

Finite-size effects on two-particle production in continuous and discrete spectrum

R. Lednický

Joint Institute for Nuclear Research, Dubna, Moscow Region, 141980, Russia

Institute of Physics ASCR, Na Slovance 2, 18221 Prague 8, Czech Republic

Abstract

The effect of a finite space-time extent of particle production region on the lifetime measurement of hadronic atoms produced by a high energy beam in a thin target is discussed. Particularly, it is found that the neglect of this effect on the ponium lifetime measurement in the experiment DIRAC at CERN could lead to the lifetime overestimation on the level of the expected 10% statistical error. It is argued that the data on correlations of identical particles obtained in the same experimental conditions, together with transport code simulation, allow to diminish the systematic error in the extracted lifetime to an acceptable level. The theoretical systematic errors arising in the calculation of the finite-size effect due to the neglect of non-equal emission times in the pair c.m.s., the space-time coherence and the residual charge are shown to be negligible.

1 Introduction

The determination, on a percent level accuracy, of the breakup probability of the $\pi^+\pi^-$ atoms produced by a high energy beam in a thin target is of principle importance for a precise lifetime measurement of these atoms in the experiment DIRAC at CERN [1-3]. This experiment aims to measure the lifetime τ_{10} of the $\pi^+\pi^-$ atoms in the ground state with 10% precision. As this lifetime of order 10^{-15} s is determined by the probability of the annihilation $\pi^+\pi^- \rightarrow \pi^0\pi^0$: $1/\tau_{10} \sim |a_0^0 - a_0^2|^2$, the DIRAC measurement enables to determine the absolute value of the difference $a_0^0 - a_0^2$ of the s-wave isoscalar and isotensor $\pi\pi$ -scattering lengths to 5%. This represents a factor of 4 improvement as compared with the present experimental data [4] except for the most recent BNL experiment [5]. The latter is based on a study of K_{e4} decays and yields the statistical error of 6% in a_0^0 , though essentially exploiting the theoretical input (the authors estimate the systematic and theoretical error on the level of several percent).

It should be stressed that the theoretical prediction for the difference $a_0^0 - a_0^2$ depends on the structure of the QCD vacuum. Thus, on the assumption of a strong quark condensate one has $a_0^0 - a_0^2 = 0.374 \pm 0.006$ fm [6]. With the decreasing condensate this difference increases and can be up to 25 % larger [7]. The DIRAC measurement thus submits the understanding of chiral symmetry breaking of QCD to a crucial test.

The method of the lifetime measurement is based on the production of the $\pi^+\pi^-$ atoms in a thin target and subsequent detection of highly correlated $\pi^+\pi^-$ pairs leaving the target as a result of the breakup of a part of the $\pi^+\pi^-$ atoms which did not decay within the target [8]. Clearly, the breakup probability is a unique function of the target geometry and material, the Lorentz factor and the ground state lifetime of the $\pi^+\pi^-$ atom. The analysis shows that, to achieve the required accuracy of 10% in the lifetime, the breakup probability, in more or less optimal conditions, should be measured to 4% [1].

There are two methods - extrapolation and subtraction ones - which can be used to measure the breakup probability (or a combination of the breakup probabilities in different targets) [2] $P_{br} = N_A^{br}/N_A$, defined as a ratio of the number of breakup atoms to the number of the atoms produced in the target. The extrapolation method requires the calculation of the number of produced $\pi^+\pi^-$ atoms N_A based on the theory of the final state interaction (FSI) in discrete and continuous spectrum [8, 9, 10]. This calculation, as well as the determination of N_A^{br} , is not required in the subtraction method which exploits the data taken on at least three different targets made out of the same material but consisting of a different number of layers of the same total thickness. However, this method needs a factor 7 larger statistics [1] and cannot yield the required precision within the approved time-scale of the experiment DIRAC.

Regarding the extrapolation method, it is sensitive to the finite space-time extent of the pion production region entering mainly through the distance r^* between the π^+ and π^- production points in their c.m.s.. In Ref. [8], the r^* -dependence was treated in an approximate way, dividing the pion sources into short-lived and long-lived ones. It was assumed that $r^* = 0$ for pion pairs arising solely from the short-lived sources (SLS) and characterized by the distances r^* much smaller than the Bohr radius $|a|$ of the $\pi^+\pi^-$ system ($a = -387.5$ fm), otherwise $r^* = \infty$.

The finite-size correction to such calculated number of free $\pi^+\pi^-$ pairs in the region of small relative momenta is determined by the three dimensionless combinations r^*/a , f_0/r^* and f_0/a of r^* , a and the s-wave $\pi^+\pi^-$ -scattering length: $f_0 = \frac{1}{3}(2a_0^0 + a_0^2) \approx 0.2$ fm. Typically $\langle r^* \rangle^{\text{SLS}} \sim 10$ fm so that the correction is dominated by the strong interaction effect and can amount up to $\sim 10\%$.

Due to a small binding energy $\epsilon_b \sim (2\mu a^2)^{-1}$, the finite-size correction to the production probability in discrete spectrum at $r^* \ll |a|$ is nearly the same as that in continuous spectrum at zero energy. Since N_A is actually determined by a ratio of the pions produced in discrete and continuous spectrum, this correction, up to $\mathcal{O}((r^*/a)^2)$ and $\mathcal{O}(f_0/a)$, would cancel out in the breakup probability provided we could measure the number of free $\pi^+\pi^-$ pairs in the region of very small relative momenta, $Q \ll 1/r^*$ [11, 12].

At small values of Q and r^* , the relative correction to the number of the free pairs is positive (due to the effect of the strong FSI $\sim 2f_0/r^*$) and changes sign at $r^* \sim 10$ fm (due to negative finite-size effect of the Coulomb FSI $\sim 2r^*/a$). For $r^* < 20$ fm, the relative correction shows a quasi-linear behavior in Q up to ~ 50 MeV/c, with almost a universal negative slope. For larger distances r^* , the slope becomes positive and has a non-trivial Q -dependence. If the pions were produced at small distances r^* of several fm, one could safely neglect the non-universal correction $\mathcal{O}((r^*/a)^2)$ and use the quasi-linear Q -dependence of the number of the free pairs to interpolate to $Q = 0$. However, there is a non-negligible tail of the distances $r^* > 10$ fm due to particle rescatterings and resonances (particularly, $r^* \sim 30$ fm in the case when one of the two pions comes from the ω -meson decay). We show that in DIRAC conditions the finite-size correction can lead to about percent underestimation of N_A and - to a similar overestimation of N_A^{br} enhanced (in case of a homogeneous target) by the ratio of the number of correlated pions to the number of breakup atoms $N_{\pi^+\pi^-}^{\text{corr}}/N_A^{br} \sim 5$. As a result, the finite-size correction in the extracted lifetime can be on a ten percent level and should be taken into account.

We discuss how to diminish the systematic error in the finite-size correction, using the correlation data on identical charged pions (containing the information about the distances r^* between the pion production points in the same experiment) together with

the complete phase-space simulations within transport models. We also show that in the calculations one can safely neglect non-equal emission times in the pair c.m.s., the space-time coherence and the residual nucleus charge.

The paper is organized now as follows. In sections 2 and 4 we give the basics of the theory of two-particle correlations due to the effects of final state interaction and quantum statistics. Sections 5 and 7 deal with the single- and two-channel wave functions in the continuous and discrete spectrum. In section 6 we consider the effect of the residual charge. In sections 3 and 8, we apply the developed formalism to estimate the finite-size effects on the pionium lifetime measurement in the experiment DIRAC at CERN. The results are summarized in section 9. In Appendices A and B we consider the effect of non-equal times and derive the analytical expression for the normalization effect of the short-range interaction on the wave function of a hadronic atom, modifying the usual $n^{-3/2}$ dependence of the pure Coulomb wave function on the main quantum number n . The reader interested mainly in practical applications can start reading from sections 3 and 8 and consult the rest of the paper to clarify the eventual questions.

2 Formalism

The production of two particles at small relative momenta is strongly influenced by their mutual final state interaction (FSI) and, for identical particles, also by quantum statistics (QS). One can separate these effects from the production amplitude provided a sufficiently long two-particle interaction time in the final state as compared with the characteristic time of the production process. This condition requires the magnitude of the relative three-momentum $\mathbf{q}^* = \mathbf{p}_1^* - \mathbf{p}_2^* \equiv 2\mathbf{k}^*$ in the two-particle c.m.s. much smaller than several hundreds MeV/c - the momentum transfer typical for particle production. For a two-particle bound state the momentum k^* in this condition has to be substituted by $(2\mu\epsilon_b)^{1/2}$, where ϵ_b is the binding energy and $\mu = m_1m_2/(m_1 + m_2)$ is the reduced mass.

Consider first the differential cross section for the production of a pair of non-identical particles 1 and 2 with the four-momenta $p_i = \{\omega_i, \mathbf{p}_i\}$ and the Lorentz factors $\gamma_i = \omega_i/m_i$. Generally, it can be expressed through the invariant production amplitudes $T(p_1, p_2; \alpha)$ in the form:

$$(2\pi)^6 \gamma_1 \gamma_2 \frac{d^6\sigma}{d^3\mathbf{p}_1 d^3\mathbf{p}_2} = \sum_{\alpha} |T(p_1, p_2; \alpha)|^2, \quad (1)$$

where the sum is done over the total spin S of the pair and its projection M (which is equivalent to the sum over helicities of the two particles) and the quantum numbers of other produced particles, including integration over their momenta with the energy-momentum conservation taken into account.

We are interested in the pairs (1,2) of the particles produced with a small relative velocity in a process with an ordinary phase space density of final state particles so that a main contribution to the double inclusive cross section comes from the configurations (1, 2, ..., i , ...) with large relative velocities of the particles 1 and 2 with respect to other produced particles ($i = 3, 4, ..n$). Due to a sharp fall of FSI with the increasing relative velocity, we can then neglect the effect of FSI in all pairs (1, i) and (2, i) except (1, 2)

and,¹ in accordance with the upper diagram in Fig. 1, write the production amplitude as

$$T(p_1, p_2; \alpha) = T_0(p_1, p_2; \alpha) + \Delta T(p_1, p_2; \alpha). \quad (2)$$

Here $T_0(p_1, p_2; \alpha)$ is the production amplitude in the case of no FSI, and $\Delta T(p_1, p_2; \alpha)$ represents the contribution of the FSI between particles 1 and 2, described by the formula

$$\Delta T(p_1, p_2; \alpha) = \frac{i\sqrt{P^2}}{2\pi^3} \int d^4\kappa \frac{T_0(\kappa, P - \kappa; \alpha) f^{S*}(p_1, p_2; \kappa, P - \kappa)}{(\kappa^2 - m_1^2 - i0)[(P - \kappa)^2 - m_2^2 - i0]}, \quad (3)$$

where $P \equiv 2p = p_1 + p_2$, $T_0(\kappa, P - \kappa; \alpha)$ is the production amplitude analytically continued off mass-shell, $f^S(p_1, p_2; \kappa, P - \kappa)$ is the scattering amplitude of particles 1 and 2 also analytically continued to the unphysical region.²

Let us express the amplitude T_0 in a form of the Fourier integral:

$$T_0(p_1, p_2; \alpha) = \int d^4x_1 d^4x_2 e^{-ip_1x_1 - ip_2x_2} \mathcal{T}(x_1, x_2; \alpha) = \int d^4x e^{-i\tilde{q}x/2} \tau_P(x; \alpha), \quad (4)$$

where the last expression arises after the integration over the pair c.m.s. four-coordinate $X = [(p_1P)x_1 + (p_2P)x_2]/P^2$ ($d^4x_1 d^4x_2 = d^4X d^4x$) based on the separation of the phase factors due to the free c.m.s. and relative motions: $e^{-ip_1x_1 - ip_2x_2} = e^{-iPX} e^{-i\tilde{q}x/2}$. Here the relative four-coordinate $x \equiv \{t, \mathbf{r}\} = x_1 - x_2$ and the generalized relative four-momentum $\tilde{q} = q - P(qP)/P^2$, $q = p_1 - p_2$; note that $qP = m_1^2 - m_2^2$. Apparently, the function $\mathcal{T}(x_1, x_2; \alpha)$ represents the production amplitude of particles 1 and 2 at the space-time points x_1 and x_2 , respectively. It should be stressed that the representation (4) concerns virtual particles as well. Inserting now in Eq. (3) the representation (4) with the substitutions $p_1 \rightarrow \kappa$, $p_2 \rightarrow P - \kappa$, we get

$$T(p_1, p_2; \alpha) = \int d^4x_1 d^4x_2 \Psi_{p_1, p_2}^{S(-)}(x_1, x_2) \mathcal{T}(x_1, x_2; \alpha) = \int d^4x \psi_q^{S(-)}(x) \tau_P(x; \alpha), \quad (5)$$

where

$$\Psi_{p_1, p_2}^{S(-)}(x_1, x_2) = [\Psi_{p_1, p_2}^{S(+)}(x_1, x_2)]^* = [e^{iPX} \psi_q^{S(+)}(x)]^* \quad (6)$$

coincides with the Bethe-Salpeter amplitude in continuous spectrum [14]. The second equality in Eq. (5) merely arises after the integration over the pair c.m.s. coordinate X as a consequence of the factorization of the free c.m.s. motion in the phase factor e^{-iPX} . Thus, on the assumption of the quasi-free propagation of the low-mass two-particle system, the momentum dependence of the two-particle amplitude is determined by the convolution of the reduced production amplitude

$$\tau_P(x; \alpha) = \int d^4X e^{-iPX} \mathcal{T}(x_1, x_2; \alpha) \quad (7)$$

¹Besides the events with a large phase-space density fluctuations, this assumption may not be justified also in low energy heavy ion reactions when the particles are produced in a strong Coulomb field of residual nuclei. To deal with this field a quantum adiabatic (factorisation) approach can be used (see Ref. [13] and section 6).

²In the case of small k^* , we are interested in, the central forces dominate so the scattering amplitude f^S is diagonal with respect to the total spin S and doesn't depend on its projections. Further, since most of the systems of our interest ($\pi^+\pi^-$, $K^\pm\pi^\mp$, π^-p , K^+K^- , K^-p , except for $\bar{p}p$) is described by a single value of S , we will often skip it to simplify the notation.

and the reduced Bethe-Salpeter amplitude $\psi_q^{S(-)}(x)$, the latter depending only on the relative four-coordinate x and the generalized relative four-momentum \tilde{q} . Using Eqs. (2)-(5), we can write

$$\psi_q^{S(+)}(x) = e^{i\tilde{q}x/2} + \Delta\psi_q^{S(+)}(x), \quad (8)$$

where the correction to the plane wave is

$$\Delta\psi_q^{S(+)}(x) = \frac{\sqrt{P^2}}{2\pi^3 i} e^{-iPx(1+Pq/P^2)/2} \int d^4\kappa \frac{e^{i\kappa x} f^S(p_1, p_2; \kappa, P - \kappa)}{(\kappa^2 - m_1^2 + i0)[(P - \kappa)^2 - m_2^2 + i0]}. \quad (9)$$

In the two-particle c.m.s., where $\mathbf{P} = 0$, $\tilde{q} = \{0, 2\mathbf{k}^*\}$, $x = \{t^*, \mathbf{r}^*\}$, the amplitude $\psi_q^{S(+)}(x)$ at $t^* \equiv t_1^* - t_2^* = 0$ coincides with a stationary solution $\psi_{-\mathbf{k}^*}^S(\mathbf{r}^*)$ of the scattering problem having at large $r^* = |\mathbf{r}^*|$ the asymptotic form of a superposition of the plane and outgoing spherical waves [15].

We see that one and the same production amplitude $\mathcal{T}(x_1, x_2; \alpha)$ or $\tau_P(x; \alpha)$, corresponding to the space-time representation, enters into relations (4) and (5). The effect of FSI manifests itself in the fact that the role of the functional basis, which the asymptotic two-particle state is projected on, is transferred from the plane waves to Bethe-Salpeter amplitudes $\Psi_{p_1, p_2}^{S(-)}(x_1, x_2)$ or $\psi_q^{S(-)}(x)$.

Eq. (5) is valid also for identical particles 1 and 2 provided the substitution of the non-symmetrized Bethe-Salpeter amplitudes $\Psi_{p_1, p_2}^{S(-)}(x_1, x_2)$ by their properly symmetrized combinations satisfying the requirements of quantum statistics:

$$\Psi_{p_1, p_2}^{S(-)}(x_1, x_2) \rightarrow \frac{1}{\sqrt{2}} [\Psi_{p_1, p_2}^{S(-)}(x_1, x_2) + (-1)^S \Psi_{p_2, p_1}^{S(-)}(x_1, x_2)]. \quad (10)$$

In this case $m_1 = m_2$, $\tilde{q} = q$ and $X = (x_1 + x_2)/2$.

After substituting the representation (5) into Eq. (1), the double inclusive cross section takes on the form

$$\begin{aligned} & (2\pi)^6 \gamma_1 \gamma_2 \frac{d^6\sigma}{d^3\mathbf{p}_1 d^3\mathbf{p}_2} \\ &= \sum_S \int d^4x_1 d^4x_2 d^4x'_1 d^4x'_2 \rho_S(x_1, x_2; x'_1, x'_2) \Psi_{p_1, p_2}^{S(-)}(x_1, x_2) \Psi_{p_1, p_2}^{S(-)*}(x'_1, x'_2) \\ &= \sum_S \int d^4x d^4x' \rho_{PS}(x; x') \psi_q^{S(-)}(x) \psi_q^{S(-)*}(x'), \end{aligned} \quad (11)$$

where the functions

$$\begin{aligned} \rho_S(x_1, x_2; x'_1, x'_2) &= \sum_{\alpha'} \mathcal{T}(x_1, x_2; S, \alpha') \mathcal{T}^*(x'_1, x'_2; S, \alpha'), \\ \rho_{PS}(x; x') &= \sum_{\alpha'} \tau_P(x; S, \alpha') \tau_P^*(x'; S, \alpha') \equiv \end{aligned} \quad (12)$$

$$\int d^4X d^4X' e^{-iP(X-X')} \rho_S\left(X + \frac{p_2 P}{P^2} x, X - \frac{p_1 P}{P^2} x; X' + \frac{p_2 P}{P^2} x', X' - \frac{p_1 P}{P^2} x'\right)$$

represent elements of the unnormalized two-particle space-time density matrices.³

³On the assumption of an instantaneous emission in the two-particle c.m.s. ($t_1^* = t_2^*$), the second expression in Eq. (11) reduces to the ansatz used in Refs. [8, 12].

Switching off the FSI and QS effects, for example, by mixing particles from different events with similar global characteristics, one can define the reference differential cross section

$$\begin{aligned} (2\pi)^6 \gamma_1 \gamma_2 \frac{d^6 \sigma_0}{d^3 \mathbf{p}_1 d^3 \mathbf{p}_2} &= \sum_S \int d^4 x_1 d^4 x_2 d^4 x'_1 d^4 x'_2 \rho_S(x_1, x_2; x'_1, x'_2) e^{-ip_1(x_1-x'_1)-ip_2(x_2-x'_2)} \\ &= \sum_S \int d^4 x d^4 x' \rho_{PS}(x; x') e^{-i\tilde{q}(x-x')/2} \end{aligned} \quad (13)$$

and rewrite Eq. (11) as

$$\begin{aligned} \frac{d^6 \sigma}{d^3 \mathbf{p}_1 d^3 \mathbf{p}_2} &= \frac{d^6 \sigma_0}{d^3 \mathbf{p}_1 d^3 \mathbf{p}_2} \sum_S \mathcal{G}_S(p_1, p_2) \left\langle \Psi_{p_1, p_2}^{S(-)}(x_1, x_2) \Psi_{p_1, p_2}^{S(-)*}(x'_1, x'_2) \right\rangle'_{p_1 p_2 S} \\ &= \frac{d^6 \sigma_0}{d^3 \mathbf{p}_1 d^3 \mathbf{p}_2} \sum_S \mathcal{G}_S(p_1, p_2) \left\langle \psi_q^{S(-)}(x) \psi_q^{S(-)*}(x') \right\rangle'_{\tilde{q} PS}, \end{aligned} \quad (14)$$

where we have introduced the quasi-averages of the bilinear products of the Bethe–Salpeter amplitudes:

$$\begin{aligned} &\left\langle \Psi_{p_1, p_2}^{S(-)}(x_1, x_2) \Psi_{p_1, p_2}^{S(-)*}(x'_1, x'_2) \right\rangle'_{p_1 p_2 S} \\ &= \frac{\int d^4 x_1 d^4 x_2 d^4 x'_1 d^4 x'_2 \rho_S(x_1, x_2; x'_1, x'_2) \Psi_{p_1, p_2}^{S(-)}(x_1, x_2) \Psi_{p_1, p_2}^{S(-)*}(x'_1, x'_2)}{\int d^4 x_1 d^4 x_2 d^4 x'_1 d^4 x'_2 \rho_S(x_1, x_2; x'_1, x'_2) e^{-ip_1(x_1-x'_1)-ip_2(x_2-x'_2)}} \\ &= \left\langle \psi_q^{S(-)}(x) \psi_q^{S(-)*}(x') \right\rangle'_{\tilde{q} PS} = \frac{\int d^4 x d^4 x' \rho_{PS}(x; x') \psi_q^{S(-)}(x) \psi_q^{S(-)*}(x')}{\int d^4 x d^4 x' \rho_{PS}(x; x') e^{-i\tilde{q}(x-x')/2}} \end{aligned} \quad (15)$$

and the statistical factors \mathcal{G}_S representing the population probabilities of the pair spin- S states out of the region of the correlation effect:

$$\begin{aligned} \mathcal{G}_S(p_1, p_2) &= \frac{\int d^4 x_1 d^4 x_2 d^4 x'_1 d^4 x'_2 \rho_S(x_1, x_2; x'_1, x'_2) e^{-ip_1(x_1-x'_1)-ip_2(x_2-x'_2)}}{\sum_S \int d^4 x_1 d^4 x_2 d^4 x'_1 d^4 x'_2 \rho_S(x_1, x_2; x'_1, x'_2) e^{-ip_1(x_1-x'_1)-ip_2(x_2-x'_2)}} \\ &= \frac{\int d^4 x d^4 x' \rho_{PS}(x; x') e^{-i\tilde{q}(x-x')/2}}{\sum_S \int d^4 x d^4 x' \rho_{PS}(x; x') e^{-i\tilde{q}(x-x')/2}}. \end{aligned} \quad (16)$$

Note that for unpolarized particles with spins j_1 and j_2 one has:⁴

$$\mathcal{G}_S = (2S+1)/[(2j_1+1)(2j_2+1)], \quad \sum_S \mathcal{G}_S = 1. \quad (17)$$

The same procedure can be also applied to describe the production of weakly bound two-particle systems, like deuterons or hadronic atoms ($\pi^+ \pi^-$ atoms, in particular). Due to a low binding energy, as compared with the energy transfers at the initial stage of the collision, there is practically no direct production of such bound systems. Their dominant production mechanism is thus due to the particle interaction in the final state. The

⁴Generally, the spin factors are sensitive to particle polarization. For example, if two spin-1/2 particles are independently emitted with the polarizations \mathbf{P}_1 and \mathbf{P}_2 , then $\mathcal{G}_0 = (1 - \mathbf{P}_1 \cdot \mathbf{P}_2)/4$ and $\mathcal{G}_1 = (3 + \mathbf{P}_1 \cdot \mathbf{P}_2)/4$.

invariant production amplitude $T_b(p_b; S, \alpha')$ of a spin- S bound system $b = \{1+2\}$ is then described by the lower diagram in Fig. 1 corresponding to the second term in the upper diagram with the free two-particle final state substituted by the bound one. Therefore, similar to Eq. (5), this amplitude is related to the Fourier transforms \mathcal{T} or τ_P of the off-mass-shell two-particle amplitude T_0 :

$$T_b(p_b; S, \alpha') = \int d^4x_1 d^4x_2 \Psi_{b,p_b}^{S(-)}(x_1, x_2) \mathcal{T}(x_1, x_2; S, \alpha') = \int d^4x \psi_b^{S(-)}(x) \tau_P(x; S, \alpha') \quad (18)$$

and the corresponding differential cross section - to the same two-particle space-time density matrices ρ_S or ρ_{PS} as enter into Eq. (11):

$$\begin{aligned} (2\pi)^3 \gamma_b \frac{d^3\sigma_b^S}{d^3\mathbf{p}_b} &= \int d^4x_1 d^4x_2 d^4x'_1 d^4x'_2 \rho_S(x_1, x_2; x'_1, x'_2) \Psi_{b,p_b}^{S(-)}(x_1, x_2) \Psi_{b,p_b}^{S(-)*}(x'_1, x'_2) \\ &= \int d^4x d^4x' \rho_{PS}(x; x') \psi_b^{S(-)}(x) \psi_b^{S(-)*}(x'). \end{aligned} \quad (19)$$

Here $\Psi_{b,p_b}^{S(-)}(x_1, x_2) = [\Psi_{b,p_b}^{S(+)}(x_1, x_2)]^* = [e^{ip_b X} \psi_b^{S(+)}(x)]^*$ is the Bethe-Salpeter amplitude for the bound system. At equal emission times in c.m.s. of the two particles, the amplitude $\psi_b^{S(+)}(x)$, describing their relative motion, coincides with the usual non-relativistic wave function in discrete spectrum $\psi_b^S(\mathbf{r}^*)$. Similar to Eq. (14), one can also rewrite the production cross section of the bound system through the reference spectrum in Eq. (13) taken at $\mathbf{p}_1 \doteq \mathbf{p}_2 \doteq \mathbf{p}_b/2$ and $\gamma_1 \doteq \gamma_2 \doteq \gamma_b$ (i.e. $\tilde{q} \doteq 0$):

$$\begin{aligned} \frac{d^3\sigma_b^S}{d^3\mathbf{p}_b} &= (2\pi)^3 \gamma_b \frac{d^6\sigma_0}{d^3\mathbf{p}_1 d^3\mathbf{p}_2} \mathcal{G}_S(p_1, p_2) \left\langle \Psi_{b,p_b}^{S(-)}(x_1, x_2) \Psi_{b,p_b}^{S(-)*}(x'_1, x'_2) \right\rangle'_{p_1 p_2 S} \\ &= (2\pi)^3 \gamma_b \frac{d^6\sigma_0}{d^3\mathbf{p}_1 d^3\mathbf{p}_2} \mathcal{G}_S(p_1, p_2) \left\langle \psi_b^{S(-)}(x) \psi_b^{S(-)*}(x') \right\rangle'_{0PS}. \end{aligned} \quad (20)$$

We see that the production of a weakly bound system $\{1+2\}$ is closely related with the production of particles 1 and 2 in continuous spectrum at small relative energies in their c.m.s. This relation was first formulated [16] in connection with the production of non-relativistic deuterons and then generalized [17] to the relativistic case and the inclusive production. Similar relation was obtained, in the limit of an instantaneous emission from a point-like region, also for the case of the production of pure Coulomb hadronic atoms [8]. A complete treatment of the production of weakly bound systems, accounting for the finite-size effects, can be found in Ref. [9].

3 Approximate description of the $\pi^+\pi^-$ production

Following Ref. [8], let us first neglect the $\pi^+\pi^-$ strong FSI and assume only two types of pion sources: short-lived sources (e.g., ρ - or Δ -resonances) characterized by small sizes or path lengths on a fm level, and long-lived sources (e.g., η , K_s or Λ) with very large or macroscopic path lengths. Since the relative space-time distance between the emission points x enters in the $\pi^+\pi^-$ pure Coulomb amplitudes $\psi_q^{(-)\text{coul}}(x)$ and $\psi_b^{(-)\text{coul}}(x)$ scaled by the Bohr radius of 387.5 fm, one can put in Eqs. (11) and (19) $\psi_q^{(-)}(x) \approx e^{-i\tilde{q}x/2} |\psi_q^{(-)\text{coul}}(0)| = e^{i\mathbf{k}^* \mathbf{r}^*} |\psi_{-\mathbf{k}^*}^{\text{coul}}(0)|$ and $\psi_b^{(-)}(x) \approx \psi_b^{(-)\text{coul}}(0) = \psi_b^{\text{coul}}(0)$ for the fraction

λ of the pairs with both pions from short-lived sources, and $\psi_q^{(-)\text{coul}}(x) \approx e^{-i\tilde{q}x/2}$ and $\psi_b^{(-)\text{coul}}(x) \approx \psi_b^{(-)\text{coul}}(\infty) = 0$ for the remaining fraction $(1 - \lambda)$. As a result, Eqs. (11) and (19) reduce to:

$$\frac{d^6\sigma}{d^3\mathbf{p}_1 d^3\mathbf{p}_2} \approx \frac{d^6\sigma_0}{d^3\mathbf{p}_1 d^3\mathbf{p}_2} [\lambda |\psi_{-\mathbf{k}^*}^{\text{coul}}(0)|^2 + (1 - \lambda)], \quad (21)$$

$$\frac{d^3\sigma}{d^3\mathbf{p}_b} \approx (2\pi)^3 \gamma_b \frac{d^3\sigma_0}{d^3\mathbf{p}_1 d^3\mathbf{p}_2} \lambda |\psi_b^{\text{coul}}(0)|^2, \quad (22)$$

where σ_0 represents the production cross section of the non-interacting pions and the expression for the production of bound $\pi^+\pi^-$ system implies $\mathbf{p}_1 \doteq \mathbf{p}_2 \doteq \mathbf{p}_b/2$ and $\gamma_1 \doteq \gamma_2 \doteq \gamma_b$. The squares of the non-relativistic Coulomb wave functions at zero separation are well known:

$$|\psi_{-\mathbf{k}^*}^{\text{coul}}(0)|^2 \equiv A_c(\eta) = 2\pi\eta/[\exp(2\pi\eta) - 1], \quad \eta = (k^*a)^{-1}, \quad (23)$$

$$|\psi_b^{\text{coul}}(0)|^2 = \delta_{l0}(\pi|a|^3 n^3)^{-1}. \quad (24)$$

Here $a = -(\mu e^2)^{-1} = -387.5$ fm is the Bohr radius accounting for the opposite signs of the pion charges. The Coulomb penetration factor $A_c(\eta)$ (sometimes called Gamow factor) enhances the production of $\pi^+\pi^-$ pairs at small $Q = 2k^*$ as $4\pi/(|a|Q)$ and at large Q approaches unity as $1 + 2\pi/(|a|Q)$. As for the bound $\pi^+\pi^-$ pairs $b = \{nl\}$, at zero separation they are produced only in the s-wave states $\{n0\}$ and the fractions with given main quantum numbers n are uniquely fixed by the n^{-3} law in Eq. (24).

The numbers N_A and N_A^{br} of produced and breakup $\pi^+\pi^-$ atoms can then be calculated in two steps [8]. First, one constructs the uncorrelated two-pion spectrum by mixing pions from different events and determines the overall normalization parameter g and the fraction λ or $\Lambda = \lambda g$ by fitting the theoretical spectrum

$$\frac{d^6 N}{d^3\mathbf{p}_1 d^3\mathbf{p}_2} \approx g \frac{d^6 N_0^{\text{mix}}}{d^3\mathbf{p}_1 d^3\mathbf{p}_2} [\lambda A_c(\eta) + (1 - \lambda)] \quad (25)$$

to the spectrum of the true pion pairs; to get rid of the pairs from the breakup of the $\pi^+\pi^-$ atoms in the target, the fit should be done in the region $Q > \sim 3$ MeV/c. In the second step, one can use the fitted parameter $\Lambda = \lambda g$ to calculate the numbers of the produced atoms in given states $b = \{n0\}$ as

$$\frac{d^3 N}{d^3\mathbf{p}_b} \approx (2\pi)^3 \gamma_b \frac{d^3 N_0^{\text{mix}}}{d^3\mathbf{p}_1 d^3\mathbf{p}_2} \Lambda |\psi_b^{\text{coul}}(0)|^2, \quad (26)$$

where $\mathbf{p}_1 \doteq \mathbf{p}_2 \doteq \mathbf{p}_b/2$. As for the number of breakup atoms, it is simply obtained by subtracting the fitted spectrum in Eq. (25) from the measured one.

Let us now consider the modification of Eqs. (25) and (26) due to the strong FSI and finite space-time separation of the particle sources. Formally one can write

$$\frac{d^6 N}{d^3\mathbf{p}_1 d^3\mathbf{p}_2} \doteq g \frac{d^6 N_0^{\text{mix}}}{d^3\mathbf{p}_1 d^3\mathbf{p}_2} \{\lambda [1 + \delta(\mathbf{k}^*)] A_c(\eta) + (1 - \lambda)\}, \quad (27)$$

$$\frac{d^3 N}{d^3\mathbf{p}_b} \doteq (2\pi)^3 \gamma_b \frac{d^3 N_0^{\text{mix}}}{d^3\mathbf{p}_1 d^3\mathbf{p}_2} \Lambda (1 + \delta_b) |\psi_b^{\text{coul}}(0)|^2, \quad (28)$$

where the correction factors are determined by the averaging of the bilinear products of the reduced Bethe–Salpeter amplitudes over the distribution of the relative space–time separations of the short–lived sources:⁵

$$1 + \delta(\mathbf{k}^*) \doteq \left\langle \psi_q^{(-)}(x) \psi_q^{(-)*}(x') \right\rangle_{\tilde{q}P}^{\text{SLS}} / A_c(\eta), \quad (29)$$

$$1 + \delta_b \doteq \left\langle \psi_b^{(-)}(x) \psi_b^{(-)*}(x') \right\rangle_{0P}^{\text{SLS}} / |\psi_b^{\text{coul}}(0)|^2. \quad (30)$$

The averaging is defined in Eq. (15) with the reduced space–time density matrix substituted by its SLS part ρ_P^{SLS} . In fact, it can be argued [11, 12] that

$$\delta_b \doteq \delta(0) \quad (31)$$

provided the characteristic separation of the pion SLS is much less than the two–pion Bohr radius $|a|$. This result immediately follows from the well known Migdal’s argument [16]. Namely, since the particles in continuous spectrum at zero kinetic energy and in discrete spectrum at very small binding energy $\kappa^2/(2\mu) \rightarrow 0$ are described by practically the same wave equations, the r^* –dependence of the corresponding wave functions at a given orbital angular momentum should be the same for the distances $r^* \ll \kappa^{-1}$ (i.e. $r^* \ll n|a|$ in the case of a hadronic atom with the main quantum number n). We show in sections 5.3 and 7 that Eq. (31) is subject to a normalization correction $\mathcal{O}(f_0/a) \sim 0.3\%/n$ and other small corrections $4\pi\mathcal{O}(k_\beta^*(f_0^{\beta\alpha})^2/a)$ and $\mathcal{O}(a^{-2})$, where $k_\beta^* = 35.5$ MeV/c is the momentum in the channel $\beta = \{\pi^0\pi^0\}$ at the threshold transition to the channel $\alpha = \{\pi^+\pi^-\}$, $f_0^{\beta\alpha} = \sqrt{2}(a_0^2 - a_0^0)/3 \approx -0.2$ fm is the transition amplitude. Taking the normalization correction explicitly into account (see Eq. (96)):

$$1 + \delta_n = (1 + \delta'_n) \left\{ 1 + \phi(n) \frac{2f_0}{n|a|} \left[1 + \mathcal{O}\left((k_\beta^* f_0^{\beta\alpha})^2\right) \right] - 4\pi^2 \mathcal{O}\left(\left(\frac{f_0}{a}\right)^2\right) \right\}, \quad (32)$$

where $\phi(n) \approx 3$ is defined in Eq. (80), one can rewrite the approximate equality in Eq. (31) as

$$\delta'_n = \delta(0) + 4\pi\mathcal{O}\left(k_\beta^*(f_0^{\beta\alpha})^2/a\right) + \mathcal{O}(a^{-2}). \quad (33)$$

In the following, we perform an analytical and numerical study of the corrections δ_n and $\delta(\mathbf{k}^*)$. Here we only mention that the condition $r^* \ll n|a|$ can be violated for pion pairs containing pions from the decays of some resonances such as ω and η' with the path lengths of about 30 and 900 fm respectively. The corresponding exponential tails are clearly seen in Fig. 2, where the r^* –distribution simulated with the UrQMD transport code [18] is shown for pion pairs produced in pNi interactions at 24 GeV in the conditions of the DIRAC experiment at CERN [19].

⁵We put approximate equalities in Eqs. (29) and (30) since they account only for the elastic transition $\alpha \rightarrow \alpha$ and ignore a small contribution of the inelastic one $\beta \rightarrow \alpha$, where $\alpha = \{\pi^+\pi^-\}$, $\beta = \{\pi^0\pi^0\}$; see section 7 for the complete treatment.

4 Space-time coherence, smoothness assumption and equal-time approximation

4.1 Non-interacting non-identical particles

To clarify the meaning of the two-particle space-time density matrix $\rho_S(x_1, x_2; x'_1, x'_2)$, let us first neglect the FSI effect and substitute the Bethe-Salpeter amplitudes by the plane waves. Changing in Eq. (11) the integration variables: $x_i, x'_i \rightarrow \bar{x}_i = \frac{1}{2}(x_i + x'_i)$, $\epsilon_i = x_i - x'_i$, we can then rewrite the production cross section of two non-identical particles as

$$(2\pi)^6 \gamma_1 \gamma_2 \frac{d^6 \sigma_0}{d^3 \mathbf{p}_1 d^3 \mathbf{p}_2} = \sum_S \int d^4 \bar{x}_1 d^4 \bar{x}_2 G_S(\bar{x}_1, p_1; \bar{x}_2, p_2) = \sum_S \int d^4 \bar{x} g_{PS}(\bar{x}, \tilde{q}), \quad (34)$$

where $\bar{x} = \bar{x}_1 - \bar{x}_2$ and the real functions

$$G_S(\bar{x}_1, p_1; \bar{x}_2, p_2) = \int d^4 \epsilon_1 d^4 \epsilon_2 e^{-ip_1 \epsilon_1 - ip_2 \epsilon_2} \rho_S(\bar{x}_1 + \frac{\epsilon_1}{2}, \bar{x}_2 + \frac{\epsilon_2}{2}; \bar{x}_1 - \frac{\epsilon_1}{2}, \bar{x}_2 - \frac{\epsilon_2}{2}),$$

$$g_{PS}(\bar{x}; \tilde{q}) = \int d^4 \bar{X} G_S(\bar{X} + \frac{p_2 P}{P^2} \bar{x}, p_1; \bar{X} - \frac{p_1 P}{P^2} \bar{x}, p_2) = \int d^4 \epsilon e^{-i\tilde{q}\epsilon/2} \rho_{PS}(\bar{x} + \frac{\epsilon}{2}, \bar{x} - \frac{\epsilon}{2}). \quad (35)$$

The function G_S , usually called emission function, being a partial Fourier transform of the space-time density matrix, is closely related to the Wigner density, the latter collecting all contributions due to free streaming of the emitted particles to given space-time points through an integral over the emission function (see Eq. (49) in Ref. [20]).

It is clear from Eqs. (34) and (35) that more narrow is the width of the diagonal of the space-time density matrix (the width of the ϵ_i -distribution), more wide is the distribution of particle four-momenta. In particular, the diagonal space-time density matrix would yield the uniform four-momentum distribution, in correspondence with the infinite uncertainty in the four-momenta of the particles localized at certain space-time points.

Consider as an example the particle emission by independent one-particle sources of various types A according to the one-particle production amplitudes (see also [21])

$$\mathcal{T}_A^{(1)}(x_1; x_A) \sim \exp[-\frac{(\mathbf{x}_1 - \mathbf{x}_A)^2}{2r_A^2} - \frac{(x_{01} - x_{0A})^2}{2\tau_A^2}] \exp(-\frac{\mathbf{x}_A^2}{4r_0^2} - \frac{x_{0A}^2}{4\tau_0^2}). \quad (36)$$

These amplitudes correspond to the sources at rest with a Gaussian distribution of the emission points $x_1 = \{t_1, \mathbf{r}_1\}$ around the source centers $x_A = \{t_A, \mathbf{r}_A\}$, also distributed according to a Gaussian law. Assuming further that the sources are sufficiently heavy, we can describe them classically. The four-coordinates of the source centers x_A can then be considered as a part of the quantum numbers α' , the sum in Eq. (12) containing the integration over x_A . Performing this integration, we get for the elements of the one-particle space-time density matrix related to a source A :

$$\rho_A^{(1)}(x_1, x'_1) \sim \exp(-\frac{\epsilon_1^2}{4r_A^2} - \frac{\epsilon_{01}^2}{4\tau_A^2}) \exp(-\frac{\bar{\mathbf{x}}_1^2}{2r_0^2 + r_A^2} - \frac{\bar{x}_{01}^2}{2\tau_0^2 + \tau_A^2}) \quad (37)$$

and for the corresponding emission function:

$$G_A^{(1)}(\bar{x}_1, p) \sim \exp(-r_A^2 \mathbf{p}^2 - \tau_A^2 p_0^2) \exp(-\frac{\bar{\mathbf{x}}_1^2}{2r_0^2 + r_A^2} - \frac{\bar{x}_{01}^2}{2\tau_0^2 + \tau_A^2}). \quad (38)$$

We may see that the source space-time dimensions r_A and τ_A determine both the space-time coherence of particle production (the non-diagonality of the space-time density matrix) and the distribution of particle four-momenta. In particular case of the sources of a vanishing space-time extent: $r_A = \tau_A = 0$ (no coherence) any particle four-momenta are equally probable.

Note that for a source moving with a non-relativistic velocity β_A and emitting a particle 1 with the mean three-momentum $\mathbf{p}_A = m_1\beta_A$, Eqs. (36) and (37) acquire phase factors $e^{i\mathbf{p}_A\mathbf{x}_1}$ and $e^{i\mathbf{p}_A\mathbf{\epsilon}_1}$ respectively and the substitution $\mathbf{p} \rightarrow \mathbf{p} - \mathbf{p}_A$ has to be done in Eq. (38). If the \mathbf{p}_A -distribution decouples from the distribution of other source characteristics in a Gaussian form of a width Δ_0 , we still arrive at Eqs. (37), (38), up to a substitution $r_A^2 \rightarrow r_A^2/[2(r_A\Delta_0)^2 + 1]$ in the first factor, corresponding to a widening of the momentum distribution due to the dispersion of the source velocities.

As for the actual values of the parameters r_A and τ_A , we can estimate them using the information about particle transverse momenta which are much less influenced by the motion of the sources than the longitudinal ones. Doing this for pions or kaons, we should however exclude the low- p_t region which is dominantly populated by the decays of low-lying resonances. We can also use the p_\perp -distributions of these resonances. In both cases the p_t -slopes are of $\sim 3 \text{ (GeV/c)}^{-2}$ (see, e.g., [22]), yielding on average $r_A^2 + \tau_A^2 \approx 0.1 \text{ fm}^2$. It is important that the estimated value of $r_A^2 + \tau_A^2$ appears to be much smaller than the effective values of the parameters r_0^2 and τ_0^2 , measured with the help of the correlations of identical particles (so called *particle interferometry* or *correlation femtoscopy*; see section 4.2 and also the reviews [23]-[28]). The latter being of about 1 fm^2 for hadron-hadron interactions and of several tens fm^2 for the collisions involving heavy nuclei.

4.2 Non-interacting identical particles

4.2.1 Correlation function

Consider the production of non-interacting identical particles. Now we have to substitute the Bethe-Salpeter amplitude by a properly symmetrized combination of the plane waves (see Eq. (10)). As a result of the interference of these waves, there appears the additional term, not present in Eq. (34):

$$\begin{aligned} (2\pi)^6 \gamma_1 \gamma_2 \frac{d^6\sigma}{d^3\mathbf{p}_1 d^3\mathbf{p}_2} &= \sum_S \int d^4\bar{x}_1 d^4\bar{x}_2 [G_S(\bar{x}_1, p_1; \bar{x}_2, p_2) + G_S(\bar{x}_1, p; \bar{x}_2, p)(-1)^S \cos(q\bar{x})] \\ &= \sum_S \int d^4\bar{x} [g_{PS}(\bar{x}, q) + g_{PS}(\bar{x}, 0)(-1)^S \cos(q\bar{x})]. \end{aligned} \quad (39)$$

Note that the off-mass-shell four-momentum $p = (p_1 + p_2)/2$ enters as an argument of the emission function G_S in the interference term.

It is convenient to define the correlation function $\mathcal{R}(p_1, p_2)$ as a ratio of the double inclusive cross section $d^6\sigma$ to the reference one $d^6\sigma_0$ which would be observed in the case of absent effects of quantum statistics and FSI:⁶

$$\mathcal{R}(p_1, p_2) = \frac{d^6\sigma(p_1, p_2)}{d^6\sigma_0(p_1, p_2)}. \quad (40)$$

⁶In the high energy collisions involving nuclei, we can neglect the kinematic constraints as well as rather weak dynamical correlations and construct the reference distribution using the particles from different events.

In case of a negligible FSI, there is no correlation for non-identical particles: $\mathcal{R}(p_1, p_2) = 1$, while for identical particles the correlation arises due to the interference effect:

$$\begin{aligned}\mathcal{R}(p_1, p_2) &= 1 + \frac{\sum_S \int d^4\bar{x}_1 d^4\bar{x}_2 G_S(\bar{x}_1, p; \bar{x}_2, p) (-1)^S \cos(q\bar{x})}{\sum_S \int d^4\bar{x}_1 d^4\bar{x}_2 G_S(\bar{x}_1, p_1; \bar{x}_2, p_2)} \equiv 1 + \sum_S \mathcal{G}_S (-1)^S \langle \cos(q\bar{x}) \rangle''_{p_1 p_2 S} \\ &= 1 + \frac{\sum_S \int d^4\bar{x} g_{PS}(\bar{x}, 0) (-1)^S \cos(q\bar{x})}{\sum_S \int d^4\bar{x} g_{PS}(\bar{x}, q)} \equiv 1 + \sum_S \mathcal{G}_S (-1)^S \langle \cos(q\bar{x}) \rangle''_{qPS},\end{aligned}\quad (41)$$

where the quasi-averages satisfy the equalities

$$\langle \cos(q\bar{x}) \rangle''_{p_1 p_2 S} \equiv \Re \langle e^{ip_1(x_1 - x'_2) + ip_2(x_2 - x'_1)} \rangle'_{p_1 p_2 S} = \langle \cos(q\bar{x}) \rangle''_{qPS} \equiv \Re \langle e^{iq(x+x')/2} \rangle'_{qPS}; \quad (42)$$

the factors \mathcal{G}_S represent the population probabilities of the pair spin- S states out of the region of the correlation effect. They are defined in Eq. (16) and can be expressed through the emission functions as:

$$\mathcal{G}_S(p_1, p_2) = \frac{\int d^4x_1 d^4x_2 G_S(x_1, p_1; x_2, p_2)}{\sum_S \int d^4x_1 d^4x_2 G_S(x_1, p_1; x_2, p_2)} = \frac{\int d^4x g_{PS}(x, q)}{\sum_S \int d^4x g_{PS}(x, q)}, \quad \sum_S \mathcal{G}_S = 1. \quad (43)$$

They can be also considered as the initial (QS switched off) statistical factors. For initially unpolarized spin- j particles: $\sum_S \mathcal{G}_S (-1)^S = (-1)^{2j} / (2j + 1)$.

Assuming, for example, that for a (generally momentum dependent) fraction λ of the pairs the particles are emitted by independent one-particle sources described by the Gaussian amplitude (36), while for the remaining fraction $(1 - \lambda)$, related to very long-lived sources (η , K_s^0 , Λ , \dots), the relative distances r^* between the emission points in the pair c.m.s. are extremely large, the correlation function

$$\mathcal{R}(p_1, p_2) = 1 + \lambda \sum_S \mathcal{G}_S (-1)^S \exp(-r_0^2 \mathbf{q}^2 - \tau_0^2 q_0^2). \quad (44)$$

We see that a characteristic feature of the correlation function of identical particles is the presence of an interference maximum or minimum at small $|\mathbf{q}|$, changing to a horizontal plateau at sufficiently large $|\mathbf{q}|$, large compared with the inverse characteristic space-time distance between the particle emission points.

4.2.2 Directional and velocity dependence

One can see from Eq. (44) that, due to the relation $q_0 = \mathbf{v}\mathbf{q} \equiv vq_L$, the correlation function at $v\tau_0 > r_0$ substantially depends on the direction of the vector \mathbf{q} even in the considered case of spherically symmetric spatial form of the production region. Thus the transverse ($\mathbf{q} \perp \mathbf{v}$) and longitudinal ($\mathbf{q} \parallel \mathbf{v}$) interferometry radii are $r_T = r_0$ and $r_L = (r_0^2 + v^2 \tau_0^2)^{1/2}$ respectively.

In principle, the directional and velocity dependence of the correlation function allows to determine the characteristic emission time and the form of the production region [23] and reveal the details of the production dynamics (such as collective flows; see, *e.g.* [29, 30]). For this, the correlation function is often analyzed in terms of the *out* (x), *side* (y) and *longitudinal* (z) components of the relative momentum vector $\mathbf{q} = \{q_x, q_y, q_z\}$.

Here the *out* and *side* denote the transverse, with respect to the reaction (event) axis, components of the vector \mathbf{q} , the *out* direction is parallel to the transverse component of the pair velocity vector.

It should be noted that particle correlations at high energies usually measure only a small part of the space-time emission volume, being only slightly sensitive to its increase related to the fast longitudinal motion of the particle sources. In fact, due to limited source decay momenta $p^{(s)}$ of a few hundred MeV/c, the correlated particles with nearby velocities are emitted by almost comoving sources and so - at nearby space-time points. In other words, the maximal contribution of the relative motion to the interferometry radii in the two-particle c.m.s. is limited by the moderate source decay length $\tau p^{(s)}/m$. The dynamical examples are sources-resonances, color strings or hydrodynamic expansion. To substantially eliminate the effect of the longitudinal motion, the correlations can be analyzed in terms of the invariant variable $Q = 2k^* \equiv (-\tilde{q}^2)^{1/2}$ and the components of the three-momentum difference in pair c.m.s. ($\mathbf{q}^* \equiv \mathbf{Q} = 2\mathbf{k}^*$) or in the longitudinally comoving system (LCMS). In LCMS, each pair is emitted transverse to the reaction axis so that the generalized relative four-momentum $\tilde{\mathbf{q}}$ coincides with \mathbf{q}^* except for the *out*-component $\tilde{q}_x = \gamma_t q_x^*$, where γ_t is the LCMS Lorentz factor of the pair. For example, in the case of one-dimensional boost invariant expansion, the longitudinal interferometry radius in the longitudinally comoving system reads [30] $r_z = (T/m_t)^{1/2}\tau$, where T is the freezeout temperature, τ is the proper freezeout time and m_t is the transverse particle mass.

Clearly, the complicated dynamics of particle production requires a detailed study of the directional and momentum dependence of the correlation functions. Moreover, the usual Gaussian parametrization of the relative distances between the emission points may happen to be insufficient. Particularly, it can lead to inconsistencies in the treatment of QS and FSI effects, the latter being more sensitive to the tail of the distribution of the relative distances. These problems can be at least partially overcome with the help of transport code simulations accounting for the dynamical evolution of the emission process and providing the phase space information required to calculate the QS and FSI effects on the correlation function.

4.2.3 Smoothness assumption

In the simple model of only one type of the sources contributing to the observable interference effect and in the absence of the relative source motion, the width of the low- $|\mathbf{q}|$ structure is solely determined by the characteristic space-time distance between the one-particle sources and does not depend on the parameters r_A and τ_A , characterizing the space-time extent of the sources themselves - see Eq. (44). It means that the enlargement of the production region related to the latter ($r_0^2 \rightarrow r_0^2 + \frac{1}{2}r_A^2$, $\tau_0^2 \rightarrow \tau_0^2 + \frac{1}{2}\tau_A^2$) is compensated in the correlation function due to the different momentum arguments of the emission functions in the numerator and denominator of Eq. (41).⁷

Generally, the particles are emitted by moving sources of different types and the correlation function depends also on their space-time extent. Particularly, for a Gaussian

⁷This is clearly seen when calculating the correlation function directly from Eq. (1), substituting the production amplitude $T(p_1, p_2; \alpha)$ by the symmetrized product of the Kopylov-Podgoretsky one-particle amplitudes in momentum representation (given by the inverse Fourier transform of Eq. (36)): $T_A^{(1)}(p, x_A) = u(p, x_A)e^{ipx_A}$, where $u(p, x_A)$ is a universal one-particle amplitude.

distribution of the mean emission three-momentum \mathbf{p}_A of a width Δ_0 , Eq. (44) is modified by the substitution [21] $r_0^2 \rightarrow r_0^2 + r_A^2/[2 + (r_A\Delta_0)^{-2}]$. Usually, the effect of a finite space-time extent of the one-particle sources is negligible:

$$r_A^2/2 \ll r_0^2, \quad \tau_A^2/2 \ll \tau_0^2. \quad (45)$$

Note that these conditions guarantee sufficiently smooth four-momentum dependence of the emission function $G_S(\bar{x}_1, p_1; \bar{x}_2, p_2)$, such that we can neglect its dependence on the four-momentum difference q in the region of the interference effect characterized by the inverse space-time distance between the particle production points. On this, so called *smoothness* assumption, Eq. (41) reduces to:

$$\mathcal{R}(p_1, p_2) \doteq 1 + \sum_S (-1)^S \mathcal{G}_S \langle \cos(qx) \rangle_{qPS}, \quad (46)$$

where

$$\langle \cos(qx) \rangle_{qPS} = \frac{\int d^4x_1 d^4x_2 G_S(x_1, p_1; x_2, p_2) \cos(qx)}{\int d^4x_1 d^4x_2 G_S(x_1, p_1; x_2, p_2)} = \frac{\int d^4x g_{PS}(x, q) \cos(qx)}{\int d^4x g_{PS}(x, q)} \quad (47)$$

and the spin factors \mathcal{G}_S are defined in Eqs. (16) and (43).

Eq. (46) is valid up to a correction representing a fraction of $(r_A^2 + v^2\tau_A^2)/(r_0^2 + v^2\tau_0^2)$. This correction composes a few percent for high energy hadron-hadron collisions and - a few per mil for the collisions involving heavy nuclei. Note that Eq. (47) is often used to calculate the correlation functions of non-interacting identical particles with the help of various classical transport codes (like RQMD, VENUS or UrQMD) [18] - the emission points are identified with the points of the last collisions or the resonance decays. One can also use the transport codes to estimate the effect of the smoothness approximation on the correlation function. Thus, using the UrQMD simulation of the pNi interactions at 24 GeV in the conditions of experiment DIRAC, we have calculated the $\pi^-\pi^-$ correlation functions as $\mathcal{R}(Q) = 1 + \langle \cos(qx) \rangle \equiv 1 + \langle \cos(\mathbf{Q}\mathbf{r}^*) \rangle$ averaging over the \mathbf{r}^* -distribution determined in various Q -intervals and found that the correlation functions corresponding to the intervals 50-100, 100-150 and 150-200 MeV/c agree with that based on the lowest Q -interval of 0-50 MeV/c within 0.2-0.9%, $\sim 3\%$ and $\sim 7\%$, respectively.

4.3 Interacting particles

It is clear that the *smoothness* condition allows one to express the production cross section through the emission function $G_S(x_1, p_1; x_2, p_2)$ also in the case of interacting particles. Thus, separating the two-particle c.m.s. motion in the phase factor $\exp[iP(X - X')] \equiv \exp[i(p_1 - \tilde{q}/2)\epsilon_1 + i(p_2 + \tilde{q}/2)\epsilon_2]$ and using the *smoothness* condition to neglect here \tilde{q} compared with $p_{1,2}$ ⁸ and substitute, in the amplitudes $\psi_q^{S(+)}(x)$, the relative coordinates $x = \bar{x} + (\epsilon_1 - \epsilon_2)/2$ and $x' = \bar{x} - (\epsilon_1 - \epsilon_2)/2$ by their mean value \bar{x} , we can rewrite Eq. (11) in a simple approximate form:

$$(2\pi)^6 \gamma_1 \gamma_2 \frac{d^6\sigma}{d^3\mathbf{p}_1 d^3\mathbf{p}_2} \doteq \sum_S \int d^4x_1 d^4x_2 G_S(x_1, p_1; x_2, p_2) |\psi_q^{S(+)}(x)|^2$$

⁸The account of \tilde{q} in the phase factor would lead to the substitution of the particle four-momenta in the emission function by their mean (off-mass-shell) values: $p_i \rightarrow Pm_i/(m_1 + m_2)$.

$$\begin{aligned}
&= \sum_S \int d^4x g_{PS}(x, \tilde{q}) |\psi_q^{S(+)}(x)|^2 \\
&\equiv (2\pi)^6 \gamma_1 \gamma_2 \frac{d^6\sigma_0}{d^3\mathbf{p}_1 d^3\mathbf{p}_2} \sum_S \mathcal{G}_S \langle |\psi_q^{S(+)}(x)|^2 \rangle_{\tilde{q}PS}, \quad (48)
\end{aligned}$$

where $d^6\sigma_0$ is the production cross section of the non-interacting particles introduced in Eq. (34). The averaging $\langle \dots \rangle_{\tilde{q}PS}$ and the initial spin factors \mathcal{G}_S are defined in Eqs. (47) and (43). The correlation function defined as a ratio $d^6\sigma/d^6\sigma_0$ then takes on the form:

$$\mathcal{R}(p_1, p_2) \doteq \sum_S \mathcal{G}_S \langle |\psi_q^{S(+)}(x)|^2 \rangle_{\tilde{q}PS}. \quad (49)$$

Recall that for identical particles the Bethe-Salpeter amplitudes $\psi_q^{S(+)}(x)$ should be symmetrized according to Eq. (10).

Note that for non-identical particles, one also arrives at Eqs. (48) and (49) using the approximate ansatz $\Psi_{p_1, p_2}^{S(+)}(x_1, x_2) \doteq e^{i(p_1 \epsilon_1 + p_2 \epsilon_2)} \Psi_{p_1, p_2}^{S(+)}(\bar{x}_1, \bar{x}_2)$ which becomes exact in the absence of FSI. For identical particles, this ansatz, applied to the non-symmetrized amplitudes $\tilde{\Psi}^{S(+)}$, leads to the correlation function (see also Eqs. (58) and (60) in Ref. [20])

$$\mathcal{R}(p_1, p_2) \doteq \sum_S \mathcal{G}_S \left[\langle |\tilde{\psi}_q^{S(+)}(x)|^2 \rangle_{qPS} + (-1)^S \Re \langle \tilde{\psi}_q^{S(+)}(x) \tilde{\psi}_{-q}^{S(+)*}(x) \rangle_{qPS}'' \right], \quad (50)$$

where $\tilde{\psi}$ is the reduced non-symmetrized Bethe-Salpeter amplitude ($\tilde{\psi}_q^{S(+)}(x) = e^{iqx/2}$ for non-interacting particles). Clearly, the smoothness condition allows one to put $\langle \dots \rangle_{qPS}'' \doteq \langle \dots \rangle_{qPS}$ and thus recover Eq. (49).

Similar to the case of non-interacting particles, the relative correction to the approximations in Eqs. (48)-(50) is determined by the ratio $(r_A^2 + v^2 \tau_A^2)/(r_0^2 + v^2 \tau_0^2)$ - a measure of the non-diagonality of the space-time density matrix. For identical particles, the correction arises mainly from the symmetrization effect and, according to previous subsection, it is expected on a few per mil level for the processes involving heavy nuclei. For non-identical particles, the correction is usually substantially smaller, being scaled by the relative finite-size contribution of the strong and Coulomb FSI.⁹

Proceeding in a similar way with the production cross section of a bound two-particle system, we arrive, on the same conditions as in the case of continuous spectrum, at the approximate form:

$$\begin{aligned}
(2\pi)^3 \gamma_b \frac{d^3\sigma_b^S}{d^3\mathbf{p}_b} &\doteq \int d^4x_1 d^4x_2 G_S(x_1, p_1; x_2, p_2) |\psi_b^{S(+)}(x)|^2 \\
&= \int d^4x g_{PS}(x, 0) |\psi_b^{S(+)}(x)|^2 \\
&\equiv (2\pi)^6 \gamma_1 \gamma_2 \frac{d^6\sigma_0}{d^3\mathbf{p}_1 d^3\mathbf{p}_2} \mathcal{G}_S \langle |\psi_b^{S(+)}(x)|^2 \rangle_{0PS}, \quad (51)
\end{aligned}$$

where $\mathbf{p}_i = \mathbf{p}_b m_i / (m_1 + m_2)$.

We will show that for two oppositely charged particles, the x -dependence of the Bethe-Salpeter amplitudes in continuous and discrete spectrum is practically the same at c.m.s.

⁹In case of $|f^S| \ll r^* \ll |a|$, we are interested in, the corresponding strong and Coulomb FSI contributions are of $2f^S/r^*$ and $2r^*/a$ respectively (see next section).

separations r^* much smaller than the Bohr radius $|a|$. Therefore, the corrections to Eqs. (48) and (51) (arising due to the use of the smoothness assumption in their derivation from Eqs. (11) and (19) respectively) practically cancel out in the ratio of the numbers of pairs produced in continuous and discrete spectrum provided $\langle r^* \rangle^{\text{SLS}} \ll |a|$.

4.4 Equal-time approximation

For non-interacting particles, the non-symmetrized Bethe-Salpeter amplitude $\psi_q^{(+)}(x) = e^{-i\mathbf{k}^*\mathbf{r}^*}$ is independent of the relative emission time t^* in c.m.s. of the pair. On the contrary, the amplitude of two interacting particles contains an explicit dependence on t^* - the interaction effect vanishes at $|t^*| \rightarrow \infty$. However, it can be shown [10] (see Appendix A) that the effect of non-equal times can be neglected on condition

$$|t^*| \ll m(t^*)r^{*2}, \quad (52)$$

where $m(t^* > 0) = m_2$ and $m(t^* < 0) = m_1$. On this condition we can use the approximation of equal emission times of the two particles in their c.m.s ($t^* = 0$) and substitute the Bethe-Salpeter amplitude by the usual non-relativistic two-particle wave function. The applicability condition (52) of the equal-time approximation is usually satisfied for heavy particles like kaons or nucleons. But even for pions this approximation merely leads to a slight overestimation (typically less than a few percent) of the strong FSI contribution to the production cross section [10]. To demonstrate this, we use the simple static Gaussian model of independent one-particle sources described by the amplitude (36). Recall, however, that in high energy collisions, such a model is relevant for a limited rapidity region only. It means that the pair velocity v in the rest frame of the sources is related to the measured velocity rather indirectly.¹⁰ In this model, the applicability condition (52) of the equal-time approximation can be roughly written in the form [10]:

$$\tau_0 \ll \mu\gamma r_0(r_0^2 + v^2\tau_0^2)^{1/2}. \quad (53)$$

For $\tau_0 \lesssim r_0$ this condition requires sufficiently small Compton wave lengths of the particles in the source rest frame: $1/\omega_i \ll r_0$, while for large characteristic emission times, $\tau_0 \gg r_0/v$, it requires small de Broglie wave lengths: $1/p_i \ll r_0$. Clearly, this condition is not satisfied for very slow particles emitted by the sources of a long lifetime. The increasing importance of the non-equal time effect with the decreasing pair velocity and increasing lifetime of the sources is demonstrated in Figs. 3 and 4 for the FSI contribution in the $\pi^0\pi^0$ correlation function. For sufficiently large velocities $v > 0.5$ and radii $r_0 > 1$ fm, we are interested in, the effect is rather small, not exceeding 5% of the FSI contribution in the low- k^* region, corresponding to the effect of a few per mil in the correlation function.

As for the effect of non-equal times on the Coulomb FSI it doesn't influence the leading zero-distance ($r^* = 0$) part and, the effect of the subleading part (expected on a similar percent level as in the case of the strong FSI) can be neglected when scaled by its contribution $\sim r^*/a$. It concerns also the case of hadronic atoms since the subleading part is the same as in the continuous spectrum at $k^* = 0$.

¹⁰We can roughly estimate $\langle v \rangle$ from the distribution of particle transverse momenta. Taking for pions the p_\perp^2 -slope of ~ 6 (GeV/c)⁻² (now we have to account for lower p_\perp -values due to indirect pions) and using $\langle v^2 \rangle \approx \langle 3p_\perp^2 / (3p_\perp^2 + m_{12}^2) \rangle$, we get $\langle v \rangle \approx 0.8$.

Adopting the equal-time approximation (with the accuracy of a few per mil), we can rewrite Eqs. (48) and (51) for the production cross sections of particles 1 and 2 in continuous and discrete spectrum at low relative or binding energies as follows:

$$\gamma_1\gamma_2\frac{d^6\sigma}{d^3\mathbf{p}_1d^3\mathbf{p}_2} \doteq \gamma_1\gamma_2\frac{d^6\sigma_0}{d^3\mathbf{p}_1d^3\mathbf{p}_2} \sum_S \mathcal{G}_S \langle |\psi_{-\mathbf{k}^*}^S(\mathbf{r}^*)|^2 \rangle_{\widetilde{q}PS}, \quad (54)$$

$$\gamma_b\frac{d^3\sigma_b^S}{d^3\mathbf{p}_b} \doteq (2\pi)^3\gamma_1\gamma_2\frac{d^6\sigma_0}{d^3\mathbf{p}_1d^3\mathbf{p}_2} \mathcal{G}_S \langle |\psi_b^S(r^*)|^2 \rangle_{0PS}, \quad (55)$$

where $b = \{n0\}$ and $\mathbf{p}_i = \mathbf{p}_b m_i / (m_1 + m_2)$ in Eq. (55); for equal-mass particles $\mathbf{p}_1 = \mathbf{p}_2 = \mathbf{p}_b/2$ and $\gamma_1 = \gamma_2 = \gamma_b$.

Particularly, for $\pi^+\pi^-$ production, one can rewrite the correction factors in Eqs. (29) and (30) as

$$1 + \delta(\mathbf{k}^*) \doteq \langle |\psi_{-\mathbf{k}^*}(\mathbf{r}^*)|^2 \rangle_{\widetilde{q}P}^{\text{SLS}} / A_c(\eta), \quad (56)$$

$$1 + \delta_n \doteq \langle |\psi_{n0}(r^*)|^2 \rangle_{0P}^{\text{SLS}} / |\psi_b^{\text{coul}}(0)|^2. \quad (57)$$

5 Wave functions

5.1 Continuous spectrum

5.1.1 Short-range FSI

Let us start with the case when at least one of the two particles is neutral and their FSI is due to the short-range forces only. In the considered region of small k^* the short-range particle interaction is dominated by s-waves. Since the radius of the s-wave interaction is usually small compared with the distance r^* between the production points of particles 1 and 2 in their c.m.s., the FSI effect is mainly determined by the asymptotic behavior of the scattered wave outside the region of the strong interaction $r^* > d$:

$$\Delta\psi_{-\mathbf{k}^*}(\mathbf{r}^*) = f(k^*)e^{ik^*r^*}/r^*. \quad (58)$$

The s-wave amplitude f depends on the magnitude of the vector \mathbf{k}^* only. Assuming the absence of inelastic transitions, it satisfies the one-channel s-wave unitarity condition $\Im f = k^*|f|^2$ or, equivalently $\Im f^{-1} = -k^*$, and so can be represented as

$$f = [\exp(2i\delta_0) - 1]/(2ik^*) = (K^{-1} - ik^*)^{-1}, \quad (59)$$

where δ_0 is the s-wave phase shift and $K^{-1} = k^* \cot \delta_0$ is a real function of k^* . Usually (for potentials vanishing with the distance exponentially or faster), this function is real also for negative kinetic energies $k^{*2}/(2\mu)$, so that its expansion can contain only even powers of k^* [15]. Retaining near threshold only the first two terms in the expansion, one can express the function K^{-1} or K through the corresponding two parameters: scattering length f_0 and effective range d_0 or curvature b_0 :

$$K^{-1} \doteq 1/f_0 + \frac{1}{2}d_0k^{*2}, \quad K \doteq f_0 + b_0k^{*2}, \quad b_0 \doteq -d_0f_0^2/2. \quad (60)$$

The expansion of K^{-1} is superior for two-nucleon systems (due to large scattering lengths, amounting to about 20 fm in the singlet case) while for other systems, the K -expansion

Table 1: The pair Bohr radius including the sign of the interaction, $a = (\mu z_1 z_2 e^2)^{-1}$, and the characteristic width of the Coulomb correlation effect, $Q_c \equiv 2k_c^* = 4\pi/|a|$, corresponding to $|\eta|^{-1} = 2\pi$ (see Eq. (23) and the first panel in Fig. 5).

Pair	$\pi^+\pi^\pm$	π^+K^\pm	$\pi^\pm p$	K^+K^\pm	$K^\pm p$	pp^\pm
a , fm	± 387.5	± 248.6	± 222.5	± 109.6	± 83.6	± 57.6
Q_c , MeV/c	6.4	10.0	11.1	22.6	29.7	43.0

is often preferred. To extend the latter to a wider energy range, it is usually written in a relativistic form and additional parameters are added. For example [6]:

$$K = \frac{2}{\sqrt{s}} \frac{s_{\text{th}} - s_0}{s - s_0} \sum_{j=0}^3 A_j x^{2j}, \quad x = 2k^*/\sqrt{s_{\text{th}}}, \quad (61)$$

where $s = (p_1 + p_2)^2 = (\omega_1^* + \omega_2^*)^2$, $\omega_{1,2}^* = (m_{1,2}^2 + k^{*2})^{1/2}$ and $s_{\text{th}} = (m_1 + m_2)^2$. The parameter s_0 takes into account the eventual resonance, specifying the value of the two-particle c.m.s. energy squared where the phase $\delta_0(k^*)$ passes through 90° .¹¹

Note that the extension of the asymptotic wave function in the inner region leads to a relative shift in the production cross section of the order $|f|^2 \frac{d}{dk^{*2}} \text{Re}(1/f)/\langle r^* \rangle^3$ [10, 31]. The leading part of this shift can be, in principle, corrected for (see section 7.3). However, being quadratic in the amplitude f , it is rather small for $\pi\pi$ -, πK - or πp -systems - usually not exceeding several percent of the short-range FSI contribution.

5.1.2 Account of the Coulomb FSI

Similar to the case of neutral particles, we will approximate (with the same accuracy) the wave function of two charged particles near threshold by the asymptotic solution outside the region of the strong interaction $r^* > d$. It is well known that the long-range Coulomb interaction modifies both the plane and spherical waves [15]:

$$\psi_{-\mathbf{k}^*}(\mathbf{r}^*) = e^{i\delta_c} \sqrt{A_c(\eta)} \left[e^{-i\mathbf{k}^* \cdot \mathbf{r}^*} F(-i\eta, 1, i\xi) + f_c(k^*) \frac{\tilde{G}(\rho, \eta)}{r^*} \right], \quad (62)$$

where $\xi = \mathbf{k}^* \cdot \mathbf{r}^* + k^* r^* \equiv \rho(1 + \cos \theta^*)$, $\rho = k^* r^*$, $\eta = (k^* a)^{-1}$, $a = (\mu z_1 z_2 e^2)^{-1}$ is the two-particle Bohr radius including the sign of the interaction, $\delta_c = \arg \Gamma(1 + i\eta)$ is the Coulomb s-wave phase shift, $A_c(\eta)$ is the Coulomb penetration factor defined in Eq. (23),

$$F(\alpha, 1, z) = 1 + \alpha z/1!^2 + \alpha(\alpha + 1)z^2/2!^2 + \dots \quad (63)$$

¹¹The actual k^* -dependence of the K -function is however not important since we are interested in the near-threshold region and, have already neglected the p-wave correction $\mathcal{O}(k^{*2} a_1/r^*)$ in Eq. (58); here a_1 is a p-wave scattering length. For $\pi^+\pi^-$ system, $a_1 \approx 0.1 \text{ fm}^3$, $f_0 \approx 0.2 \text{ fm}$, $d_0 \approx -10 \text{ fm}$ and the relative p-wave contribution to the k^{*2} term due to the short-range FSI composes in the production cross section $\sim a_1/(a_1 - d_0 f_0^2/2 - f_0^3/3) \sim 30\%$; the relative contribution of the k^{*2} term $\sim (a_1 - d_0 f_0^2/2 - f_0^3/3)k^{*2}/f_0$ being less than 1% of the total short-range FSI contribution for $Q = 2k^* < 30 \text{ MeV}/c$.

is the confluent hypergeometric function and $\tilde{G} = \sqrt{A_c}(G_0 + iF_0)$ is a combination of the regular (F_0) and singular (G_0) s-wave Coulomb functions (see, e.g., [32]):

$$\tilde{G}(\rho, \eta) = P(\rho, \eta) + 2\eta\rho[\ln|2\eta\rho| + 2C - 1 + \chi(\eta)]B(\rho, \eta). \quad (64)$$

Here $C \doteq 0.5772$ is the Euler constant, the functions

$$\begin{aligned} B(\rho, \eta) &= \sum_{s=0}^{\infty} B_s, \quad B_0 = 1, \quad B_1 = \eta\rho, \quad B_2 = (\eta\rho)^2/3 - \rho^2/6, \quad \dots, \\ P(\rho, \eta) &= \sum_{s=0}^{\infty} P_s, \quad P_0 = 1, \quad P_1 = 0, \quad P_2 = -3(\eta\rho)^2 - \rho^2/2, \quad \dots \end{aligned} \quad (65)$$

are given by the following recurrence relations:¹²

$$\begin{aligned} (n+1)(n+2)B_{n+1} &= 2\eta\rho B_n - \rho^2 B_{n-1}, \\ n(n+1)P_{n+1} &= 2\eta\rho P_n - \rho^2 P_{n-1} - (2n+1)2\eta\rho B_n \end{aligned} \quad (66)$$

and the function

$$\chi(\eta) = h(\eta) + iA_c(\eta)/(2\eta), \quad (67)$$

where the function $h(\eta)$ is expressed through the digamma function $\psi(z) = \Gamma'(z)/\Gamma(z)$:¹³

$$h(\eta) = [\psi(i\eta) + \psi(-i\eta) - \ln(\eta^2)]/2. \quad (68)$$

The amplitude $f_c(k^*) = f(k^*)/A_c(\eta)$, where $f(k^*)$ is the amplitude of the low-energy s-wave elastic scattering due to the short-range interaction renormalized by the long-range Coulomb forces. Assuming again the absence of inelastic transitions, the amplitude $f(k^*) = (e^{2i\delta_0} - 1)/(2ik^*)$ and satisfies the one-channel s-wave unitarity condition. Similar to the case of neutral particles, one then has [15]:

$$f_c(k^*) = \left(K^{-1} - \frac{2\chi(\eta)}{a} \right)^{-1}, \quad (69)$$

where the function K is real for real kinetic energies, including negative ones (provided the short-range potential vanishes with the distance exponentially or faster), and can be parametrized according to Eqs. (60) or (61).

Note that $\delta_c \rightarrow 0$, $A_c \rightarrow 1$ for $\eta \rightarrow 0$ ($k^* \gg |a|^{-1}$) and $\tilde{G} \rightarrow e^{i\rho}$, $F \rightarrow 1$ for $\eta\rho \equiv r^*/a \rightarrow 0$. So, the two-particle wave function in the absence of the long-range Coulomb forces is recovered provided r^* , f_0 and $1/k^*$ are much smaller than the Bohr radius $|a|$.

In Fig. 5, we plot $A_c(\eta)$ and $\chi(\eta)$ as functions of the variable $|\eta|^{-1} = |ak^*|$. For the system of two charged pions, this variable approximately corresponds to $Q = 2k^*$ in MeV/c. One may see that, at $k^* \rightarrow 0$, the Coulomb penetration factor $A_c(\eta)$ respectively tends to 0 and ∞ for like and unlike particle charges. With the increasing k^* , this factor slowly approaches unity: $A_c(\eta) \approx 1 - \pi\eta$ for $k^* > 2\pi/|a|$. Note that the quadratic behavior of $\Re\chi(\eta) \equiv h(\eta) \approx \eta^{-2}/12$ at $|\eta|^{-1} < 1$ is changed by a steep quasi-linear rise in the interval $1 < |\eta|^{-1} < 5$; the corresponding slope being about 0.26. As for $\Im\chi(\eta) \equiv A_c(\eta)/(2\eta)$, at $k^* = 0$ it equals to 0 and $-\pi$ for like and unlike charges respectively, and, for $k^* > 2\pi/|a|$, it approaches the linear k^* -dependence: $\Im\chi(\eta) \approx (\eta^{-1} - \pi)/2$.

¹²Note that $B(\eta, \rho) \equiv F_0/(\rho\sqrt{A_c}) \rightarrow \sin(\rho)/\rho$ and $P(\eta, \rho) \rightarrow \cos(\rho)$ in the limit $\eta\rho \equiv r^*/a \rightarrow 0$.

¹³For $|\eta| < 0.3$ the function $h(\eta) \doteq 1.2\eta^2 - \ln|\eta| - C$, while at large $|\eta|$ this function can be represented by a truncated series in inverse powers of η^2 : $h(\eta) = \eta^{-2}/12 + \eta^{-4}/120 + \dots$.

5.1.3 The small- and large- r^* limits

Since we are interested in the region of small relative distances r^* compared with the Bohr radius $|a|$ and small relative momenta $Q = 2k^*$ compared with $1/r^*$, it is useful to write the first terms in the expansion of the hypergeometric functions F and \tilde{G} in r^*/a and $\rho \equiv k^*r^*$. We have ($x = \cos \theta^*$):

$$\begin{aligned} F(-i\eta, 1, i\xi) &= 1 + \frac{r^*}{a}(1+x) \left[1 + \frac{i\rho}{4}(1+x) - \frac{\rho^2}{18}(1+x)^2 + \mathcal{O}(\rho^3) \right] + \mathcal{O}\left(\left(\frac{r^*}{a}\right)^2\right), \\ \tilde{G}(\rho, \eta) &= 1 - \frac{\rho^2}{2} + 2\frac{r^*}{a} \left[\ln|2\frac{r^*}{a}| + 2C - 1 + \chi(\eta) \right] \left(1 - \frac{\rho^2}{6} \right) + \mathcal{O}(\rho^4) + \mathcal{O}\left(\left(\frac{r^*}{a}\right)^2\right). \end{aligned} \quad (70)$$

Since for the systems of interest ($\pi\pi$, πK , πp), $|f_0|^2 < |f_0 d_0| < \sim m_\pi^{-2} \ll r^{*2}$, one can neglect the Q -dependence of the scattering amplitude and, after the averaging over the uniform x -distribution,¹⁴ write the correlation function at a fixed separation r^* $\mathcal{R}(k^*; r^*) = \langle |\psi_{-\mathbf{k}^*}(\mathbf{r}^*)|^2 \rangle$ as

$$\begin{aligned} \mathcal{R}(k^*; r^*) &= A_c(\eta) \left\langle |F|^2 + 2\Re \left(e^{i\mathbf{k}^* \cdot \mathbf{r}^*} F^* \tilde{G} \frac{f_0}{r^*} \right) + \mathcal{O}\left(\left(\frac{f_0}{r^*}\right)^2\right) \right\rangle \\ &= A_c(\eta) \left\{ 1 + 2\frac{r^*}{a} + 2\frac{f_0}{r^*} + 2\frac{f_0}{a} \left[1 + 2 \left(\ln|2\frac{r^*}{a}| + 2C - 1 + h(\eta) \right) \right] \right. \\ &\quad \left. - \rho^2 \left(\frac{2}{9} \frac{r^*}{a} + \frac{4}{3} \frac{f_0}{r^*} \right) + \mathcal{O}\left(\left(\frac{f_0}{r^*}\right)^2\right) + \mathcal{O}\left(\left(\frac{r^*}{a}\right)^2\right) + \mathcal{O}(\rho^4) \right\}. \end{aligned} \quad (71)$$

In Figs. 6, 7 and 8, we show the Q -dependence of the functions $B(\rho, \eta)$, $P(\rho, \eta)$, $\tilde{G}(\rho, \eta)$ and the reduced correlation function \mathcal{R}/A_c as well as the corresponding main contributions due to the interference term and the modulus squared of the hypergeometric function for the $\pi^+\pi^-$ system at $r^* = 5, 15, 50$ fm. One may see that the almost universal quasilinear decrease of \mathcal{R}/A_c for $r^* < \sim 20$ fm is due to the interference term, and that it is changed, for higher r^* -values, by a steep rise due to the $|F|^2$ -term. From the results of table 2 one can conclude that the linear fits of \mathcal{R}/A_c recover the intercept better than to 2 per mil for $r^* < \sim 20$ fm and - better than to 2 percent even for $r^* = 50$ fm.

To clarify the origin of the quasilinear behavior of the reduced correlation function \mathcal{R}/A_c , one can use Eq. (71) to estimate the slope at small Q :

$$\left(\frac{\mathcal{R}}{A_c}\right)' \equiv \frac{d}{dQ} \left(\frac{\mathcal{R}}{A_c}\right) \doteq \pm 2f_0 \frac{dh}{d|\eta|^{-1}} - \left(\pm \frac{1}{9} \frac{r^*}{|a|} + \frac{2}{3} \frac{f_0}{r^*} \right) r^{*2} Q, \quad (72)$$

where the sign $+$ ($-$) corresponds to the Coulomb repulsion (attraction). Using the fact that $dh/d|\eta|^{-1} \approx 0.26$ for $1 < |\eta|^{-1} < 5$, one has $(\mathcal{R}/A_c)' \approx -(0.61 + bQ)$ (GeV/c)⁻¹ for the $\pi^+\pi^-$ -system at $1 < Q < 5$ MeV/c, where $b = 0.019, 0.035$ and -0.72 (MeV/c)⁻¹ at $r^* = 5, 15$ and 50 fm respectively. For $Q > 5$ MeV/c, the absolute value of the slope due to the h -function decreases as $\sim 2.35|\eta|$. It appears, that for $r^* < \sim 20$ fm, this decrease is approximately compensated by the Q -dependence of the functions B , P and F , so that $(\mathcal{R}/A_c)' \approx -0.5$ (GeV/c)⁻¹ up to $Q = 50$ MeV/c.

¹⁴In case of an anisotropic \mathbf{r}^* -distribution, this implies the integration over the direction of the vector $\mathbf{k}^* = \mathbf{Q}/2$, distributed isotropically for uncorrelated particles at $Q \rightarrow 0$.

Table 2: Results of the linear fits of the reduced $\pi^+\pi^-$ correlation function: $\mathcal{R}/A_c = c_0 + c_1 Q$ in different intervals $0 < Q < Q_{\max}$. The function \mathcal{R}/A_c is calculated at $r^* = 5, 15$ and 50 fm in the approximation of a constant scattering amplitude $f_c(k^*) = f_0 = 0.232$ fm and, assuming the uniform distribution of the cosine of the angle between the vectors \mathbf{r}^* and $\mathbf{k}^* = \mathbf{Q}/2$. Also shown are the corresponding values of \mathcal{R}/A_c at $Q = 0$ (the intercepts).

r^* , fm	Intercept	Q_{\max} , MeV/c	10	20	30	40	50
5	1.077	c_0	1.077	1.077	1.077	1.077	1.078
		$c_1, (\text{GeV}/c)^{-1}$	-0.55	-0.47	-0.48	-0.52	-0.57
15	0.961	c_0	0.961	0.961	0.961	0.960	0.959
		$c_1, (\text{GeV}/c)^{-1}$	-0.59	-0.56	-0.55	-0.51	-0.42
50	0.783	c_0	0.778	0.768	0.766	0.773	0.783
		$c_1, (\text{GeV}/c)^{-1}$	2.55	4.61	4.99	4.38	3.69

Note that, at $\xi \gg 1 + \eta^2$,

$$\sqrt{A_c(\eta)}F(-i\eta, 1, i\xi) \rightarrow \left(1 - i\frac{\eta^2}{\xi}\right) e^{i(-\delta_c + \eta \ln \xi)} + \frac{\eta}{\xi} e^{i(\delta_c + \xi - \eta \ln \xi)} \quad (73)$$

and, at $\rho \gg 1 + \eta^2$,

$$\tilde{G}(\rho, \eta) \rightarrow \sqrt{A_c(\eta)} e^{i(\delta_c + \rho - \eta \ln 2\rho)}, \quad (74)$$

so that both the effects of the Coulomb and strong FSI vanish in the cross section as r^{*-2} . In fact, the asymptotic expression for the F -function in Eq. (73) is not valid in the case of nearly opposite directions of the vectors \mathbf{k}^* and \mathbf{r}^* ($\cos \theta^* \approx -1$) when the variable $\xi = \rho(1 + \cos \theta^*)$ is suppressed even at large $\rho = k^* r^*$. This leads, after averaging over the angles, to a slower vanishing of the Coulomb effect, as r^{*-1} , in agreement with the classical Jacobian factor $[1 - 2/(ar^* k^{*2})]^{1/2} \approx 1 - (ar^* k^{*2})^{-1}$.

5.2 Discrete spectrum

Since the Schrödinger equation at a small negative energy $-\epsilon_b = -\kappa^2/(2\mu)$ practically coincides with that in continuous spectrum at zero energy, the r^* -dependence of the corresponding wave functions at given orbital angular momentum l and $r^* \ll \kappa^{-1}$ is the same.¹⁵ In fact, both solutions (at positive and negative energies) can be written in the same form for any r^* , up to an energy dependent normalization factor \mathcal{N} . Outside the region of the short-range interaction, $r^* > d$, we can write the s-wave solution as a combination of the regular and singular Coulomb functions:

$$\psi_{l=0}(r^*) = \mathcal{N}(\eta) \left[\frac{F_0(\rho, \eta)}{\rho \sqrt{A_c(\eta)}} + f_c(k^*) \frac{\tilde{G}(\rho, \eta)}{r^*} \right]. \quad (75)$$

¹⁵This important conclusion was first stated by Migdal for the pn -system [16].

At $d < r^* \ll |a|$ and $|\rho| \ll 1$ it takes on the form:

$$\begin{aligned} \psi_{l=0}(r^*) = \mathcal{N} \left\{ \left(1 + \frac{r^*}{a}\right) + \mathcal{O}\left(\left(\frac{r^*}{a}\right)^2\right) + \mathcal{O}(\rho^2) + \right. \\ \left. + f_c \frac{1}{r^*} \left[1 + 2\frac{r^*}{a} \left(\ln \left|2\frac{r^*}{a}\right| + 2C - 1 + \chi\right) \left(1 + \frac{r^*}{a}\right) + \mathcal{O}\left(\left(\frac{r^*}{a}\right)^2\right) + \mathcal{O}(\rho^2)\right] \right\}. \end{aligned} \quad (76)$$

For positive energies, $\mathcal{N} = e^{i\delta_c} \sqrt{A_c(\eta)}$ and, at $k^* \rightarrow 0$, $f_c = f_0/[1 - 2f_0\chi(\pm\infty)/a]$, $\chi(+\infty) = 0$ ($a > 0$) or $\chi(-\infty) = -i\pi$ ($a < 0$). In the case of opposite charges ($a < 0$), Eq. (76) yields:

$$\begin{aligned} \psi_{k^*, l=0} = e^{i\delta_c} \sqrt{A_c} \left\{ \left(1 - \frac{r^*}{|a|}\right) \left[1 - 2\frac{f_0}{|a|} \left(\ln \left|2\frac{r^*}{a}\right| + 2C - 1\right)\right] + \frac{f_0}{r^*} + \right. \\ \left. + \left(1 + \frac{f_0}{r^*}\right) \left[2i\pi \frac{f_0}{|a|} + \mathcal{O}\left(\left(\frac{r^*}{a}\right)^2\right) + \mathcal{O}(\rho^2)\right] \right\}. \end{aligned} \quad (77)$$

For the discrete levels at negative energies, the substitution $k^* \rightarrow i\kappa_n$ has to be done, particularly yielding [15, 31]:

$$\chi(\eta_n) = \frac{\pi}{2} \cot\left(\frac{\pi}{\kappa_n|a|}\right) + \frac{1}{2} \left[2 \ln(\kappa_n|a|) + \psi\left(\frac{1}{\kappa_n|a|}\right) + \psi\left(-\frac{1}{\kappa_n|a|}\right)\right], \quad (78)$$

where $\eta_n = (i\kappa_n a)^{-1}$. Later on, we will use a more compact form of Eq. (78) following from the relation $\psi(-x) = \psi(x) + \pi \cot(\pi x) + x^{-1}$:

$$\chi(\eta_n) = \pi \cot(\pi x_n) - (2x_n)^{-1} [\phi(x_n) - 3], \quad x_n = (\kappa_n|a|)^{-1}, \quad (79)$$

$$\phi(x) = 2 + 2x[\ln x - \psi(x)]. \quad (80)$$

For a pure Coulombic atom ($a < 0$, $f_0 = 0$), only the solution F_0/ρ , regular at $r^* \rightarrow 0$, contributes and the requirement of its exponential damping at large distances fixes the energy levels. The corresponding κ -values at a given principle quantum number n are equal to $\kappa_n^c = (n|a|)^{-1}$. The wave functions $\psi_{nl}^{\text{coul}}(r^*)$ can then be expressed in terms of the Laguerre polynomials $L_{n+l-1}^{2l+1}(z)$. For $l = 0$,

$$\psi_{n0}^{\text{coul}}(r^*) = \psi_{n0}^{\text{coul}}(0) \exp\left(-\frac{r^*}{n|a|}\right) L_{n-1}^1\left(\frac{2r^*}{n|a|}\right) / (n \cdot n!). \quad (81)$$

The square of the wave function $\psi_{n0}^{\text{coul}}(0)$ at zero separation is given in Eq. (24) and the Laguerre polynomials are defined by the following recurrence relations:

$$L_{n-1}^1(z) = (n \cdot n!) \sum_{s=0}^{n-1} l_{n-1}^s(z), \quad l_{n-1}^0(z) = 1, \quad l_{n-1}^s(z) = -\frac{z(n-s)}{s(s+1)} l_{n-1}^{s-1}(z). \quad (82)$$

At $r^* \ll n|a|$,

$$\psi_{n0}^{\text{coul}}(r^*) = \psi_{n0}^{\text{coul}}(0) \left[1 - \frac{r^*}{|a|} + \mathcal{O}\left(\left(\frac{r^*}{na}\right)^2\right)\right]. \quad (83)$$

The strong interaction slightly shifts the Coulombic energy levels thus making the regular part of the general solution (75) divergent at large distances. Therefore, the amplitude f_c has to have a pole at $k^* = i\kappa_n$, and so, according to Eq. (69),

$$\chi(\eta_n) = -\frac{|a|}{2K(i\kappa_n)} = -\frac{|a|}{2f_0} \left[1 + \mathcal{O}\left(\frac{f_0 d_0}{(na)^2}\right)\right]. \quad (84)$$

Using Eqs. (79) and (84), one can fix the energy levels $E_n = -\kappa_n^2/(2\mu)$ in discrete spectrum with the relative error of $\mathcal{O}(a^{-3})$:¹⁶

$$\kappa_n = \kappa_n^c \left\{ 1 + 2f_0\kappa_n^c \left[1 + f_0\kappa_n^c[\phi(n) - 1] - \frac{4\pi^2}{3}\mathcal{O}\left(\frac{f_0^2}{a^2}\right) + \mathcal{O}\left(\frac{f_0d_0}{n^2a^2}\right) \right] \right\}, \quad \kappa_n^c = (n|a|)^{-1}, \quad (85)$$

where the function $\phi(n)$ is defined in Eq. (80) and the digamma function for the integer values of the argument is given by the recurrence relation:

$$\psi(n+1) = \psi(n) + 1/n, \quad \psi(1) = -C \doteq -0.5772. \quad (86)$$

Note that $\phi(n) \approx 3$ is nearly constant: $\phi(1) = 2 + 2C \doteq 3.15443$, $\phi(2) \doteq 3.08145$, $\phi(3) \doteq 3.05497$, ..., $\phi(\infty) = 3$.

Since $N(\eta_n) = 0$ (to compensate for the pole of the amplitude f_c at $k^* = i\kappa_n$), the s-wave solutions in discrete spectrum are now given (for $r^* > d$) by the second term in Eq. (75), exponentially vanishing at large distances:

$$\psi_{n0}(r^*) = \mathcal{N}'(n)K(i\kappa_n)\frac{\tilde{G}(\rho_n, \eta_n)}{r^*} = \mathcal{N}'(n)f_0\frac{\tilde{G}(\rho_n, \eta_n)}{r^*} \left[1 + \mathcal{O}\left(\frac{f_0d_0}{n^2a^2}\right) \right]. \quad (87)$$

The arguments ρ_n and η_n are taken at $k^* = i\kappa_n$ and the normalization factor

$$\mathcal{N}'(n) = \mathcal{N}(\eta_n)f_c(i\kappa_n)/K(i\kappa_n) \quad (88)$$

is set by the requirement

$$\int |\psi_{n0}(r^*)|^2 d^3\mathbf{r}^* = 1. \quad (89)$$

Note that the extension in the integral (89) of the asymptotic wave function (87) into the inner region $r^* < d$ leads to negligible relative errors $\mathcal{O}(f_0d^2/(na)^3)$, $\mathcal{O}(f_0^2d/(na)^3)$ in the normalization factor \mathcal{N}' . Comparing the expansion of the wave function $\psi_{n0}(r^*)$ for the distances $d < r^* \ll |a|$:¹⁷

$$\begin{aligned} \psi_{n0}(r^*) = \mathcal{N}'(n) \left\{ \left(1 - \frac{r^*}{|a|} \right) \left[1 - 2\frac{f_0}{|a|} \left(\ln \left| \frac{2r^*}{a} \right| + 2C - 1 \right) \right] + \frac{f_0}{r^*} \right. \\ \left. + \mathcal{O}\left(\frac{f_0d_0}{n^2a^2}\right) + \mathcal{O}\left(\frac{f_0r^*}{a^2}\right) \right\} \end{aligned} \quad (90)$$

with the low- r^* expansion (83) of the pure Coulombic wave function and, also taking into account the exponential damping at large distances, one can approximate the wave function (87) at $r^* \ll |a|^2/f_0$ by the expression:

$$\psi_{n0}^{\text{app}}(r^*) = \frac{\mathcal{N}'(n)}{\psi_{n0}^{\text{coul}}(0)} \psi_{n0}^{\text{coul}}(r^*) \left[1 - 2\frac{f_0}{|a|} \left(\ln \left| \frac{2r^*}{a} \right| + 2C - \frac{3}{2} \right) + \frac{f_0}{r^*} \right]. \quad (91)$$

¹⁶To show this, one can put $\kappa_n = \kappa_n^c(1 + \epsilon)$, $x_n = |\kappa_n a|^{-1} = n/(1 + \epsilon)$ and use the equality $\tan(\pi x_n) = -\tan(\pi x_n \epsilon) = -(\pi x_n \epsilon)[1 + (\pi^2 n^2/3)\mathcal{O}(\epsilon^2)]$ and the inequality $|\phi(x_n) - \phi(n)| < \mathcal{O}(\epsilon)$, the latter following from the fact that $\phi'(n)$ vanishes faster than n^{-1} . Note that Eq. (85) is in agreement with the result of Ref. [33] for the relative energy shift $\epsilon(n, 0) \equiv (2 + \epsilon)\epsilon \doteq \epsilon_0(n, 0)[1 + \epsilon_0(n, 0)p_1(n, 0)]$, where $\epsilon_0(n, 0) = 4f_0\kappa_n^c$ and $p_1(n, 0) = \phi(n)/4$.

¹⁷See the expansion of the \tilde{G} -function in the square brackets in Eq. (76) and use Eq. (84) for $\chi(\eta_n)$.

From the results of calculations for the s-wave $\pi^+\pi^-$ atoms, presented in upper panel of Fig. 9, one can see that the squares of the approximate and exact expressions (91) and (87) practically coincide for the distances up to several tens fm and that the agreement is better than percent even at $r^* \sim |a|$.

It follows from Eq. (91) that the relative difference of the normalization factors $\mathcal{N}'(n)$ and $\psi_{n0}^{\text{coul}}(0)$ scales as $\mathcal{O}(f_0/a)$. In fact, this difference can be fixed when extending the theory to a multichannel case and requiring the equality of the total width $\Gamma_n = -2\Im E_n$ and the sum of the partial widths (see Eqs. (B.1) and (B.5) or, Eqs. (B.7) and (B.4)). As a result:

$$|\mathcal{N}'(n)/\psi_{n0}^{\text{coul}}(0)|^2 - 1 \doteq \phi(n) \frac{2f_0}{n|a|}. \quad (92)$$

We have checked Eq. (92), calculating \mathcal{N}' from the integral (89) for various values of the scattering length f_0 , Bohr radius $|a|$ and the principle quantum number n .

5.3 Universality

Comparing Eqs. (77) and (90), valid for the distances $d < r^* \ll |a|$, one confirms the important conclusion, already stated at the beginning of the previous subsection, about the universality of the r^* -behavior of the moduli squared of the s-wave solutions in continuous ($k^* \rightarrow 0$) and discrete spectrum, up to corrections vanishing as inverse squares of the Bohr radius $|a|$. Assuming $f_0 < \sim d$, one has:

$$\Delta_{n0}^{k^*}(r^*) \equiv \left| \frac{\psi_{k^*0}(\mathbf{r}^*)/\psi_{k^*0}^{\text{coul}}(0)}{\psi_{n0}(r^*)/\mathcal{N}'(n)} \right|^2 - 1 = 4\pi^2 \mathcal{O}\left(\frac{f_0^2}{a^2}\right) + \mathcal{O}\left(\frac{f_0 d_0}{n^2 a^2}\right) + \mathcal{O}\left(\frac{r^{*2}}{a^2}\right) + \mathcal{O}(\rho^2). \quad (93)$$

The universality holds with the same accuracy also if the s-wave solution in continuous spectrum were substituted by the complete wave function (recall that $\psi_{-\mathbf{k}^*}^{\text{coul}}(0) = \psi_{k^*0}^{\text{coul}}(0) \equiv A_c^{1/2}$), provided the averaging over the angle between the the vectors \mathbf{r}^* and \mathbf{k}^* :

$$\Delta_n^{k^*}(r^*) \equiv \left\langle \left| \frac{\psi_{-\mathbf{k}^*}(\mathbf{r}^*)/\psi_{-\mathbf{k}^*}^{\text{coul}}(0)}{\psi_{n0}(r^*)/\mathcal{N}'(n)} \right|^2 \right\rangle - 1 = 4\pi^2 \mathcal{O}\left(\frac{f_0^2}{a^2}\right) + \mathcal{O}\left(\frac{f_0 d_0}{n^2 a^2}\right) + \mathcal{O}\left(\frac{r^{*2}}{a^2}\right) + \mathcal{O}(\rho^2). \quad (94)$$

This result follows from the fact that, at $k^* \rightarrow 0$ and typical distances $r^* \ll |a|$, the total wave function in continuous spectrum almost coincides with the s-wave amplitude $\psi_{k^*0}(r^*)$ (see the lower panel in Fig. 8):

$$\psi_{-\mathbf{k}^*}(\mathbf{r}^*) = \psi_{k^*0}(r^*) + e^{i\delta_c} \sqrt{A_c} \frac{\mathbf{k}^* \mathbf{r}^*}{k^* a} + \mathcal{O}\left(\frac{r^{*2}}{a^2}\right) + \mathcal{O}(\rho^2) \quad (95)$$

and, that the relatively significant correction term $\mathcal{O}(r^*/a)$ vanishes after the averaging over the directions of the relative three-momentum $\mathbf{Q} = 2\mathbf{k}^*$.¹⁸ From the lower panel of Fig. 9, one can see that for the $\pi^+\pi^-$ system, the universality holds to better than percent for $r^* < \sim 50$ fm.¹⁹

¹⁸The distribution of these directions has to be eventually corrected for the experimental acceptance provided the latter is asymmetric with respect to $\mathbf{Q} \rightarrow -\mathbf{Q}$.

¹⁹Note that Δ_{n0}^0 (not shown in Fig. 9) is negative and, contrary to Δ_n^0 , it shows the strongest deviation from zero for $n = 1$, achieving a per mil level already at $r^* \approx 20$ fm.

Comparing Eqs. (54) and (55), one can see that the number N_A of produced $\pi^+\pi^-$ atoms is determined by the number of free $\pi^+\pi^-$ pairs in the region of small k^* . So, N_A is actually proportional to the ratio $\langle |\psi_{n0}(r^*)|^2 \rangle_{0P} / \langle |\psi_{-\mathbf{k}^*}(\mathbf{r}^*)|^2 \rangle_{\tilde{q}P}$ in which the effects of the r^* -dependence as well as the corrections due to non-equal emission times ($t^* \neq 0$) and smoothness assumption are to a large extent compensated for, being practically the same for the wave functions in continuous spectrum at $k^* \rightarrow 0$ and discrete spectrum at $r^* \ll |a|$. In fact, according to Eqs. (92-94), one can write the ratio of the finite-size correction factors at small relative momenta ($k^* \ll \langle 1/r^* \rangle^{\text{SLS}}$) and moderate distances between the particle emitters ($\langle r^* \rangle^{\text{SLS}} \ll |a|$) as

$$\begin{aligned} \frac{1 + \delta_n}{1 + \delta(k^*)} &\equiv \frac{\langle |\psi_{n0}(r^*)/\psi_{n0}^{\text{coul}}(0)|^2 \rangle_{0P}^{\text{SLS}}}{\langle |\psi_{-\mathbf{k}^*}(\mathbf{r}^*)/\psi_{k^*0}^{\text{coul}}(0)|^2 \rangle_{\tilde{q}P}^{\text{SLS}}} \equiv \left| \frac{N'(n)}{\psi_{n0}^{\text{coul}}(0)} \right|^2 \frac{1 + \delta'_n}{1 + \delta(k^*)} \\ &= \left[1 + \phi(n) \frac{2f_0}{n|a|} \right] \left\{ 1 + \mathcal{O}\left(\frac{\langle r^{*2} \rangle^{\text{SLS}}}{a^2}\right) + \mathcal{O}(k^{*2} \langle r^{*2} \rangle^{\text{SLS}}) \right\}, \end{aligned} \quad (96)$$

thus leading to Eq. (33) up to a small correction due to the transition $\pi^0\pi^0 \rightarrow \pi^+\pi^-$ (see Eq. (126)). Recall that though the k^* -dependence of the correction factor in braces is quadratic at very low values of k^* , in fact, in a wider k^* -interval and for sufficiently small values $\langle r^* \rangle^{\text{SLS}} < \sim 10$ fm, it shows a quasi-linear and almost universal behavior (see Fig. 8 and Ref. [1]).

Note that a relation similar to Eq. (96) without the correction factors has been used in Ref. [8] for a simple calculation of the number of produced atoms (see Eqs. (21) and (22)).²⁰ Particularly, the n^{-3} dependence of the latter has been predicted. The correction $2\phi(n)f_0/(n|a|) \approx 6f_0/(na)$ slightly modifies this dependence, the modification being the largest for low values of n . For example, for the $\pi^+\pi^-$ -atom ($f_0 \approx 0.2$ fm), this correction is about 0.3% at $n = 1$ (see also the central panel of Fig. 9).

In Refs. [34, 35], the effect of the strong interaction on the n -dependence of the pionium wave function has been studied numerically, solving the corresponding Schrödinger equations. Thus, in Ref. [34], the ratio $R_n = \psi_{n0}/\psi_{n0}^{\text{coul}}$ and the difference $\Delta R_n = R_1 - R_n$ have been calculated for $n = 1 - 3$ using an exponential form of the short-range potential. According to Eqs. (83), (90) and (92), one has, up to corrections $\mathcal{O}(f_0/a)$ and $\mathcal{O}(r^{*2}/a^2)$:

$$R_n \equiv \frac{\psi_{n0}(r^*)}{\psi_{n0}^{\text{coul}}(r^*)} \doteq 1 + \frac{f_0}{r^*}, \quad \Delta R_n \equiv R_1 - R_n \doteq \frac{f_0}{|a|} \left\{ \phi(1) - \frac{1}{n}\phi(n) \right\} \left(1 + \frac{f_0}{r^*} \right). \quad (97)$$

From Fig. 1 of Ref. [34], one can deduce a value of ~ 0.15 fm for the scattering length f_0 to achieve an agreement with the prediction of Eq. (97) for the ratio R_n at $d < r^* \ll |a|$. The differences ΔR_n , presented in Fig. 1 of Ref. [34] for $n = 2$ and 3, are however by a factor 1.6 higher than the corresponding predictions of Eq. (97). For example, for $10^3 \Delta R_n$ at $r^* = 8$ fm, $n = 2$ and 3, one can read from this figure the values²¹ 1.0 and 1.3 while, Eq. (97) respectively predicts 0.6 and 0.8. This discrepancy may indicate that the calculation error, declared in Ref. [34] to be better than 10^{-4} , was underestimated by a factor of 5.

²⁰Originally, this relation was obtained on the assumption of an instantaneous emission from a point-like region ($r^* \ll |a|$) and a negligible short-range FSI [8], the latter shown later on as unnecessary [12].

²¹One should correct the figure by interchanging the curves. The author is grateful to O. Voskresenskaya for pointing out this misprint.

In Ref. [35], a more refined numerical study of the n -dependence has been done accounting for the second channel ($\pi^0\pi^0$) and extended charges. The hadronic $\pi\pi$ potentials have been chosen to reproduce the phase shifts given by two-loop chiral perturbation theory. The quantity $d_n = n^{3/2}\psi_{n0}/\psi_{10} - 1$ has been calculated for $n = 1 - 4$. Similar to Eq. (97), one has for $d < r^* \ll |a|$

$$d_n \equiv n^{3/2} \frac{\psi_{n0}(r^*)}{\psi_{10}(r^*)} - 1 \doteq -\frac{f_0}{|a|} \left\{ \phi(1) - \frac{1}{n} \phi(n) \right\}, \quad (98)$$

up to corrections $\mathcal{O}(f_0 r^*/a^2)$ and $\mathcal{O}(r^{*2}/a^2)$. The results of numerical calculations presented in Fig. 2 of Ref. [35] are in qualitative agreement with Eq. (98), d_n being almost constant (except for the region of very small r^*) and showing the right n -dependence: $d_n \sim -(1 - 1/n)$. Similar to Ref. [34], the numerical results for $|d_n|$ are however higher, now by a factor of 2.5, than the predictions of Eq. (98) calculated with $f_0 = 0.2$ fm which should correspond within $\sim 10\%$ to the choice of the potentials in Ref. [35]. Since the presence of the second channel leads to a negligible modification of Eq. (98) (see next chapter) and the correction due to the extended charges is also expected to be negligible ($\sim -\frac{1}{6}\langle r^2 \rangle_\pi/a^2$), the discrepancy in the size of the correction d_n has to be attributed to the insufficient calculation accuracy or, to the incorrect matching of the scattering length.

6 The effect of residual charge

The formalism of section 2 assumes a free motion of a given particle pair in the last stage of the collision. Here we will estimate the effect of the residual charge present in the collisions involving nuclei. Since the energy of the collisions producing hadronic atoms is sufficiently large, this effect can be expected of minor importance. Therefore, we will estimate its upper limit considering rather unfavourable conditions.

Generally, instead of the two-particle Bethe-Salpeter amplitude $\Psi_{p_1 p_2}^{(+S)}(x_1, x_2)$, the correlation function is determined by the amplitude $\Psi_{p_1 p_2}^{(+S\{\alpha\})}(x_1, x_2)$ representing the solution of a complicated multi-body problem, taking into account interaction between the two particles and also their interaction with the residual system described by the quantum numbers $\{\alpha\}$. For our purpose, it is sufficient to approximate these quantum numbers by an effective (comoving with a given pair) pointlike residual charge Ze and consider a thermal motion of the two particles with the temperature $T \sim m_\pi$ in the rest frame of this charge.

Let us start with the hypothetical case of particles that interact with the charge Ze but their mutual interaction is "switched off". In such a situation we can treat the systems $(1, Z)$ and $(2, Z)$ independently. Then the interaction with the Coulomb center just leads to the substitution of the spatial parts of the plane waves $e^{ip_i x_i}$ by the usual Coulomb wave functions: $e^{-i\mathbf{p}_i \mathbf{r}_i} \rightarrow e^{-i\mathbf{p}_i \mathbf{r}_i} \Phi_{\mathbf{p}_i}^{z_i Z}(\mathbf{r}_i)$, where $\Phi_{\mathbf{p}_i}^{z_i Z}(\mathbf{r}_i) = e^{i\delta_i} \sqrt{A_c(\eta_i)} F(-i\eta_i, 1, i\rho_i)$, $\rho_i = \mathbf{p}_i \mathbf{r}_i + p_i r_i$, $\eta_i = (p_i a_i)^{-1}$, $a_i = (\omega_i z_i Z e^2)^{-1}$ is the Bohr radius of the system (i, Z) (taking into account the sign of the interaction) generalized to the relativistic case by the substitution $m_i \rightarrow \omega_i$ of the particle masses by their energies, δ_i is the Coulomb s-wave phase shift, $A_c(\eta_i)$ is the Coulomb penetration factor and $F(\alpha, 1, z)$ is the confluent hypergeometrical function; see Eqs. (23), (62) and (63). For the complete amplitude we have:

$$\tilde{\Psi}_{p_1 p_2}^{(+Z)}(x_1, x_2) = e^{ip_1 x_1 + ip_2 x_2} \Phi_{\mathbf{p}_1}^{z_1 Z}(\mathbf{r}_1) \Phi_{\mathbf{p}_2}^{z_2 Z}(\mathbf{r}_2) \equiv e^{iPX} e^{-i\mathbf{k}^* \mathbf{r}^*} \Phi_{\mathbf{p}_1}^{z_1 Z}(\mathbf{r}_1) \Phi_{\mathbf{p}_2}^{z_2 Z}(\mathbf{r}_2). \quad (99)$$

Note that a small contribution of spin-dependent electromagnetic forces is neglected here so that $\tilde{\Psi}^{(+)\text{SZ}} \equiv \tilde{\Psi}^{(+)\text{Z}}$ is independent of the total spin S of the particle pair.

Let us now "switch on" the interaction between particles 1 and 2. Since we consider the relative motion of the two particles at characteristic distances much slower compared with their motion with respect to the Coulomb center, it is natural to assume that in such a case the plane wave $e^{-i\mathbf{k}^*\mathbf{r}^*}$ in Eq. (99) will be basically substituted by the Bethe-Salpeter amplitude $\psi_q^S(x)$ describing the relative motion of isolated interacting particles. After this substitution we get the amplitude in so called adiabatic (factorization) approximation [13]:

$$\Psi_{p_1 p_2}^{(+)\text{SZ}}(x_1, x_2) = e^{iPX} \psi_q^S(x) \Phi_{\mathbf{p}_1}^{z_1 Z}(\mathbf{r}_1) \Phi_{\mathbf{p}_2}^{z_2 Z}(\mathbf{r}_2). \quad (100)$$

Instead of the 6-dimensional correlation function $\mathcal{R}(p_1, p_2)$ we calculate the 1-dimensional one, $\mathcal{R}^Z(k^*)$, with the numerator and denominator integrated over the simulated particle spectra. In the equal-time approximation,

$$\mathcal{R}^Z(k^*) = \sum_{i=1}^{N(k^*)} \sum_S \rho_S |\psi_{-\mathbf{k}_i^*}^S(\mathbf{r}_i^*) \Phi_{\mathbf{p}_{1_i}}^{z_1 Z}(\mathbf{r}_{1_i}) \Phi_{\mathbf{p}_{2_i}}^{z_2 Z}(\mathbf{r}_{2_i})|^2 \bigg/ \sum_{i=1}^{N(k^*)} |\Phi_{\mathbf{p}_{1_i}}^{z_1 Z}(\mathbf{r}_{1_i}) \Phi_{\mathbf{p}_{2_i}}^{z_2 Z}(\mathbf{r}_{2_i})|^2, \quad (101)$$

where $N(k^*)$ is the number of generated particle pairs in a given k^* bin. To separate the pure effect of the residual Coulomb field on particle correlations, we compare the correlation function $\mathcal{R}^Z(k^*)$ with the one, $\mathcal{R}^{\text{"Z"}}(k^*)$, taking into account for the latter the effect of the nucleus Coulomb field on one-particle spectra but not on particle correlations (i.e., simulating the argument \mathbf{r}^* independently of the arguments \mathbf{r}_1 and \mathbf{r}_2). Note that due to the velocity dependence of the correlation function, $\mathcal{R}^{\text{"Z"}} = \mathcal{R}^{Z=0}$ only at a fixed pair velocity v . In Fig. 10, we present the ratios of the $\pi^+\pi^-$ correlation functions \mathcal{R}^Z and $\mathcal{R}^{\text{"Z"}}$ assuming that the pions are emitted in the rest frame of the residual charge Z according to the thermal law with a temperature of 140 MeV at the space-time points distributed according to a product of Gauss functions with the dispersions $r_0^2 = c^2 \tau_0^2$. One may see that even for the radius as low as 2 fm the effect of the residual comoving charge as large as $Z = 60$ is less than a few per mil. Taking into account that the effective radius r_0 is larger than 2 fm even for proton collisions with low- Z nuclei and that the effective residual charge is only a fraction of the target nucleus charge, one can conclude that the effect of the residual charge is on a negligible level of a fraction of per mil.

7 Two-channel systems

7.1 Continuous spectrum in both channels

It was implied until now that a long-time FSI takes place and can be separated in the Bethe-Salpeter amplitudes in the near-threshold final state elastic transitions $1 + 2 \rightarrow 1 + 2$ only. In principle, however, it can be separated also in the inelastic transitions, $1 + 2 \rightarrow 3 + 4$, characterized by a slow relative motion in both entrance and exit channels. The necessary condition for such a separation is an approximate equality of the sums of particle masses in the intermediate ($m_3 + m_4$) and final ($m_1 + m_2$) states. Some examples are the transitions $\pi^+\pi^- \leftrightarrow \pi^0\pi^0$, $\pi^-K^+ \leftrightarrow \pi^0K^0$ or $\pi^-p \leftrightarrow \pi^0n$. For such processes only the second term in the upper diagram in Fig. 1 contributes, now with the particles 3, 4 in the intermediate state. In the equal-time approximation, the corresponding amplitudes

Table 3: The β -channel momenta k_β^* calculated at the α -channel thresholds $k_\alpha^* = 0$. Also shown are the relative shifts $\Delta k_\beta^*/k_\beta^*$ arising from the non-relativistic approximation in the second formula in Eq. (103).

α $\rightarrow \beta$	$\pi^+\pi^-$ $\rightarrow \pi^0\pi^0$	π^-K^+ $\rightarrow \pi^0K^0$	π^-p $\rightarrow \pi^0n$	K^+K^- $\rightarrow K^0\bar{K}^0$	K^-p $\rightarrow \bar{K}^0n$	$\bar{p}p$ $\rightarrow \bar{n}n$
k_β^* , MeV/c	35.5	11.3	28.0	i 62.9	i 58.6	i 49.3
k_β^{*-1} , fm	5.6	17.5	7.0	-i 3.1	-i 3.4	-i 4.0
$\Delta k_\beta^*/k_\beta^*$, %	-0.84	-0.07	-0.46	0.20	0.13	0.03

reduce to the wave functions describing a two-channel scattering of the particles 1, 2 with the inverse direction of the relative three-momentum: $\mathbf{k}^* \rightarrow -\mathbf{k}^*$ (the scattering is viewed in the diagram from right to left so that the final state particles 1, 2 are in the entrance scattering channel). We will denote the channels as $\alpha = \{1+2\}$ and $\beta = \{3+4\}$, and the corresponding wave functions describing the scattering $\alpha \rightarrow \alpha$ and $\alpha \rightarrow \beta$ - as ψ^α and ψ^β respectively. Outside the range of the strong FSI, $r^* > d$, they can be written, for the α - and β -channel continuous spectrum, as [31]:

$$\begin{aligned} \psi_{-\mathbf{k}^*}^\alpha(\mathbf{r}^*) &= \mathcal{N}(\eta_\alpha) \left[e^{-i\mathbf{k}^*\mathbf{r}^*} F(-i\eta_\alpha, 1, i\xi_\alpha) + f_c^{\alpha\alpha}(k^*) \frac{\tilde{G}(\rho_\alpha, \eta_\alpha)}{r^*} \right], \\ \psi_{-\mathbf{k}^*}^\beta(\mathbf{r}^*) &= \mathcal{N}(\eta_\alpha) f_c^{\beta\alpha}(k^*) \sqrt{\frac{\mu_\beta}{\mu_\alpha}} \frac{\tilde{G}(\rho_\beta, \eta_\beta)}{r^*} \rightarrow \mathcal{N}(\eta_\alpha) f_c^{\beta\alpha}(k^*) \sqrt{\frac{\mu_\beta}{\mu_\alpha}} \frac{\exp(i\rho_\beta)}{r^*}, \end{aligned} \quad (102)$$

where $\mathcal{N}(\eta_\alpha) = e^{i\delta_c(\eta_\alpha)} \sqrt{A_c(\eta_\alpha)}$, $\mathbf{k}^* \equiv \mathbf{k}_\alpha^*$ and

$$k_\beta^{*2} = \frac{[m_4^2 - m_3^2 + (\omega_1^* + \omega_2^*)^2]^2}{4(\omega_1^* + \omega_2^*)^2} - m_4^2 \doteq \frac{\mu_\beta}{\mu_\alpha} k_\alpha^{*2} + 2\mu_\beta(m_1 + m_2 - m_3 - m_4). \quad (103)$$

The approximate equality in Eq. (103) corresponds to the non-relativistic expressions for the energies: $\omega_j^* = m_j + k_\alpha^{*2}/(2m_j)$, $j = 1 - 4$. We consider here the systems with the Coulomb interaction absent in the channel β , so $a_\beta = \infty$, $\eta_\beta = 0$, $A_c(\eta_\beta) = 1$, $\tilde{G}(\rho_\beta, \eta_\beta) = \exp(i\rho_\beta)$ and $\chi(\eta_\beta)/a_\beta = ik_\beta^*$; the amplitude ψ^β in Eq. (102) then reduces to the expression indicated by the arrow. The β -channel momenta at the α -channel thresholds ($k_\alpha^* = 0$) for $\pi\pi^-$, πK^- , πN^- , KK^- , KN^- and $\bar{N}N^-$ -systems are given in table 3. This table also demonstrates that even close to the α -channel threshold, the use of the non-relativistic approximation can lead to noticeable shifts in k_β^* .

Similar to the single-channel case, the amplitudes

$$f_c^{\lambda\lambda'} = f^{\lambda\lambda'} / [A_c(\eta_\lambda) A_c(\eta_{\lambda'})]^{1/2}, \quad (104)$$

where $f^{\lambda\lambda'}$ are the amplitudes of the low-energy s-wave scattering due to the short-range interaction renormalized by the long-range Coulomb forces, $\lambda, \lambda' = \alpha, \beta$. The time-reversal invariance requires $f^{\lambda\lambda'} = f^{\lambda'\lambda}$. It is convenient to consider the amplitudes $f_c^{\lambda\lambda'}$ and $f^{\lambda\lambda'}$ as the elements of the symmetric matrices \hat{f}_c and \hat{f} related by the matrix equation

$$\hat{f}(k^*) = [A_c(\hat{\eta})]^{1/2} \hat{f}_c(k^*) [A_c(\hat{\eta})]^{1/2}. \quad (105)$$

The single-channel expression (69) for the amplitude f_c can then be rewritten in a matrix form:

$$\hat{f}_c(k^*) = \left(\hat{K}^{-1} - \frac{2\chi(\hat{\eta})}{\hat{a}} \right)^{-1}, \quad (106)$$

where the matrices \hat{a} , $\hat{\eta}$, $\chi(\hat{\eta})$ and $A_c(\hat{\eta})$ are diagonal in the (α, β) -channel representation, for example, $[A_c(\hat{\eta})]_{\lambda\lambda'} = A_c(\eta_\lambda)\delta_{\lambda\lambda'}$. The symmetric matrix \hat{K} has to be real for the energies above both thresholds due to the two-channel s-wave unitarity condition [15]

$$\Im \hat{f} = \hat{f}^+ \Re \hat{k} \hat{f}, \quad (107)$$

where the diagonal matrix $k_{\lambda\lambda'} = k_\lambda^* \delta_{\lambda\lambda'}$. Usually, the \hat{K} -matrix is real also for negative kinetic energies (provided sufficiently fast vanishing of the short-range potential with the distance), and so it can be expanded in even powers of $k^* \equiv k_\alpha^*$, similar to Eqs. (60) or (61) with the parameters substituted by the corresponding matrices (e.g., $f_0 \rightarrow \hat{f}_0$).

Since, in the cases of practical interest, the particles (pions, kaons, nucleons) in the channels α and β are members of the corresponding isotopic multiplets, one can assume the parameter matrices diagonal in the representation of the total isospin [31]. The elements of the amplitude matrix in the channel representation are then given by the corresponding isospin projections. Particularly, for $\alpha = \{\pi^+\pi^-\}$, $\beta = \{\pi^0\pi^0\}$, one has:

$$f_0^{\alpha\alpha} = \frac{2}{3}f_0^{(0)} + \frac{1}{3}f_0^{(2)}, \quad f_0^{\alpha\beta} = f_0^{\beta\alpha} = -\frac{\sqrt{2}}{3}(f_0^{(0)} - f_0^{(2)}), \quad f_0^{\beta\beta} = \frac{1}{3}f_0^{(0)} + \frac{2}{3}f_0^{(2)}. \quad (108)$$

Analogous relations, with the substitutions (0) \rightarrow (1/2) and (2) \rightarrow (3/2), take place for the channels $\alpha = \{\pi^-p, \pi^-K^+, \pi^+K^-\}$, $\beta = \{\pi^0n, \pi^0K^0, \pi^0\bar{K}^0\}$. For the channels $\alpha = \{K^+K^-, K^-p, \bar{p}p\}$, $\beta = \{K^0\bar{K}^0, \bar{K}^0n, \bar{n}n\}$, one has

$$f_0^{\alpha\alpha} = f_0^{\beta\beta} = \frac{1}{2}(f_0^{(0)} + f_0^{(1)}), \quad f_0^{\alpha\beta} = f_0^{\beta\alpha} = -\frac{1}{2}(f_0^{(0)} - f_0^{(1)}), \quad (109)$$

where the parameters $f_0^{(0)}$ and $f_0^{(1)}$ have now positive imaginary parts due to the effective inclusion of the additional channels opened at the energies of the elastic thresholds ($k_\alpha^* = 0$) in the reactions $K\bar{K} \rightarrow \pi\pi, \pi\eta$, $\bar{K}N \rightarrow \pi's\Lambda, \pi's\Sigma$, $\bar{N}N \rightarrow$ mesons.

Note that the use of the isospin relations (108) and (109) implies that the violation of isotopic invariance is solely associated with the Coulomb factors $A_c(\eta_j)$ (strongly deviating from unity at $k_j^* < 2\pi/|a_j|$) and the mass differences between the members of the same multiplets ($k_\alpha^* \neq k_\beta^*$). These relations however neglect the direct violation of isotopic invariance due to the renormalization effect of the Coulomb interaction on the scattering lengths, usually leading to the shifts on the level of several percent.²² Within this uncertainty, one can also use Eqs. (108) or (109) directly for the elements of the matrix \hat{K}^{-1} .

The difference between the channel momenta can be neglected sufficiently far from the threshold. Then, one can apply Eqs. (108) or (109) to the amplitudes $\tilde{f}_{jj'}$ in the absence of the Coulomb interaction²³ and, switch on this interaction in a similar way as in the

²²Note however that in the case of a large scattering length (e.g., for two protons), the contribution to the direct isospin violation of order $\mathcal{O}(f_0/a)$ can alone amount to several tens percent.

²³Note that Eqs. (108), (109) correspond to the two-dimensional unitary transformation $\hat{f}_0 = \hat{U}^{-1}\hat{f}_0'\hat{U}$, $U_{11} = U_{22} = \cos \varphi$, $U_{12} = -U_{21} = \sin \varphi$. Since it applies also to the \hat{d}_0 -matrix, one immediately arrives at the same transformation of the complete amplitude \hat{f} in the case of absent Coulomb interaction and $\hat{k} = k^*\hat{1}$.

single-channel case [36]:

$$\hat{f}(k^*) = [A_c(\hat{\eta})]^{1/2} \left\{ \hat{f}^{-1}(k^*) + i\hat{k} - \frac{2\chi(\hat{\eta})}{\hat{a}} \right\}^{-1} [A_c(\hat{\eta})]^{1/2}. \quad (110)$$

7.2 Discrete spectrum in the α -channel

One can repeat the same arguments as for the single-channel case, starting from the general solution in Eq. (75) with the substitution $f_c \rightarrow f_c^{\alpha\alpha}$. For a discrete energy level $E_n = -\kappa_n^2/(2\mu)$, the amplitude f_c has to have a pole or, equivalently, $\det \hat{f}_c^{-1}(i\kappa_n) = 0$. Following Ref. [33] and introducing the matrix

$$(\hat{A}^{-1})^{\lambda\lambda'} = (\hat{K}^{-1})^{\lambda\lambda'} - i\delta_{\lambda\lambda'}\delta_{\lambda\beta}k_\beta^*, \quad (111)$$

one can rewrite this requirement in a form of Eq. (84) modified by the substitution $K(i\kappa_n) \rightarrow A^{\alpha\alpha}(i\kappa_n)$ and thus, fix the discrete energy levels similar to Eq. (85):

$$\kappa_n = \kappa_n^c \left\{ 1 + 2A^{\alpha\alpha}\kappa_n^c \left[1 + A^{\alpha\alpha}\kappa_n^c[\phi(n) - 1] - \frac{4\pi^2}{3}\mathcal{O}((A^{\alpha\alpha}/a)^2) \right] \right\}, \quad \kappa_n^c = (n|a|)^{-1}, \quad (112)$$

$$A^{\alpha\alpha} = \frac{K^{\alpha\alpha} - ik_\beta^* \det \hat{K}}{1 - ik_\beta^* K^{\beta\beta}} = K^{\alpha\alpha} + \frac{ik_\beta^* (K^{\beta\alpha})^2}{1 - ik_\beta^* K^{\beta\beta}}, \quad (113)$$

where $a = a_\alpha$. Since $\hat{K}(i\kappa_n) = \hat{K}(0)[1 + \text{Tr}\mathcal{O}(\hat{f}_0\hat{d}_0/(na)^2)]$ and $k_\beta^*(i\kappa_n) = k_\beta^*(0)[1 + \mathcal{O}((nak_\beta^*)^{-2})]$, one can safely make the substitutions $\hat{K}(i\kappa_n) \rightarrow \hat{f}_0 \equiv \hat{K}(0)$ and $k_\beta^*(i\kappa_n) \rightarrow k_\beta^*(0)$ and write, with the relative errors $\mathcal{O}(a^{-2})$ less than a fraction of per mil,

$$A^{\lambda\lambda'} = \frac{K^{\lambda\lambda'} - ik_\beta^* \det \hat{K} \delta_{\lambda\lambda'} \delta_{\lambda\alpha}}{1 - ik_\beta^* K^{\beta\beta}} \doteq \frac{f_0^{\lambda\lambda'} - ik_\beta^* \det \hat{f}_0 \delta_{\lambda\lambda'} \delta_{\lambda\alpha}}{1 - ik_\beta^* f_0^{\beta\beta}}, \quad (114)$$

particularly,

$$\begin{aligned} \Re A^{\alpha\alpha} &= K^{\alpha\alpha} - K^{\beta\beta} \frac{(k_\beta^* K^{\beta\alpha})^2}{1 + (k_\beta^* K^{\beta\beta})^2} \doteq f_0^{\alpha\alpha} - f_0^{\beta\beta} \frac{(k_\beta^* f_0^{\beta\alpha})^2}{1 + (k_\beta^* f_0^{\beta\beta})^2}, \\ \Im A^{\alpha\alpha} &= \frac{k_\beta^* (K^{\beta\alpha})^2}{1 + (k_\beta^* K^{\beta\beta})^2} \doteq \frac{k_\beta^* (f_0^{\beta\alpha})^2}{1 + (k_\beta^* f_0^{\beta\beta})^2}. \end{aligned} \quad (115)$$

In Eqs. (114) and (115), k_β^* simply denotes $k_\beta^*(0)$ or $k_\beta^*(i\kappa_n)$. It can be seen from table 3 that k_β^{*-1} represents a scale which is intermediate between the Bohr radius $|a|$ and the elements of the matrix \hat{f}_0 . As a result, the terms like $\mathcal{O}(k_\beta^* (f_0^{\lambda\lambda'})^2/a)$ or $\mathcal{O}((ak_\beta^*)^{-2})$ contribute less than a fraction of per mil and can be omitted. As for the terms $\mathcal{O}((k_\beta^* f_0^{\lambda\lambda'})^2)$, their contribution is on a per mil level and is retained.

The s-wave solutions corresponding to the α -channel discrete spectrum are again given by the second term in Eq. (75) ($\mathcal{N}(\eta_n) = 0$) with the finite normalization $\mathcal{N}' = \mathcal{N}f_c^{\alpha\alpha}/A^{\alpha\alpha}$ introduced in the same way as in Eq. (88) modified by the substitution $K \rightarrow A^{\alpha\alpha}$. As

for the corresponding β -channel s-wave solutions $\psi_{n0}^\beta(r^*)$, they are given by the second of equations (102) with

$$\mathcal{N}f_c^{\beta\alpha} = \mathcal{N}'A^{\alpha\alpha}\frac{f_c^{\beta\alpha}}{f_c^{\alpha\alpha}} = \mathcal{N}'\frac{K^{\beta\alpha}}{1 - ik_\beta^*K^{\beta\beta}} \equiv \mathcal{N}'A^{\beta\alpha}, \quad (116)$$

the second equality following from Eq. (113) and the explicit inversion of the symmetric matrix \hat{f}_c^{-1} .²⁴

$$\begin{aligned} Df_c^{\alpha\alpha} &= K^{\alpha\alpha} - ik_\beta^* \det \hat{K}, & Df_c^{\beta\alpha} &= K^{\beta\alpha}, \\ Df_c^{\beta\beta} &= K^{\beta\beta} + \frac{2\chi}{|a|} \det \hat{K}, & \det \hat{K} &= K^{\alpha\alpha}K^{\beta\beta} - (K^{\beta\alpha})^2, \\ D &= \det \hat{f}_c^{-1} \det \hat{K} = 1 - ik_\beta^*K^{\beta\beta} + \frac{2\chi}{|a|}(K^{\alpha\alpha} - ik_\beta^* \det \hat{K}), \end{aligned} \quad (117)$$

where χ denotes here $\chi(\eta_\alpha)$; recall that $\chi(\eta_\beta)/a_\beta = ik_\beta^*$ due to the absent Coulomb interaction in the channel β . As a result,

$$\begin{aligned} \psi_{n0}^\alpha(r^*) &= \mathcal{N}'(n)A^{\alpha\alpha}\frac{\tilde{G}}{r^*} = \mathcal{N}'(n)\frac{f_0^{\alpha\alpha} - ik_\beta^* \det \hat{f}_0}{1 - ik_\beta^*f_0^{\beta\beta}}\frac{\tilde{G}}{r^*} \left[1 + \text{Tr}\mathcal{O}\left(\frac{\hat{f}_0\hat{d}_0}{n^2a^2}\right) \right], \\ \psi_{n0}^\beta(r^*) &= \mathcal{N}'(n)A^{\beta\alpha}\sqrt{\frac{\mu_\beta}{\mu_\alpha}}\frac{e^{ik_\beta^*r^*}}{r^*} = \frac{\mathcal{N}'(n)f_0^{\beta\alpha}}{1 - ik_\beta^*f_0^{\beta\beta}}\sqrt{\frac{\mu_\beta}{\mu_\alpha}}\frac{e^{ik_\beta^*r^*}}{r^*} \left[1 + \text{Tr}\mathcal{O}\left(\frac{\hat{f}_0\hat{d}_0}{n^2a^2}\right) \right], \end{aligned} \quad (118)$$

where $\tilde{G} = \tilde{G}(\rho_n, \eta_n)$ with the arguments ρ_n and η_n taken at $k_\alpha^* = i\kappa_n$ (κ_n is expressed through \hat{f}_0 in Eqs. (112) and (115)), and $\mathcal{N}'(n) = \psi_{n0}^{\text{coul}}(0)[1 + \mathcal{O}(f_0^{\alpha\alpha}/a)]$ is fixed by the normalization integral (89) for the wave function $\psi_{n0}^{\alpha\alpha}$. It can be calculated also analytically using Eq. (92) with the substitution $f_0 \rightarrow \Re A^{\alpha\alpha} \approx f_0^{\alpha\alpha}$ (see Appendix B):

$$|\mathcal{N}'(n)/\psi_{n0}^{\text{coul}}(0)|^2 - 1 = \phi(n)\frac{2\Re A^{\alpha\alpha}}{n|a|} - 4\pi^2\mathcal{O}\left(\left(\frac{\Re A^{\alpha\alpha}}{a}\right)^2\right). \quad (119)$$

Using Eqs. (117), one can express the amplitudes $f_c^{\lambda\lambda'}(k^*)$ at $k_\alpha^* = 0$ ($\chi = -i\pi$, $\hat{K} = \hat{f}_0$) through the elements of the A-matrix (related to the scattering lengths $f_0^{\lambda\lambda'}$ in Eq. (114)) with the relative error $\mathcal{O}(a^{-2})$ less than a fraction of per mil:

$$f_c^{\lambda\lambda'}(0) = A^{\lambda\lambda'} \left[1 + \frac{2i\pi}{|a|}A^{\alpha\alpha} + \mathcal{O}(a^{-2}) \right] - \frac{2i\pi}{|a|}\frac{\det \hat{f}_0}{1 - ik_\beta^*f_0^{\beta\beta}}\delta_{\lambda\lambda'}\delta_{\lambda\beta}. \quad (120)$$

7.3 Universality

Comparing Eqs. (102) and (118), one may see that the universal r^* -behavior of the s-wave amplitudes ψ^λ in continuous ($k^* \rightarrow 0$) and discrete spectrum takes place with similar

²⁴Note that the product $Df_c^{\lambda\lambda'}$ is finite since the amplitude pole for a bound state is compensated by the corresponding zero of the factor $D \propto \det \hat{f}_c^{-1}$. For the continuous spectrum at the α -channel threshold, $\hat{K} = \hat{f}_0$ and $D = 1 - ik_\beta^*f_0^{\beta\beta} - (2i\pi/|a|)(f_0^{\alpha\alpha} - ik_\beta^* \det \hat{f}_0)$.

accuracy as in the single-channel case. Thus, for the measures of the universality violation defined as in Eq. (93), one has²⁵

$$\begin{aligned}\Delta_{n0}^{\alpha,k^*}(r^*) &= 4\pi\mathcal{O}\left(\frac{k_\beta^*(f_0^{\beta\alpha})^2}{a}\right) + 4\pi^2\mathcal{O}\left(\frac{(f_0^{\alpha\alpha})^2}{a^2}\right) + \text{Tr}\mathcal{O}\left(\frac{\hat{f}_0\hat{d}_0}{n^2a^2}\right) + \mathcal{O}\left(\frac{r^{*2}}{a^2}\right) + \mathcal{O}(\rho^2), \\ \Delta_{n0}^{\beta,k^*}(r^*) &= \text{Tr}\mathcal{O}\left(\frac{\hat{f}_0\hat{d}_0}{n^2a^2}\right) + \mathcal{O}\left(\frac{r^{*2}}{a^2}\right) + \mathcal{O}(\rho^2).\end{aligned}\quad (121)$$

The presence of the second channel manifests itself through a new scale k_β^* (see table 3), basically leading to the additional correction of $4\pi\mathcal{O}(k_\beta^*(f_0^{\beta\alpha})^2/a)$ which is still on the negligible level less than a fraction of per mil.

For the production cross sections, instead of Eqs. (54) and (55), we now have:

$$\begin{aligned}\gamma_1\gamma_2\frac{d^6\sigma}{d^3\mathbf{p}_1d^3\mathbf{p}_2} &= \gamma_1\gamma_2\frac{d^6\sigma_0^\alpha}{d^3\mathbf{p}_1d^3\mathbf{p}_2}\sum_S\mathcal{G}_{S,\alpha}\langle|\psi_{-\mathbf{k}^*}^{S,\alpha}(\mathbf{r}^*)|^2\rangle_{\tilde{q}PS} \\ &\quad + \gamma_3\gamma_4\frac{d^6\sigma_0^\beta}{d^3\mathbf{p}_3d^3\mathbf{p}_4}\sum_S\mathcal{G}_{S,\beta}\langle|\psi_{-\mathbf{k}^*}^{S,\beta}(\mathbf{r}^*)|^2\rangle_{\tilde{q}PS},\end{aligned}\quad (122)$$

$$\begin{aligned}\gamma_b\frac{d^3\sigma_b^S}{d^3\mathbf{p}_b} &= (2\pi)^3\gamma_1\gamma_2\frac{d^6\sigma_0^\alpha}{d^3\mathbf{p}_1d^3\mathbf{p}_2}\mathcal{G}_{S,\alpha}\langle|\psi_b^{S,\alpha}(r^*)|^2\rangle_{0PS} \\ &\quad + (2\pi)^3\gamma_3\gamma_4\frac{d^6\sigma_0^\beta}{d^3\mathbf{p}_3d^3\mathbf{p}_4}\mathcal{G}_{S,\beta}\langle|\psi_b^{S,\beta}(r^*)|^2\rangle_{0PS},\end{aligned}\quad (123)$$

where $\mathbf{p}_i = \mathbf{p}_b m_i/(m_1 + m_2)$ in Eq. (123) and $b = \{n0\}$. Since the particles 1, 3 and 2, 4 are usually the members of the same isospin multiplets, we can take $\gamma_1\gamma_2d^6\sigma_0^\alpha \doteq \gamma_3\gamma_4d^6\sigma_0^\beta$ as a common factor in Eqs. (122) and (123) and also put $\mathcal{G}_{S,\alpha} \doteq \mathcal{G}_{S,\beta}$.

The two-channel effects in the production cross section, being quadratic in the amplitude $f_0^{\beta\alpha}$, usually represent less than several percent of the strong FSI contribution (a fraction of percent in the cross section). Thus, for a near-threshold two-pion system produced according to a Gaussian r^* -distribution (131) with the characteristic radius $r_G = 3$ fm and, taking the two-pion s-wave amplitudes from Ref. [6] ($f_0^{\alpha\alpha} = 0.186$ fm, $f_0^{\beta\alpha} = -0.176$ fm), the contributions of the FSI transitions $\pi^+\pi^- \leftrightarrow \pi^+\pi^-$ and $\pi^+\pi^- \leftrightarrow \pi^0\pi^0$ to the $\pi^+\pi^-$ production cross section respectively compose 7.72% and 0.16%, ; these contributions are somewhat higher, 9.66% and 0.20%, for the amplitudes from Ref. [4] ($f_0^{\alpha\alpha} = 0.232$ fm, $f_0^{\beta\alpha} = -0.192$ fm). At large r_G , the elastic and inelastic contributions vanish as $f_0^{\alpha\alpha}/r_G$ and $|f_0^{\beta\alpha}/r_G|^2$ respectively. One should also account for the correction due to the deviation of the solutions in Eqs. (102) and (118) from the exact ones in the inner region $r^* < d$. Though this correction vanishes as r_G^{-3} , at $r_G = 3$ fm it is still comparable to the contribution of the inelastic two-pion transition, composing 0.25% and 0.20% for the amplitudes from Ref. [6] and [4], respectively.

Note that assuming $\gamma_1\gamma_2d^6\sigma_0^\alpha\mathcal{G}_{S,\alpha} \doteq \gamma_3\gamma_4d^6\sigma_0^\beta\mathcal{G}_{S,\beta}$, the correction to the correlation function at a given total spin S , total four-momentum P and a small generalized relative four-momentum $\tilde{q} = \{0, 2\mathbf{k}^*\} \rightarrow 0$ can be written as

$$\Delta\mathcal{R} \doteq \int d^3r^*W_P(r^*)\{[|\psi_{-\mathbf{k}^*}^\alpha(\mathbf{r}^*)|^2 + |\psi_{-\mathbf{k}^*}^\beta(\mathbf{r}^*)|^2] - [|\tilde{\psi}_{-\mathbf{k}^*}^\alpha(\mathbf{r}^*)|^2 + |\tilde{\psi}_{-\mathbf{k}^*}^\beta(\mathbf{r}^*)|^2]\}, \quad (124)$$

²⁵For the amplitude ψ^α , one can use the expansions in Eqs. (77) and (90), respectively modified by the substitutions $f_0 \rightarrow f_c^{\alpha\alpha}(0)$ and $f_0 \rightarrow A^{\alpha\alpha}$.

where $W_P(\mathbf{r}^*) = \int dt^* g_P(t^*, \mathbf{r}^*; 0) / \int d^4x g_P(x; 0)$ is the normalized distribution of the vector \mathbf{r}^* of the relative distances between the emission points in the pair c.m.s. and $\tilde{\psi}$ denotes the solutions in Eqs. (102) extended to the inner region $r^* < d$. In the case of only two open channels α and β , one can write the leading part of the correction as [31]²⁶

$$\Delta\mathcal{R} \approx -4\pi W_P(0) A_c(\eta_\alpha).$$

$$\left[|f_c^{\alpha\alpha}|^2 \frac{d}{dk^{*2}} (\hat{K}^{-1})^{\alpha\alpha} + |f_c^{\beta\alpha}|^2 \frac{d}{dk^{*2}} (\hat{K}^{-1})^{\beta\beta} + 2\Re(f_c^{\alpha\alpha} f_c^{\beta\alpha*}) \frac{d}{dk^{*2}} (\hat{K}^{-1})^{\beta\alpha} \right]; \quad (125)$$

at $k^* = 0$, twice the derivatives of the inverse \hat{K} -matrix elements coincide with the effective radii $d_0^{\lambda\lambda'}$. Similarly, in the case of discrete spectrum, the leading correction to $\langle |\tilde{\psi}_{n0}^\alpha(\mathbf{r}^*)|^2 + |\tilde{\psi}_{n0}^\beta(\mathbf{r}^*)|^2 \rangle$ is also given by Eq. (125) with the substitutions $A_c(\eta_\alpha) \rightarrow N'(n)$ and $f_c^{\lambda\lambda'} \rightarrow A^{\lambda\lambda'}$.

It is important that the presence of the second channel does not practically modify the ratio (96) of the finite-size correction factors in discrete and continuous ($k^* \rightarrow 0$) spectrum at moderate distances $r^* \ll |a|$. The only modifications are the substitution $f_0 \rightarrow \Re A^{\alpha\alpha} \approx f_0^{\alpha\alpha}$ and the appearance of the negligible correction $4\pi\mathcal{O}(k^*(f_0^{\beta\alpha})^2/|a|)$:

$$\begin{aligned} \frac{1 + \delta_n}{1 + \delta(k^*)} &\equiv \frac{[\mathcal{G}_\alpha \langle |\psi_{n0}^\alpha(r^*)|^2 \rangle_{0P}^{\text{SLS}} + \mathcal{G}_\beta \langle |\psi_{n0}^\beta(r^*)|^2 \rangle_{0P}^{\text{SLS}}] / |\psi_{n0}^{\text{coul}}(0)|^2}{[\mathcal{G}_\alpha \langle |\psi_{-\mathbf{k}^*}^\alpha(\mathbf{r}^*)|^2 \rangle_{qP}^{\text{SLS}} + \mathcal{G}_\beta \langle |\psi_{-\mathbf{k}^*}^\beta(\mathbf{r}^*)|^2 \rangle_{qP}^{\text{SLS}}] / |\psi_{k^*0}^{\text{coul}}(0)|^2} \equiv \left| \frac{N'(n)}{\psi_{n0}^{\text{coul}}(0)} \right|^2 \frac{1 + \delta'_n}{1 + \delta(k^*)} \\ &= \left[1 + \phi(n) \frac{2\Re A^{\alpha\alpha}}{n|a|} \right] \left\{ 1 + \mathcal{O}\left(\frac{\langle r^{*2} \rangle^{\text{SLS}}}{a^2}\right) + \mathcal{O}(k^{*2} \langle r^{*2} \rangle^{\text{SLS}}) + 4\pi\mathcal{O}\left(\frac{k_\beta^* (f_0^{\beta\alpha})^2}{|a|}\right) \right\}. \quad (126) \end{aligned}$$

8 Finite-size effects in the experiment DIRAC

8.1 $\pi^+\pi^-$ system

We will use the results of the UrQMD transport code simulations of the pion production in pNi interactions at 24 GeV in the conditions of the DIRAC experiment at CERN [19]. Since we are interested in the region of very small relative momenta $Q = 2k^* < 20$ MeV/c, where the angular distribution of the vector \mathbf{Q} is isotropic for uncorrelated pions and, for $Q < 10$ MeV/c, the detector acceptance is practically independent of the direction of the vector \mathbf{Q} , one can simplify the analysis integrating over this direction. The finite-size effect is then determined by the distribution of the relative distance r^* between the pion production points in the pair c.m.s., irrespective of the angular distribution of the vector \mathbf{r}^* . The simulated r^* -distribution is shown in Fig. 2. We have checked that the tail of this distribution ($r^* > 50 fm$) is dominated by pion pairs containing at least one pion from the decays of the ω and η' resonances with the respective path lengths of about 30 and 900 fm in the rest frame of the decay pion; the path length $l \approx \tau \langle p_{\text{dec}} \rangle / m_\pi$ is determined by the resonance lifetime τ and the four-velocity p_{dec}/m_π of the decay pion. As a consequence of the exponential decay law, the corresponding r^* -distributions are

²⁶In Ref. [31], the correction $\Delta\mathcal{R} = W(0)J_2$ and J_2 is expressed through the amplitudes $f^{\lambda\lambda'}$ in Eq. (44). It reduces to our Eq. (125) after a straightforward though lengthy algebra. For the Gaussian r^* -distribution, Eq. (125) is valid up to subleading contributions $\mathcal{O}(k^{*2}a_1/r_G)$ (see a footnote after Eq. (61)) and $\mathcal{O}(f_0^{\alpha\alpha}d^4/r_G^5)$.

nearly exponential ones except for the region of small r^* dominated by the phase space suppression factor $\propto r^{*2}$. Actually, these distributions may deviate from the exponential ones due to a continuous spectrum of the decay momenta and averaging over the emission points of the second pion. We have found that the simulated η' contribution ($\sim 1\%$ of pion pairs at $Q < 50$ MeV/c) can be sufficiently well parametrized by a single exponential formula interpolating between the phase space and exponential behavior:

$$\sum_i \frac{dN(\pi_{\eta'}\pi_i)}{dr^*} \doteq n_{\eta'} \mathcal{F}(r^*; r_{\eta'}, l_{\eta'}), \quad (127)$$

$$\mathcal{F}(r^*; r_{\eta'}, l_{\eta'}) = \frac{x^2}{2.2} \left\{ 1 - \exp \left[-\frac{2.2}{x^2} \left(1 + 0.2x^2 \frac{1 + 0.15x^2 r_{\eta'}/l_{\eta'}}{1 + x^5/125} \right) \right] \right\} \exp \left(-\frac{r^*}{l_{\eta'}} \right), \quad x = \frac{r^*}{r_{\eta'}}, \quad (128)$$

where $r_{\eta'} = 2$ fm, $l_{\eta'} = 790$ fm. At the same time, a good description of the ω -contribution ($\sim 19\%$ of low-Q pion pairs) requires a superposition of the two exponential-like expressions:

$$\sum_{i \neq \eta'} \frac{dN(\pi_{\omega}\pi_i)}{dr^*} \doteq n_{1\omega} \mathcal{F}(r^*; r_{1\omega}, l_{1\omega}) + n_{2\omega} \mathcal{F}(r^*; r_{2\omega}, l_{2\omega}), \quad (129)$$

where $r_{1\omega} = 1.07$ fm, $l_{1\omega} = 43.0$ fm, $r_{2\omega} = 2.65$ fm, $l_{2\omega} = 25.5$ fm and $n_{1\omega}/n_{2\omega} = 0.991$. The rest of the r^* -distribution (due to the pions produced directly in the collision, in the rescatterings or in the decays of resonances with the path lengths shorter than l_{ω}) is peaked at ~ 3 fm and its main part ($\sim 60\%$ of low-Q pion pairs) including the tail for $r^* = 10 - 100$ fm can be effectively described by a power-like expression:

$$\mathcal{M}(r^*; r_M, \alpha, \beta) = r^{*2} \left[1 + \left(\frac{r^*}{r_M} \right)^{2\alpha} \right]^{-2\beta}, \quad (130)$$

where $r_M = 9.20$ fm, $\alpha = 0.656$, $\beta = 2.86$; note that the tail vanishes as $(r^*)^{-5.5}$, i.e. much faster than the Lorentzian ($\alpha = \beta = 1$). The remaining short-distance part of the r^* -distribution ($\sim 20\%$ of low-Q pion pairs) is strongly shifted towards the origin because the UrQMD code assumes the point-like regions of the decays and rescatterings; particularly, $r^* = 0$ for $\sim 8\%$ of low-Q $\pi^+\pi^-$ pairs. Therefore, we will represent this part by a Gaussian distribution:

$$\mathcal{G}(r^*; r_G) = r^{*2} \exp \left(-\frac{r^{*2}}{4r_G^2} \right), \quad (131)$$

where the Gaussian radius r_G is expected on the level of a few fm. As a result,

$$\sum_{i,j \neq \omega, \eta'} \frac{dN(\pi_i\pi_j)}{dr^*} \doteq n_M \mathcal{M}(r^*; r_M, \alpha, \beta) + n_G \mathcal{G}(r^*; r_G). \quad (132)$$

The correction factors $1 + \delta(k^*)$ and $1 + \delta_n$ corresponding to the r^* -distributions $\eta', \omega, \mathcal{M}, \mathcal{G}$, required to calculate the $\pi^+\pi^-$ production cross section in the continuous and discrete spectrum, are shown in Fig. 11. The two sets of histograms denoted by the same lines (dotted, full, dash-dotted, dashed and full) correspond to the two-pion scattering amplitudes from Ref. [6] (lower) and Ref. [4] (upper). In increasing order,

they correspond to the r^* -distributions η' , ω , $\mathcal{G}(r^*; 3\text{fm})$, $\mathcal{M}(r^*; 9.20\text{fm}, 0.656, 2.86)$ and $\mathcal{G}(r^*; 2\text{fm})$. One may see that the correction factors corresponding to the η' -contribution are practically independent of the two-pion scattering amplitudes and, noticeably deviate from the infinite-size correction factors $1 + \delta^\infty(k^*) = 1/A_c(\eta)$ (the curve) and $1 + \delta_n^\infty = 0$. We thus do not include the η' -meson in the class of long-lived sources, unlike the η -meson with the path-length of $\sim 10^5$ fm.

The calculation of the correction factors was done according to the two-channel expressions given in the numerator and denominator of the first equality in Eqs. (126):

$$1 + \delta(\mathbf{k}^*) \doteq \left\langle |\psi_{-\mathbf{k}^*}^\alpha(\mathbf{r}^*)|^2 + |\psi_{-\mathbf{k}^*}^\beta(\mathbf{r}^*)|^2 \right\rangle_{\tilde{q}P}^{\text{SLS}} / A_c(\eta), \quad (133)$$

$$1 + \delta_n \doteq \left\langle |\psi_{n0}^\alpha(r^*)|^2 + |\psi_{n0}^\beta(r^*)|^2 \right\rangle_{0P}^{\text{SLS}} / |\psi_{n0}^{\text{coul}}(0)|^2, \quad (134)$$

where α and β respectively denote the channels $\pi^+\pi^-$ and $\pi^0\pi^0$. However, the account for the coupled $\pi^0\pi^0$ channel, as well as for the leading correction due to the approximate treatment of the wave function inside the range of the strong interaction, does not practically influence the results corresponding to the η' - and ω -contributions and only slightly ($< 1\%$) shifts up the correction factors corresponding to the short-distance \mathcal{M} - and \mathcal{G} -ones. A shift of the correction factors can arise also from the uncertainty in the s-wave elastic $\pi^+\pi^-$ scattering length f_0 . The shift due to the difference of the two-pion scattering amplitudes from Ref. [6] ($f_0 = 0.186$ fm) and Ref. [4] ($f_0 = 0.232$ fm) is $\sim 2 - 3\%$ for the short-distance \mathcal{M} - and \mathcal{G} -contributions and $\sim 1\%$ for the ω -one. The global shifts are however not important since they can be absorbed in the product $\lambda g = \Lambda$ in Eqs. (27) and (28)

In accordance with the results in table 2 and Fig. 8, one may see in Fig. 11 the nearly universal slope of the factors $1 + \delta(k^*)$ corresponding to the short-distance \mathcal{M} - and \mathcal{G} -contributions. In accordance with Eq. (72), the slope scales with f_0 and is $\sim 20\%$ steeper when using the two-pion amplitudes from Ref. [4]. This is clearly seen in Fig. 12, where we plot the same correction factors as in Fig. 11 in a larger scale and with the subtracted intercepts $1 + \delta(0)$. At $Q > 20$ GeV/c, there is also seen $\sim 5 - 10\%$ variation of the slope corresponding to different short-distance distributions.

Figs. 11 and 12 also demonstrate the violation of the universality relation $\delta_n \doteq \delta(0)$ up to $\sim 0.4\%$ for the short-distance and ω -contributions and up to $\sim 9\%$ for the η' -one. The most right panel in Fig. 12 shows that this violation is partly related to the effect of the strong interaction on the normalization of the ponium wave function. Indeed, the difference $\delta'_n - \delta(0)$, corrected for this effect according to Eq. (32), shows weaker dependence on the main quantum number n and, its short-distance part practically vanishes.

In Fig. 13 we plot the correction factors corresponding to the mixture of 1% η' - and 19% ω -contributions, as expected from the UrQMD simulation; to show the effect of a possible uncertainty in the remaining short-distance part, we describe it by the Gaussians with different characteristic radii $r_G = 3$ and 2 fm. To account for the uncertainty in the two-pion scattering amplitudes, we have used those from Ref. [6] ($f_0 = 0.186$ fm) and Ref. [4] ($f_0 = 0.232$ fm). One may see that the corresponding global variations of the correction factors compose $\sim 5\%$ and $\sim 2\%$, respectively. In Fig. 14, we plot the same factors with the subtracted values of the intercept $1 + \delta(0)$. One may conclude from this figure that the uncertainty in the short-distance part of the r^* -distribution is of minor importance for the relative momenta $Q < 20$ MeV/c, including the Q -interval of $\sim (4 - 20)$ MeV/c in

which the non-atomic $\pi^+\pi^-$ pairs are usually analyzed in the DIRAC experiment. As for the effect of $\sim 20\%$ increase of the s-wave elastic $\pi^+\pi^-$ scattering length, in the middle of the DIRAC Q -interval, i.e. at $Q = 12$ MeV/c, it leads to a decrease of the difference $\delta(k^*) - \delta(0)$ by ~ 0.0015 .

To estimate the effect of the uncertainties in the ω - and η' -contributions, we plot in Fig. 15 the differences $\delta - \delta(0)$, varying these contributions by $\sim 30\%$. One may see that the corresponding variations of $\delta(k^*) - \delta(0)$ at $Q = 12$ MeV/c compose ~ 0.0025 and ~ 0.0015 , respectively.

Concerning the uncertainty in the η' -contribution, one has to take into account that, in the considered Q -interval, the corresponding correction factor is quite close to the infinite-size contribution $1/A_c$. The latter is included in the fit of the non-atomic Q -spectrum and this essentially reduces the corresponding uncertainty in the correction factor $1 + \delta(k^*)$. This is demonstrated in table 4 where the results of the fits of the non-atomic $\pi^+\pi^-$ spectra corresponding to different mixtures of the η' -, ω - and \mathcal{G} -contributions are presented. One may see that the rather conservative uncertainties in the short-distance and η' -contributions lead to negligible variations of the fitted non-atomic low- Q spectrum on a level of a fraction of per mil.

The inclusion of the infinite-size contribution in the fit also essentially influences the systematic shift related with the use of simplified Eqs. (21) and (22). As seen from table 4, for 19% ω -contribution the fit in the interval $Q = 4 - 20$ MeV/c leads to $\sim 0.9\%$ underestimation of the number of the non-atomic low- Q $\pi^+\pi^-$ pairs, instead of $\sim 0.8\%$ overestimation expected from the correction factor $1 + \delta(k^*)$ alone. The corresponding overestimation of the number N_A^{br} of breakup atoms is enhanced (in case of a homogeneous target) by the ratio of the number of correlated pions to the number of breakup atoms $N_{\pi^+\pi^-}^{corr}/N_A^{br} \sim 5$ and composes $\sim 4.5\%$. Taking into account $\sim 1\%$ underestimation of the number of produced atoms (see Δ_n^1 in table 4), the overestimation of the breakup probability composes $\sim 5.5\%$ and corresponds to $\sim 14\%$ overestimation of the pionium lifetime.

Taking rather conservative 30% and 10% uncertainties in the ω -contribution and the s-wave elastic $\pi^+\pi^-$ scattering length, the respective uncertainties in the breakup probability compose (see the differences $\Delta^i - \Delta^1$ in table 4) $\sim 3\% = 5 \cdot 0.5\% + 0.5\%$ and $\sim 0.7\% = 5 \cdot 0.12\% + 0.1\%$, corresponding to $\sim 7.5\%$ and $\sim 1.8\%$ uncertainties in the extracted pionium lifetime. One can also see from table 4 that the fits in the Q -interval of 3 – 20 MeV/c yield the systematic shifts and uncertainties by $\sim 20\%$ lower.

It should be noted that the results in table 4 assume a uniform population of the Q -interval and neglect of the errors in Q . A more accurate estimate of the uncertainties and the optimization of the fit Q -interval require the fits of the real $\pi^+\pi^-$ spectra with the account of the experimental resolution.

8.2 $\pi^-\pi^-$ and $\pi^+\pi^+$ systems

As a by-product, the experiment DIRAC provides a high statistics data on the correlation functions of identical charged pions which contains the information on the space-time characteristics of pion production and can be used to check the results of the UrQMD simulations.

Contrary to the case of the $\pi^+\pi^-$ system, the correlation effect in the system of identical pions extends and is measured up to the relative momenta $Q \sim 200$ MeV/c, so

Table 4: The relative differences $\Delta^i(0) = [\delta^i - \delta(0)]/[1 + \delta(0)]$ and $\Delta_n^i = [\delta^i - \delta_n]/[1 + \delta_n]$ resulting from the fits ($i = 1-6$) of the non-atomic $\pi^+\pi^-$ spectra corresponding to different mixtures of the η' -, ω - and \mathcal{G} -contributions. Unless stated otherwise, the Gaussian radius $r_G = 3$ fm and the fit interval $Q = 4-20$ MeV/c. The fits were done according to Eq. (27) with a constant $\delta(k^*) = \delta^i$, assuming about uniform population in Q .

FIT i	1	2	3	4	5	6	Comment
ω %	19	25	13	19	19	19	
η' %	1.0	1.0	1.0	1.3	0.7	1.0	
$\pi\pi$ phase shifts	[6]	[6]	[6]	[6]	[6]	[4]	
$\Delta^i(0)$ %	-0.88 -0.92 -0.72	-1.39 -1.40 -1.11	-0.39 -0.45 -0.34	-0.93 -0.97 -0.77	-0.83 -0.88 -0.68	-0.63 -0.70 -0.54	$r_G = 2$ fm $Q = 3 - 20$ MeV/c
$\Delta^i(0) - \Delta^1(0)$ %	0 0 0	-0.51 -0.48 -0.39	0.49 0.47 0.38	-0.05 -0.05 -0.05	0.05 0.04 0.04	0.25 0.22 0.18	$r_G = 2$ fm $Q = 3 - 20$ MeV/c
Δ_n^i %	-1.11 -0.88 -0.81 -0.78 -0.77	-1.60 -1.36 -1.30 -1.27 -1.25	-0.62 -0.41 -0.35 -0.32 -0.30	-1.14 -0.90 -0.83 -0.80 -0.79	-1.09 -0.86 -0.79 -0.76 -0.75	-0.93 -0.67 -0.60 -0.56 -0.54	n=1 n=2 n=3 n=4 n=5
$\Delta_n^i - \Delta_n^1$ %	0 0 0 0 0	-0.49 -0.48 -0.49 -0.49 -0.48	0.49 0.47 0.46 0.46 0.47	-0.03 -0.02 -0.02 -0.02 -0.02	0.02 0.02 0.02 0.02 0.02	0.18 0.21 0.21 0.22 0.23	n=1 n=2 n=3 n=4 n=5

neither the distribution of the vector \mathbf{Q} nor the detector acceptance can be considered independent of the direction of this vector. Since further the angular distribution of the vector \mathbf{r}^* is not isotropic (particularly, the characteristic width of the out component of the \mathbf{r}^* -distribution increases with the transverse momentum while those of the side and longitudinal ones decrease), the required space-time information does not reduce to the distribution of the relative distance r^* between the pion production points in the pair c.m.s.; generally, the 3-dimensional distribution of the vector \mathbf{r}^* is required. Here we however neglect this complication and calculate the 1-dimensional correlation function of two identical charged pions in the same way as for the previously considered case of the near-threshold $\pi^+\pi^-$ system, i.e. assuming the uniform distribution of the cosine of the angle between the vectors \mathbf{Q} and \mathbf{r}^* for the uncorrelated pions. The calculated correlation functions corresponding to the r^* -distributions η' , ω , $\mathcal{M}(r^*; 9.20\text{fm}, 0.656, 2.86)$, $\mathcal{G}(r^*; 3\text{fm})$ and $\mathcal{G}(r^*; 2\text{fm})$ are shown in Fig. 16. In Fig. 17, we show the correlation function corresponding to 1% η' -, 19% ω -, 60% $\mathcal{M}(r^*; 9.20\text{fm}, 0.656, 2.86)$ - and 20% $\mathcal{G}(r^*; 3\text{fm})$ -contributions, the same as expected for $\pi^+\pi^-$ pairs from the UrQMD simulations.²⁷ To demonstrate the sensitivity to the ω -contribution, we show in this figure also the correlation functions calculated with this contribution varied by $\sim 30\%$ - the corresponding change in the peak value is $\sim 1.5\%$. One can conclude, that the different shape of the ω -contribution as compared with the shapes of the short-distance ones (\mathcal{M} and \mathcal{G}) allows, in principle, to determine its fraction - the most critical parameter required to calculate the finite-size $\pi^+\pi^-$ correction factors. To control the systematic error due to the ω -fraction to $\sim 2\%$ in the lifetime, one has to determine this fraction better than to 10%, i.e. measure the correlation function of the identical charged pions to a few per mil.

9 Conclusions

We have developed a practical formalism allowing one to quantify the effect of a finite space-time extent of particle emission region on the two-particle production in continuous and discrete spectrum. We have considered the effects of non-equal emission times in the pair c.m.s., the space-time coherence and the residual nucleus charge. We have shown that these effects are on a per mil level and, being nearly the same for the near-threshold free and bound particles, can be safely neglected. We have applied this formalism to the problem of lifetime measurement of hadronic atoms produced by a high energy beam in a thin target. Particularly, we have found that the neglect of the finite-size effect on the ponium lifetime measurement in the experiment DIRAC at CERN could result in a systematic shift comparable with the expected 10% statistical error. Based on the transport code simulations, we have calculated so called correction factors that can be used to take into account the finite size of the production region by multiplying the usual point-like production cross sections of the free and bound $\pi^+\pi^-$ pairs. We have shown that the uncertainty in the parametrization of the short-distance contribution can lead to a several percent global shift of the correction factors that is however of minor importance for the lifetime measurement; the most important are the uncertainties in the ω -fraction and the s-wave elastic $\pi^+\pi^-$ scattering length f_0 that, besides leading to a few percent global shift of the correction factors, affect also their Q - and n -dependence. Assuming rather

²⁷In fact, the relative η' - and ω -contributions to $\pi^-\pi^-$ and $\pi^+\pi^+$ pairs are $\sim 40\%$ higher than those to $\pi^+\pi^-$ pairs due to a lower multiplicity of the pairs of identical charged pions.

conservative $\sim 30\%$ and $\sim 10\%$ uncertainties in the ω -fraction and f_0 , one respectively arrives at $\sim 7.5\%$ and $\sim 1.8\%$ uncertainties in the extracted pionium lifetime. It is shown that the dominant uncertainty due to the ω -fraction can be substantially diminished with the help of the DIRAC data on correlations of identical charged pions. Since the DIRAC lifetime data can be used to constrain the scattering length f_0 with $\sim 5\%$ error, one can thus decrease the uncertainty in the extracted lifetime to $\sim 3\%$. The lifetime uncertainty can be further essentially reduced in future experiments using the multi-layer targets [2] since it will be basically determined by the uncertainty in the calculated number N_A of produced atoms only; even for the conservative $\sim 30\%$ and $\sim 10\%$ uncertainties in the ω -fraction and f_0 , the corresponding uncertainties in the lifetime will be quite small: $\sim 1.3\%$ and $\sim 0.3\%$. The lifetime uncertainty can be also somewhat reduced by decreasing the lower boundary of the Q -interval; thus decreasing it from 4 to 3 MeV/c reduces the uncertainty by $\sim 20\%$. To optimize the choice of the fit Q -interval and get a more accurate estimate of the lifetime uncertainty one should fit the real $\pi^+\pi^-$ spectra and account for the experimental resolution.

Acknowledgements

The author thanks Vladimir Lyuboshitz, Leonid Nemenov, Jan Smolík and Valery Yazkov for useful discussions. This work was supported by the Grant Agency of the Czech Republic under contracts 202/01/0779 and 202/04/0793.

Appendix A: Non-equal emission times

We consider here the role of non-equal emission times in the Bethe-Salpeter amplitude $\psi_q(x) = e^{i\tilde{q}x/2} + \Delta\psi_q^{(+)}(x)$, where the correction $\Delta\psi$ to the plane wave is given in Eq. (9). We will consider the amplitude in the pair c.m.s., in which the plane wave $e^{i\tilde{q}x/2} = e^{-i\mathbf{k}^*\mathbf{r}^*}$ is independent of the emission times. First, we will prove the integral relation between the Bethe-Salpeter amplitude and the corresponding non-relativistic wave function, derived on the condition $k^{*2} \ll \mu^2$ [10]:

$$\psi_q^{(+)}(x) = \int d^3\mathbf{r}' \delta_{k^*}(\mathbf{r}^* - \mathbf{r}', t^*) \psi_{-\mathbf{k}^*}(\mathbf{r}'), \quad (\text{A.1})$$

$$\delta_{k^*}(\mathbf{r}^* - \mathbf{r}', t^*) = \frac{1}{(2\pi)^3} \int d^3\boldsymbol{\kappa} e^{-i\boldsymbol{\kappa}(\mathbf{r}^* - \mathbf{r}')} \exp(-i\frac{\boldsymbol{\kappa}^2 - \mathbf{k}^{*2}}{2m(t^*)}|t^*|), \quad (\text{A.2})$$

where $m(t^* > 0) = m_2$ and $m(t^* < 0) = m_1$.

We start by splitting the product of the propagators into four terms, each containing only two poles in the complex κ_0 -plane, situated in the opposite upper and lower half-planes. Taking into account that in pair c.m.s. $\mathbf{P} = 0$ and that the pair energy coincides with its effective mass: $P_0 = m_{12}$, we get

$$\begin{aligned} & \{(\kappa^2 - m_1^2 + i0)[(P - \kappa)^2 - m_2^2 + i0]\}^{-1} = \\ & = [(\kappa_0 - \tilde{\omega}_1 + i0)(\kappa_0 + \tilde{\omega}_1 - i0)(\kappa_0 - m_{12} - \tilde{\omega}_2 + i0)(\kappa_0 - m_{12} + \tilde{\omega}_2 - i0)]^{-1} \\ & = [m_{12}^2 - (\tilde{\omega}_1 - \tilde{\omega}_2)^2]^{-1} \cdot \\ & \cdot \{[(\kappa_0 - \tilde{\omega}_1 + i0)(\kappa_0 + \tilde{\omega}_1 - i0)]^{-1} + [(\kappa_0 - m_{12} - \tilde{\omega}_2 + i0)(\kappa_0 - m_{12} + \tilde{\omega}_2 - i0)]^{-1} \\ & - [(\kappa_0 - \tilde{\omega}_1 + i0)(\kappa_0 - m_{12} + \tilde{\omega}_2 - i0)]^{-1} - [(\kappa_0 + \tilde{\omega}_1 - i0)(\kappa_0 - m_{12} - \tilde{\omega}_2 + i0)]^{-1}\}, \quad (\text{A.3}) \end{aligned}$$

where $\tilde{\omega}_i = (m_i^2 + \boldsymbol{\kappa}^2)^{1/2}$. Assuming now that the amplitude $f^S \equiv f^S(\kappa_0, m_{12} - \kappa_0)$ is an analytical function in the complex κ_0 -plane, we can integrate over κ_0 using the residue theorem. Consider first $t^* > 0$. In this case the integration contour has to be closed in the upper half-plane, Eq. (9) then giving

$$\begin{aligned} \Delta\psi_q^{(+)}(x) = & \frac{1}{\pi^2} m_{12} e^{-i[m_{12} + (m_1^2 - m_2^2)/m_{12}]t^*/2} \int \frac{d^3\boldsymbol{\kappa} e^{-i\boldsymbol{\kappa}\mathbf{r}^*}}{m_{12}^2 - (\tilde{\omega}_1 - \tilde{\omega}_2)^2} \cdot \\ & \cdot [e^{-i\tilde{\omega}_1 t^*} f(-\tilde{\omega}_1, m_{12} + \tilde{\omega}_1) \left(\frac{1}{m_{12} + \tilde{\omega}_1 + \tilde{\omega}_2} - \frac{1}{2\tilde{\omega}_1} \right) - \\ & - e^{i(m_{12} - \tilde{\omega}_2)t^*} f(m_{12} - \tilde{\omega}_2, \tilde{\omega}_2) \left(\frac{1}{m_{12} - \tilde{\omega}_1 - \tilde{\omega}_2 + i0} + \frac{1}{2\tilde{\omega}_2} \right)]. \end{aligned} \quad (\text{A.4})$$

Since we are interested in the limit of small c.m.s. particle momenta: $k^{*2} \ll \mu^2$ and since the integral (A.4) is dominated by $\boldsymbol{\kappa}^2 \approx \mathbf{k}^{*2}$, we can use the following non-relativistic approximations (recall that $\mu = m_1 m_2 / (m_1 + m_2)$ is the reduced mass of the two-particle system):

$$\begin{aligned} m_{12} &\doteq m_1 + m_2 + \frac{\mathbf{k}^{*2}}{2\mu}, \quad m_{12} + (m_1^2 - m_2^2)/m_{12} \doteq 2 \left(m_1 + \frac{m_2}{m_1 + m_2} \frac{\mathbf{k}^{*2}}{2\mu} \right) \\ \tilde{\omega}_i &\doteq m_i + \frac{\boldsymbol{\kappa}^2}{2m_i}, \quad m_{12}^2 - (\tilde{\omega}_1 - \tilde{\omega}_2)^2 \doteq 4m_1 m_2, \quad m_{12} - \tilde{\omega}_1 - \tilde{\omega}_2 \doteq \frac{\mathbf{k}^{*2} - \boldsymbol{\kappa}^2}{2\mu}. \end{aligned} \quad (\text{A.5})$$

Retaining in the integral (A.4) only the dominant pole term $\sim [m_{12} - \tilde{\omega}_1 - \tilde{\omega}_2 + i0]^{-1}$, we get

$$\Delta\psi_q^{(+)}(x) = \frac{1}{2\pi^2} \int \frac{d^3\boldsymbol{\kappa} e^{-i\boldsymbol{\kappa}\mathbf{r}^*}}{\boldsymbol{\kappa}^2 - \mathbf{k}^{*2} - i0} \exp\left(-i \frac{\boldsymbol{\kappa}^2 - \mathbf{k}^{*2}}{2m_2} t^*\right) f(m_{12} - \tilde{\omega}_2, \tilde{\omega}_2). \quad (\text{A.6})$$

Using now the equalities $\Delta\psi_q^{(+)}(\mathbf{r}^*, t^* = 0) \equiv \Delta\psi_{-\mathbf{k}^*}(\mathbf{r}^*)$ and $\delta^{(3)}(\boldsymbol{\kappa} - \boldsymbol{\kappa}') = (2\pi)^{-3} \int d^3\mathbf{r}' \cdot \exp[i(\boldsymbol{\kappa} - \boldsymbol{\kappa}')\mathbf{r}']$, we can write:

$$\begin{aligned} \Delta\psi_q^{(+)}(x) &= \frac{1}{2\pi^2} \int d^3\boldsymbol{\kappa}' \delta^{(3)}(\boldsymbol{\kappa} - \boldsymbol{\kappa}') \frac{d^3\boldsymbol{\kappa} e^{-i\boldsymbol{\kappa}\mathbf{r}^*}}{\boldsymbol{\kappa}'^2 - \mathbf{k}^{*2} - i0} \exp\left(-i \frac{\boldsymbol{\kappa}^2 - \mathbf{k}^{*2}}{2m_2} t^*\right) f(m_{12} - \tilde{\omega}_2', \tilde{\omega}_2') \\ &= \int d^3\mathbf{r}' \int \frac{d^3\boldsymbol{\kappa}}{(2\pi)^3} e^{-i\boldsymbol{\kappa}(\mathbf{r}^* - \mathbf{r}')} \exp(-i \frac{\boldsymbol{\kappa}^2 - \mathbf{k}^{*2}}{2m(t^*)} t^*) \frac{1}{2\pi^2} \int \frac{d^3\boldsymbol{\kappa}' e^{-i\boldsymbol{\kappa}'\mathbf{r}'}}{\boldsymbol{\kappa}'^2 - \mathbf{k}^{*2} - i0} f(m_{12} - \tilde{\omega}_2', \tilde{\omega}_2') \\ &\equiv \int d^3\mathbf{r}' \delta_{k^*}(\mathbf{r}^* - \mathbf{r}', t^*) \Delta\psi_{-\mathbf{k}^*}(\mathbf{r}'), \end{aligned} \quad (\text{A.7})$$

where the δ_{k^*} -function is given in Eq. (A.2). Noting that the δ_{k^*} -function in the integral (A.7) acts on the plane wave $e^{-i\mathbf{k}^*\mathbf{r}'}$ as a δ -function, we finally arrive at the integral relation in Eq. (A.1) for $t^* > 0$. The prove of this relation in the case of $t^* < 0$ is done in a similar way, the integration κ_0 -contour being now closed in the lower half-plane. The result is the same as in Eqs. (A.4)-(A.7), up to the substitutions $m_2 \rightarrow -m_1$ in the time-dependent phase factor and $\tilde{\omega}_2 \rightarrow m_{12} - \tilde{\omega}_1$ in the arguments of the scattering amplitude f .

At $t^* = 0$ the function $\delta_{k^*}(\mathbf{r}^* - \mathbf{r}', 0) = \delta^{(3)}(\mathbf{r}^* - \mathbf{r}')$ and at $t^* > 0$

$$\delta_{k^*}(\mathbf{r}^* - \mathbf{r}', t^*) = \left(\frac{m_2}{2\pi i t^*} \right)^{3/2} \exp\left[i \left(\frac{k^{*2} t^*}{2m_2} + \frac{(\mathbf{r}^* - \mathbf{r}')^2 m_2}{2t^*} \right) \right]. \quad (\text{A.8})$$

For negative t^* -values, the substitution $m_2 \rightarrow -m_1$ has to be done in Eq. (A.8). It is clear from Eq. (A.8) that, at small k^* ($k^* \ll m(t^*)r^*/|t^*|$), the function $\delta_{k^*}(\mathbf{r}^* - \mathbf{r}', t^*)$ practically coincides with the δ -function $\delta^{(3)}(\mathbf{r}^* - \mathbf{r}')$ on condition (52).

Since the particles start to feel each other only after both of them are created, it is clear that a large difference in the emission times generally leads to a suppression of particle interaction at small k^* : $|\Delta\psi_q^{(+)}(x)| \leq |\Delta\psi_{-\mathbf{k}^*}(\mathbf{r}^*)|$; $\Delta\psi_q^{(+)}(x) \rightarrow 0$ at $|t^*| \rightarrow \infty$. Particularly instructive is the case when one of the two particles is very heavy, say $m_2 \gg m_1$. Then the two-particle interaction is suppressed provided the light particle is emitted prior the emission of the heavy one ($m(t^* < 0) = m_1$ in Eq. (A.2)). Otherwise, the large mass $m(t^* > 0) = m_2$ prevents the suppression even if the light particle were emitted much later than the heavy one. Below we consider the effect of non-equal emission times on two-particle production in some detail.

We start with the FSI due to the short-range forces only. Inserting the spherical wave (58) into the integral relation (A.1) or (A.7), we get [10]

$$\Delta\psi_q^{(+)}(x) = \frac{f(k^*)}{r^*} \left\{ i \sin(k^* r^*) + \frac{1-i}{2} [E_1(z_-) e^{ik^* r^*} + E_1(z_+) e^{-ik^* r^*}] \right\}, \quad (\text{A.9})$$

where $z_{\pm} = \left(\frac{m(t^*)}{2|t^*|} \right)^{1/2} \left(r^* \pm \frac{k^* |t^*|}{m(t^*)} \right)$ and $E_1(z) = \sqrt{\frac{2}{\pi}} \int_0^z dy e^{iy^2}$ is the Fresnel integral. Note that the length $k^* |t^*| / m(t^*) \equiv l_{k^*}$ can be interpreted classically, for large $k^* r^*$, as a distance traveled by the first emitted particle until the creation moment of the second one. The absolute value of the factor $(r^* \pm l_{k^*})$ in the argument z_{\pm} (z_{\pm}) thus corresponds to the maximal (minimal) possible c.m.s. distance between the particles at the later of the two creation moments. The effect of non-equal emission times however doesn't reduce to the modification of the distance r^* , it survives even at $k^* = 0$. This effect vanishes in the limit of small $|t^*|$, when $z_{\pm} \gg 1$, $E_1(z_{\pm}) \rightarrow (1+i)/2$ and (A.9) reduces to the spherical wave (58). In the opposite limit of large $|t^*|$, when $[m(t^*)r^*^2/(2|t^*|)]^{1/2} \ll 1$, the interaction is suppressed and the scattered wave $\Delta\psi_q^{(+)}(x)$ tends to zero for arbitrary k^* -values.

In the simple static Gaussian model of independent one-particle sources described by the amplitude (36), the applicability condition (52) of the equal-time approximation can be roughly written in the form (53). Clearly, the latter condition is not satisfied for very slow particles emitted by the sources of a long lifetime. This is demonstrated in Figs. 3 and 4 for the FSI contribution in the $\pi^0 \pi^0$ correlation function.

Note that the change of the character of the effect of non-equal times at $v \approx 0.6$ and its increase with the increasing velocity is not expected from condition (53). The increase of the effect for relativistic particles ($v \rightarrow 1$) is specific for the systems of not very large sizes and lifetimes $\tau_0 \sim r_0$, when the population of the light-cone region $\mathbf{r} \sim \mathbf{v}t$ is not negligible. Indeed, in this region the arguments of the Fresnel integrals at $k^* = 0$ can be small even at large γ : $z_{\pm} \approx (\gamma m |r_L - t|/2)^{1/2}$, leading to the modification of the spherical wave.

Consider finally the effect of non-equal emission times on the correlations of two charged particles. Since, at not very large $|t^*|$, the function $\delta_{k^*}(\mathbf{r}^* - \mathbf{r}')$ is close to the δ -function, we can neglect the terms of higher orders in (r'/a) in Eq. (A.1).²⁸ The non-equal time correction is thus mainly generated by the subleading term r^*/a , similar to

²⁸Of course, at large $|t^*|$ the neglect of these terms is not possible; in particular, the \mathbf{r}' -dependence of the hypergeometric function F guarantees the vanishing of the Coulomb interaction at $|t^*| \rightarrow \infty$.

the case of strong FSI, where it arises from a small finite-size contribution f/r^* . It concerns also the case of hadronic atoms since the Schrödinger equation at a small negative energy $-\epsilon_b = -\kappa^2/(2\mu)$ practically coincides with that in continuous spectrum at zero energy. As a result, for $r^* \ll \kappa^{-1} \doteq n|a|$ (n being the main atomic quantum number), the r^* -dependence of the corresponding wave functions at given orbital angular momentum l is the same.

Appendix B: Decay rate and normalization

The decay rate (partial width) Γ_n^β of a bound α -channel state decay into the β -channel is given by the square of the wave function ψ_{n0}^β in Eq. (118) (at a distance $r^* > d$), multiplied by the product of the surface $4\pi r^{*2}$ and the relative velocity $v_\beta = k_\beta^*/\mu_\beta$:²⁹

$$\Gamma_n^\beta = 4\pi r^{*2} \frac{k_\beta^*}{\mu_\beta} |\psi_{n0}^\beta|^2 = 4\pi \frac{k_\beta^*}{\mu_\alpha} |N'(n)|^2 \frac{(K^{\beta\alpha})^2}{1 + (k_\beta^* K^{\beta\beta})^2}. \quad (\text{B.1})$$

In the considered two-channel case, the β -channel is the only open one, so the decay rate coincides with the inverse lifetime (total width) of the bound α -channel state which can be calculated from the imaginary part of the energy $E_n = -\kappa_n^2/(2\mu_\alpha)$:

$$1/\tau_n \equiv \Gamma_n = -2\Im E_n \equiv 2\Re \kappa_n \Im \kappa_n / \mu_\alpha. \quad (\text{B.2})$$

Using Eq. (112), one has (neglecting $\Im A^{\alpha\alpha}$ as compared with the $\Re A^{\alpha\alpha}$ in the correction terms)

$$\begin{aligned} \Re \kappa_n &= \kappa_n^c \left[1 + 2\Re A^{\alpha\alpha} \kappa_n^c + \mathcal{O}\left((2\Re A^{\alpha\alpha} \kappa_n^c)^2\right) \right], \\ \Im \kappa_n &= 2\Im A^{\alpha\alpha} (\kappa_n^c)^2 \left\{ 1 + 2[\phi(n) - 1] \Re A^{\alpha\alpha} \kappa_n^c - 4\pi^2 \mathcal{O}\left((\Re A^{\alpha\alpha}/a)^2\right) \right\}, \end{aligned} \quad (\text{B.3})$$

$$\Gamma_n = \frac{4}{\mu_\alpha} \left\{ 1 + 2\phi(n) \Re A^{\alpha\alpha} \kappa_n^c - 4\pi^2 \mathcal{O}\left((\Re A^{\alpha\alpha}/a)^2\right) \right\} (\kappa_n^c)^3 \Im A^{\alpha\alpha}. \quad (\text{B.4})$$

Using the relation $(\kappa_n^c)^3 = \pi |\psi_{n0}^{\text{coul}}|^2$ and Eq. (115) for $\Im A^{\alpha\alpha}$, one finally gets, in agreement with Refs. [33, 37]:

$$\Gamma_n = 4\pi \frac{k_\beta^*}{\mu_\alpha} |\psi_{n0}^{\text{coul}}|^2 \left\{ 1 + 2\phi(n) \frac{\Re A^{\alpha\alpha}}{n|a|} - 4\pi^2 \mathcal{O}\left(\left(\frac{\Re A^{\alpha\alpha}}{a}\right)^2\right) \right\} \frac{(K^{\beta\alpha})^2}{1 + (k_\beta^* K^{\beta\beta})^2}. \quad (\text{B.5})$$

Inserting Eqs. (B.1) and (B.5) into the equality $\Gamma_n = \Gamma_n^\beta$, one proves the relation (119) between the normalization factors $\mathcal{N}'(n)$ and $\psi_{n0}^{\text{coul}}(0)$.

In the case of two or more open decay channels, the two-channel (α, β) matrix \hat{K} is no more real, particularly, in the presence of one additional channel j , one has:

$$K^{\alpha\alpha} = \mathcal{K}^{\alpha\alpha} + \frac{ik_j^* (\mathcal{K}^{j\alpha})^2}{1 - ik_j^* \mathcal{K}^{jj}}, \quad K^{\beta\alpha} = \mathcal{K}^{\beta\alpha} + \frac{ik_j^* \mathcal{K}^{j\beta} \mathcal{K}^{j\alpha}}{1 - ik_j^* \mathcal{K}^{jj}}, \quad K^{\beta\beta} = \mathcal{K}^{\beta\beta} + \frac{ik_j^* (\mathcal{K}^{j\beta})^2}{1 - ik_j^* \mathcal{K}^{jj}}, \quad (\text{B.6})$$

²⁹In case of two identical bosons in the channel β , the twice as large square of the symmetrized wave function is compensated by twice as small surface so that the result is the same.

where $\mathcal{K}^{\lambda\lambda'}$ are the elements of a real three-channel matrix \mathcal{K} .³⁰ Generally, one has to account for the possible imaginary parts of the elements of the two-channel K -matrix as well as, for a possibility of a pure imaginary value of the momentum k_β^* in the case of a closed channel β ($k_\beta^{*2} < 0$, $k_\beta^* = i(-k_\beta^{*2})^{1/2}$, $\Gamma_n^\beta = 0$). Then³¹

$$\begin{aligned}\Re A^{\alpha\alpha} &= \Re K^{\alpha\alpha} - \frac{\Im k_\beta^* \Re(K^{\beta\alpha})^2 + \Re k_\beta^* \Im(K^{\beta\alpha})^2 + |k_\beta^*|^2 [\Re K^{\beta\beta} \Re(K^{\beta\alpha})^2 + \Im K^{\beta\beta} \Im(K^{\beta\alpha})^2]}{|1 - ik_\beta^* K^{\beta\beta}|^2}, \\ \Im A^{\alpha\alpha} &= \Im K^{\alpha\alpha} - \frac{\Im k_\beta^* \Im(K^{\beta\alpha})^2 - \Re k_\beta^* \Re(K^{\beta\alpha})^2 + |k_\beta^*|^2 [\Re K^{\beta\beta} \Im(K^{\beta\alpha})^2 + \Im K^{\beta\beta} \Re(K^{\beta\alpha})^2]}{|1 - ik_\beta^* K^{\beta\beta}|^2} \\ &= k_\beta^* \left| \frac{K^{\beta\alpha}}{1 - ik_\beta^* K^{\beta\beta}} \right|^2 \theta(k_\beta^{*2}) + \sum_j k_j \left| \frac{Df_c^{j\alpha}}{1 - ik_\beta^* K^{\beta\beta}} \right|^2 = \frac{\mu_\alpha}{4\pi|N'(n)|^2} \left[\Gamma_n^\beta + \sum_j \Gamma_n^j \right], \quad (\text{B.7})\end{aligned}$$

where $\theta(x) = 1$ for $x \geq 0$, $\theta(x) = 0$ for $x < 0$. Inserting the last equality in Eqs. (B.7) into Eq. (B.4), one proves Eq. (119) for the case of any number of open decay channels.

References

- [1] B. Adeva et al.: Lifetime measurement of $\pi^+\pi^-$ atoms to test low energy QCD predictions, Proposal to the SPSLC, CERN/SPSLC 95-1, updated 10 November 1995.
- [2] B. Adeva et al.: Lifetime measurement of $\pi^+\pi^-$ and $\pi^\pm K^\mp$ atoms to test low energy QCD, CERN-SPSC-2004-009, SPSC-P-284 Add. 4, 21 April 2004.
- [3] B. Adeva et al., J.Phys. G: Nucl. Part. Phys. **30** (2004) 1929.
- [4] M.N. Nagels et al., Nucl. Phys. B **147** (1979) 189.
- [5] S. Pislak et al., Phys. Rev. Lett. **87** (2001) 221801.
- [6] G. Colangelo, J. Gasser, H. Leutwyler, Phys. Rev. Lett. **86** (2001) 5008.
- [7] M. Knecht et al., Nucl. Phys. B **457** (1995) 513; *ibid.* **471** (1996) 445.
- [8] L. Nemenov, Yad. Fiz. **41** (1985) 980.
- [9] V.L. Lyuboshitz, Yad. Fiz. **48** (1988) 1501 (Sov. J. Nucl. Phys. **48** (1988) 956).

³⁰Note that in the case of a two-pion system ($\alpha = \pi^+\pi^-$, $\beta = \pi^0\pi^0$), the third channel is $j = \gamma\gamma$ so that the elements $\mathcal{K}^{j\beta}$ and \mathcal{K}^{jj} can be safely neglected. Then, only the element $K^{\alpha\alpha}$ acquires the imaginary part: $K^{\alpha\alpha} = \mathcal{K}^{\alpha\alpha} + ik_j^*(\mathcal{K}^{j\alpha})^2$.

³¹The second expression for $\Im A^{\alpha\alpha}$ in Eq. (B.7) follows from a straightforward though lengthy matrix algebra. The last equality follows from an obvious generalization of Eq. (B.1), using the relation $K^{\beta\alpha} = Df_c^{\beta\alpha}$.

- [10] R. Lednicky, V.L. Lyuboshitz, *Yad. Fiz.* **35** (1982) 1316 (*Sov. J. Nucl. Phys.* **35** (1982) 770); *Proc. Int. Workshop on Particle Correlations and Interferometry in Nuclear Collisions*, CORINNE 90, Nantes, France, 1990 (ed. D. Ardouin, World Scientific, 1990) p. 42; *Heavy Ion Physics* **3** (1996) 1.
- [11] R. Lednicky: On the breakup probability of $\pi^+\pi^-$ atoms, DIRAC meeting, CERN, 26 February 1998; Finite-size effects on $\pi^+\pi^-$ production in continuous and discrete spectrum, DIRAC meeting, CERN, 27 February 1999; *Workshop on Hadronic Atoms*, ITP, University of Bern, 14-15 October 1999; HadAtom99, BUTP-99/26, BUHE-99-08 (hep-ph/9911339), p.7.
- [12] L. Afanasyev, O. Voskresenskaya, *Phys. Letters B* **453** (1999) 302.
- [13] R. Lednicky et al., SUBATECH-94-22, Nantes (1994); B. Erazmus et al., *Nucl. Phys. A* **583** (1995) 395; L. Martin et al., *Nucl. Phys. A* **604** (1996) 69; R. Lednicky, *Nukleonika* **43** (1998) 345.
- [14] S.S. Schweber, H.A. Bethe, F. Hoffmann, *Mesons and Fields*, vol. 1, Fields, Sect. 25.6, Row, Peterson and Comp., New York, 1955.
- [15] L.D. Landau, E.M. Lifshitz, *Quantum Mechanics: Non-Relativistic Theory*, 3-rd Ed., Sect. 136, Pergamon Press, Oxford, 1977.
- [16] A.B. Migdal, *Zh. Eksp. Theor. Fiz.* **28** (1955) 3, 10 (*Sov. Phys. JETP* **1** (1955) 2, 7).
- [17] V.V. Anisovich, L.G. Dakhno, M.M. Makarov, *Yad. Fiz.* **32** (1980) 1521 (*Sov. J. Nucl. Phys.* **32** (1980) 788).
- [18] S.A. Bass et al., *Prog. Part. Nucl. Phys.* **41** (1998) 225.
- [19] J. Smolik: Simulation results on $\pi^+\pi^-$ correlations in DIRAC experiment, DIRAC meeting, CERN, 21 October 2002; R. Lednicky, J. Smolik: The influence of finite-size effects on ponium lifetime measurements, DIRAC meetings, CERN, 6 June 2003; 8 April 2004.
- [20] S.V. Akkelin, R. Lednicky, Yu.M. Sinyukov, *Phys. Rev. C* **65** (2002) 064904.
- [21] R. Lednicky et al., *Phys. Rev. C* **61** (2000) 034901.
- [22] J. Ridky, *Fortschr. Phys.* **36** (1988) 707.
- [23] M.I. Podgoretsky, *Fiz. Elem. Chast. Atom. Yad.* **20** (1989) 628 (*Sov. J. Part. Nucl.* **20** (1989) 266).
- [24] B. Lorstad, *J. Mod. Phys. A* **4** (1989) 2861.
- [25] D.H. Boal, C.-K. Gelbke, B.K. Jennings, *Rev. Mod. Phys.* **62** (1990) 553.
- [26] U.A. Wiedemann and U. Heinz, *Phys. Rept.* **319** (1999) 145.
- [27] T. Csörgö, *Heavy Ion Phys.* **15** (2002) 1.

- [28] R. Lednicky, Phys. of Atomic Nuclei **67** (2004) 71.
- [29] S. Pratt, Phys. Rev. Lett. **53** (1984) 1219; *Phys. Rev. D* **33** (1986) 1314;
S. Pratt, T. Csorgo, J. Zimanyi, Phys. Rev. C **42** (1990) 2646.
- [30] A.N. Makhlin, Yu.M. Sinyukov, Yad. Fiz. **46** (1987) 637; Z. Phys. C **39** (1988) 69;
Yu.M. Sinyukov, Nucl. Phys. A **498** (1989) 151c.
- [31] R. Lednicky, V.V. Lyuboshitz, V.L. Lyuboshitz, Phys. of Atomic Nuclei **61** (1998) 2050.
- [32] M. Gmitro, J. Kvasil, R. Lednicky, V.L. Lyuboshitz, Czech. J. Phys. B **36** (1986) 1281.
- [33] G. Rasche, W.S. Woolcock, Nucl. Phys. A **381** (1982) 405.
- [34] I. Amirkhanov et al., Phys. Letters B **452** (1999) 155.
- [35] A. Gashi, G. Rasche, W.S. Woolcock, Phys. Letters B **513** (2001) 269.
- [36] J.D. Jackson, J.O. Blatt, Rev. Mod. Phys. **22** (1950) 77.
- [37] U. Moor, G. Rasche, W.S. Woolcock, Nucl. Phys. A **587** (1995) 747.

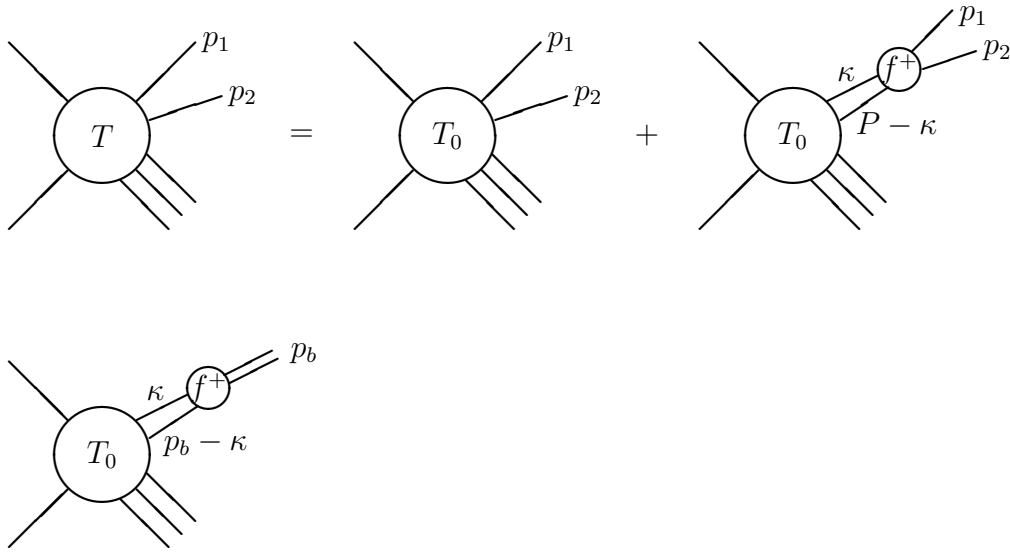


Figure 1: The diagrams describing production of particles 1 and 2 in continuous and discrete spectrum.

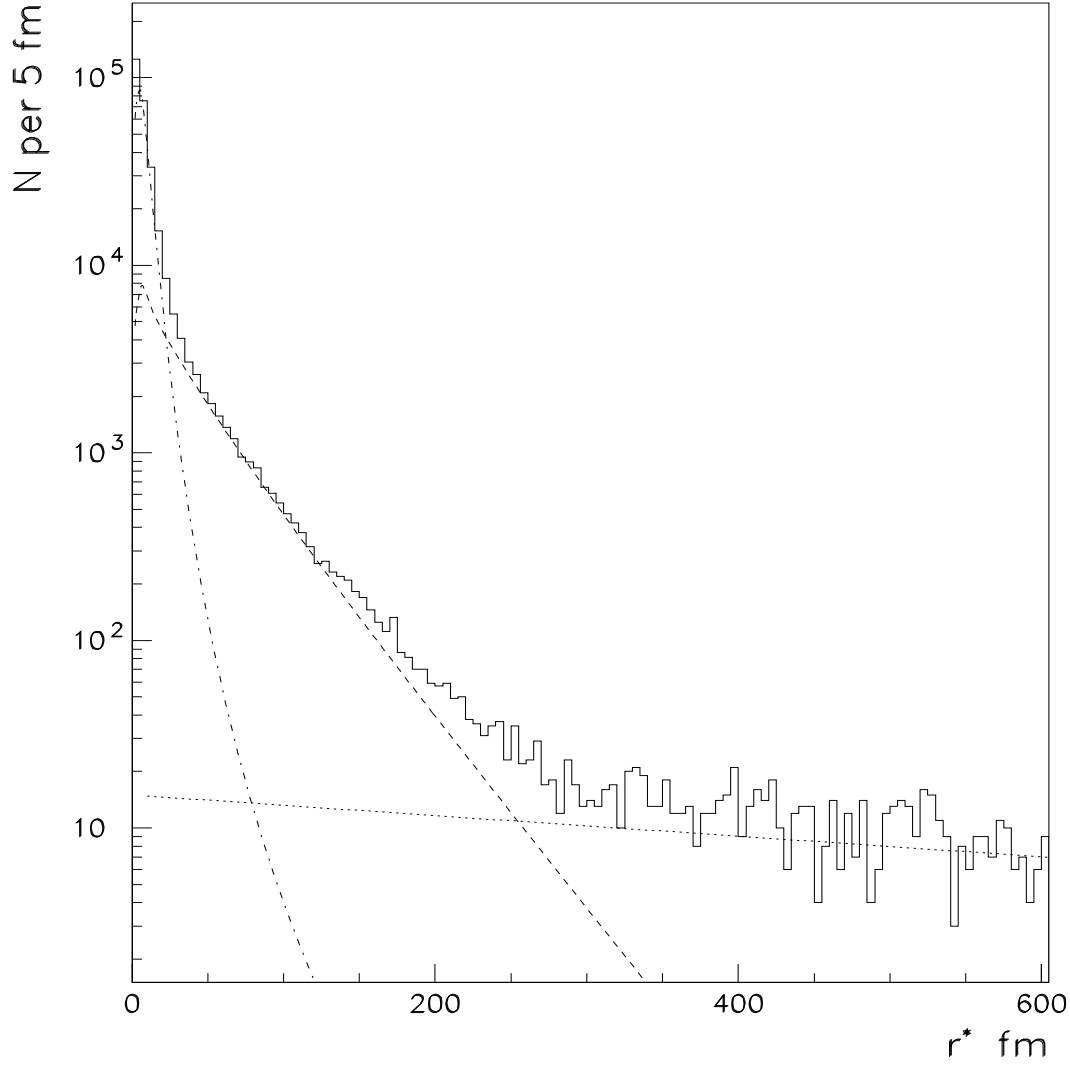


Figure 2: The distribution of the relative distance r^* between the pion production points in the pair c.m.s. simulated with the UrQMD transport code [18] for pNi interactions at 24 GeV and the relative momenta in the pair c.m.s. $Q = 2k^* < 50$ MeV/c in the conditions of the DIRAC experiment at CERN [19]. The curves are the results of the fits to short-distance, ω and η' contributions described in the text.

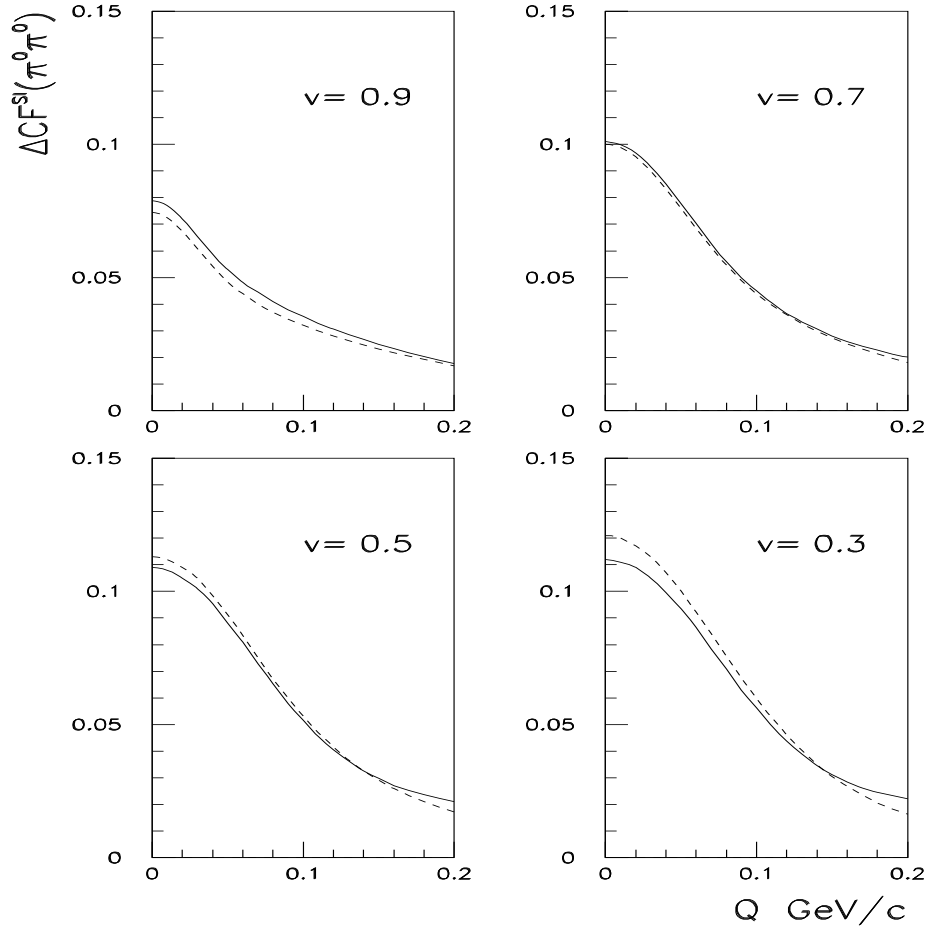


Figure 3: The FSI contribution to the $\pi^0\pi^0$ correlation function calculated for different values of the pair velocity v in a model of independent one-particle sources distributed according to a Gaussian law with the spatial and time width parameters $r_0 = 2$ fm and $\tau_0 = 2$ fm/c. The exact results (solid curves) are compared with those obtained in the equal-time approximation (dash curves).

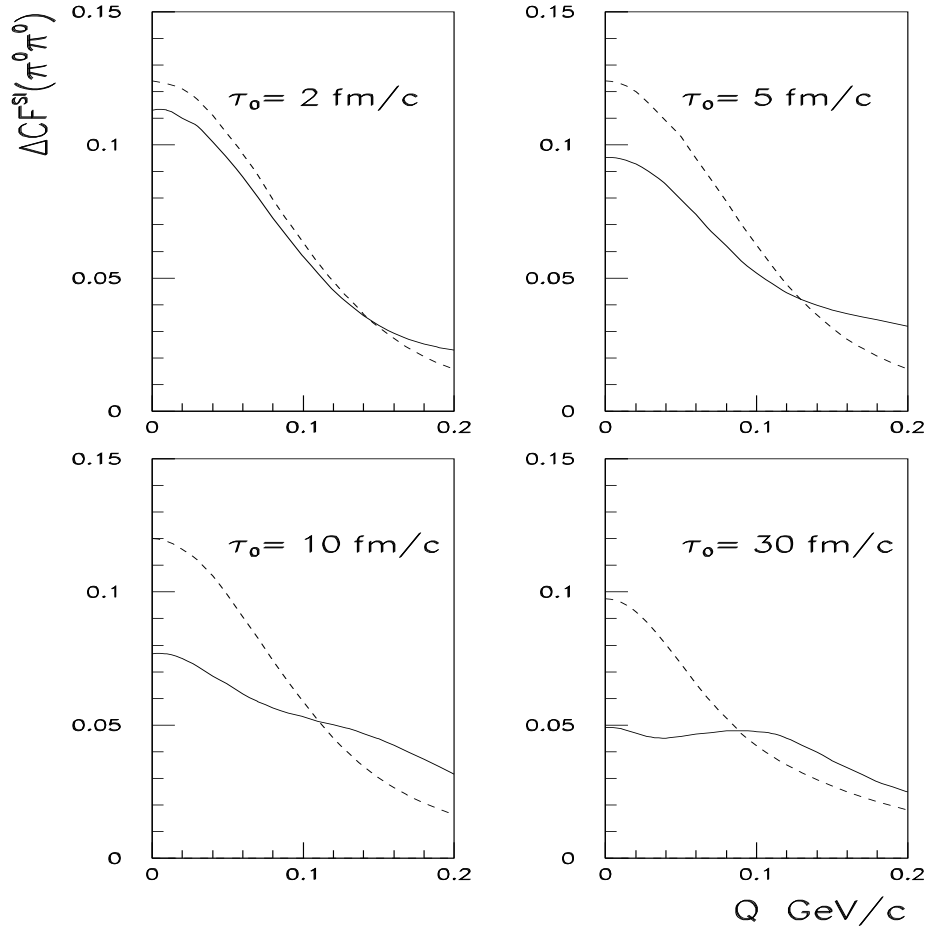


Figure 4: The same as in Fig. 3 for the pair velocity $v = 0.1$, the spatial width parameter $r_0 = 2$ fm and different values of the time width parameter τ_0 .

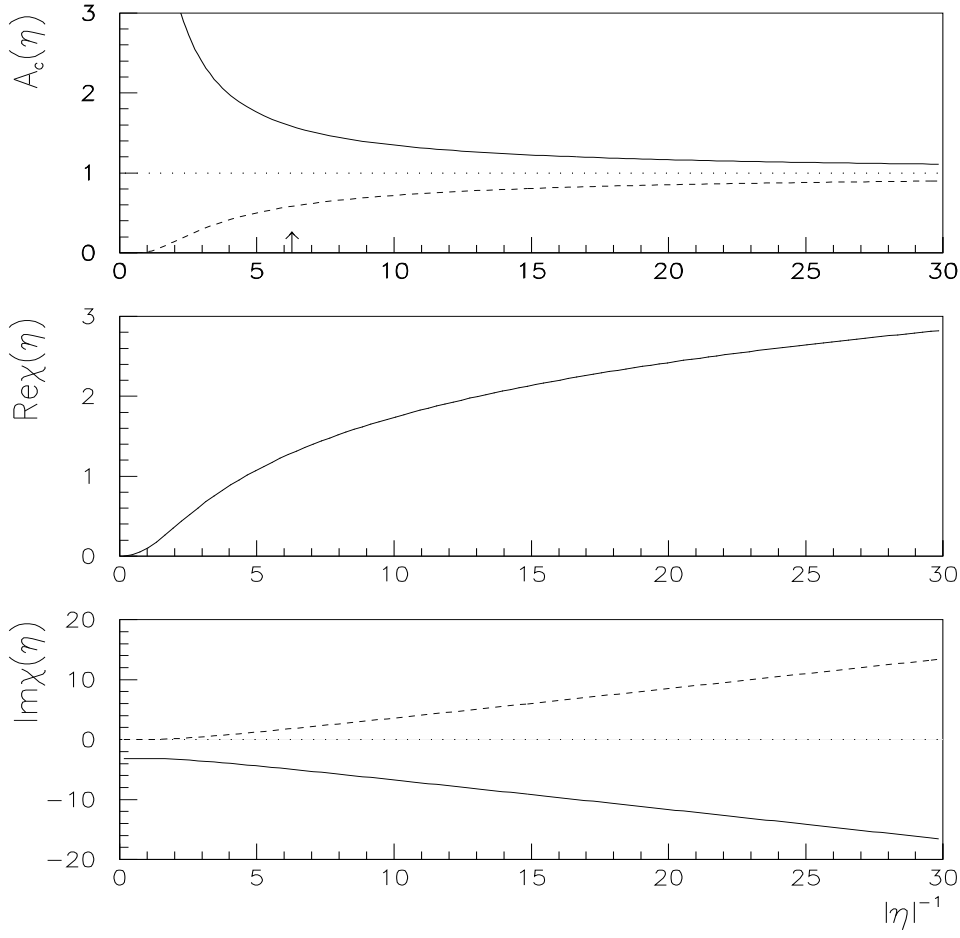


Figure 5: The functions $A_c(\eta)$, $\Re\chi(\eta) \equiv h(\eta)$ and $\Im\chi(\eta) = A_c(\eta)/(2\eta)$ defined in Eqs. (23), (67) and (68). The solid and dash curves correspond to the attraction ($\eta < 0$) and repulsion ($\eta > 0$) respectively. For two-pion systems, the variable $|\eta|^{-1} \equiv |ak^*|$ approximately coincides with the relative three-momentum $Q = 2k^*$ in MeV/c: $|\eta|^{-1} \doteq 0.98Q/(MeV/c)$. The arrow in the first panel indicates the characteristic width $|\eta|^{-1} = 2\pi$ of the Coulomb effect.

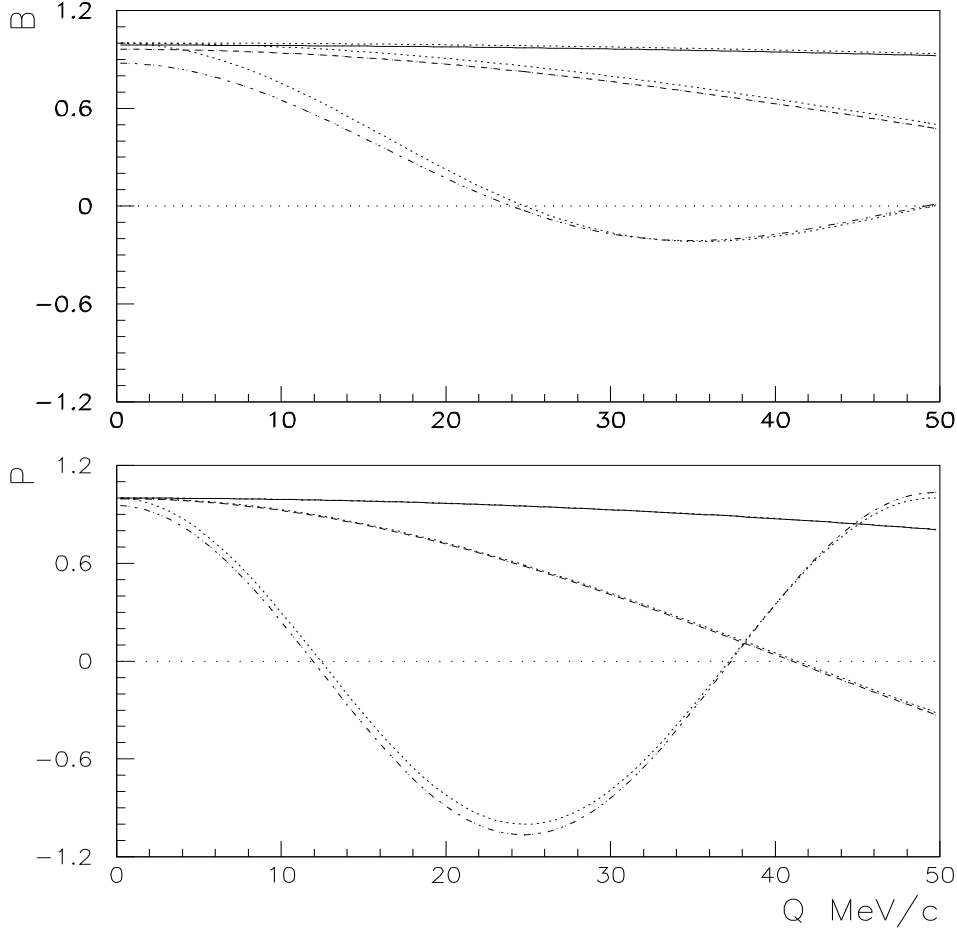


Figure 6: The functions $B(\rho, \eta)$ and $P(\rho, \eta)$ defined in Eqs. (65), (66) and calculated for the $\pi^+\pi^-$ system. The solid, dash and dash-dotted curves correspond to $r^* = 5, 15$ and 50 fm respectively. The dotted curves represent the functions $B(\rho, 0) = \sin \rho / \rho$ and $P(\rho, 0) = \cos \rho$ corresponding to the case of neutral particles.

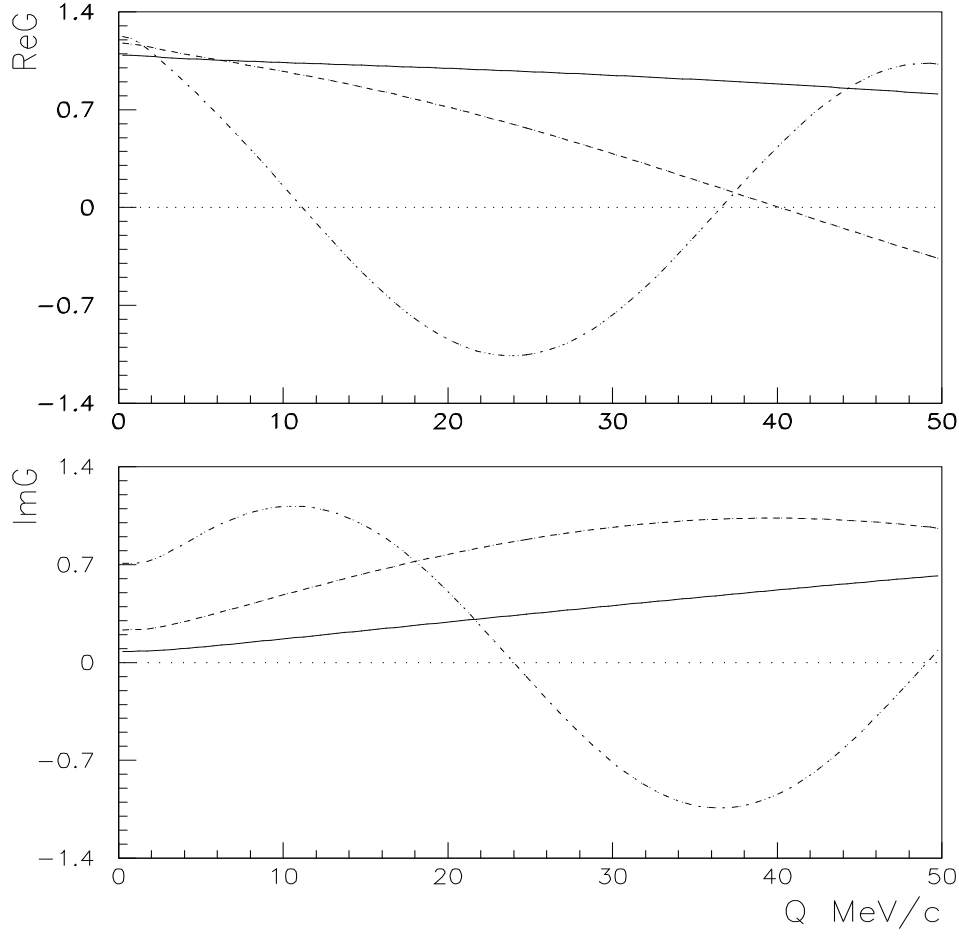


Figure 7: The function $\tilde{G}(\rho, \eta)$ defined in Eq. (64) and calculated for the $\pi^+\pi^-$ system. The solid, dash and dash-dotted curves correspond to $r^* = 5, 15$ and 50 fm respectively.

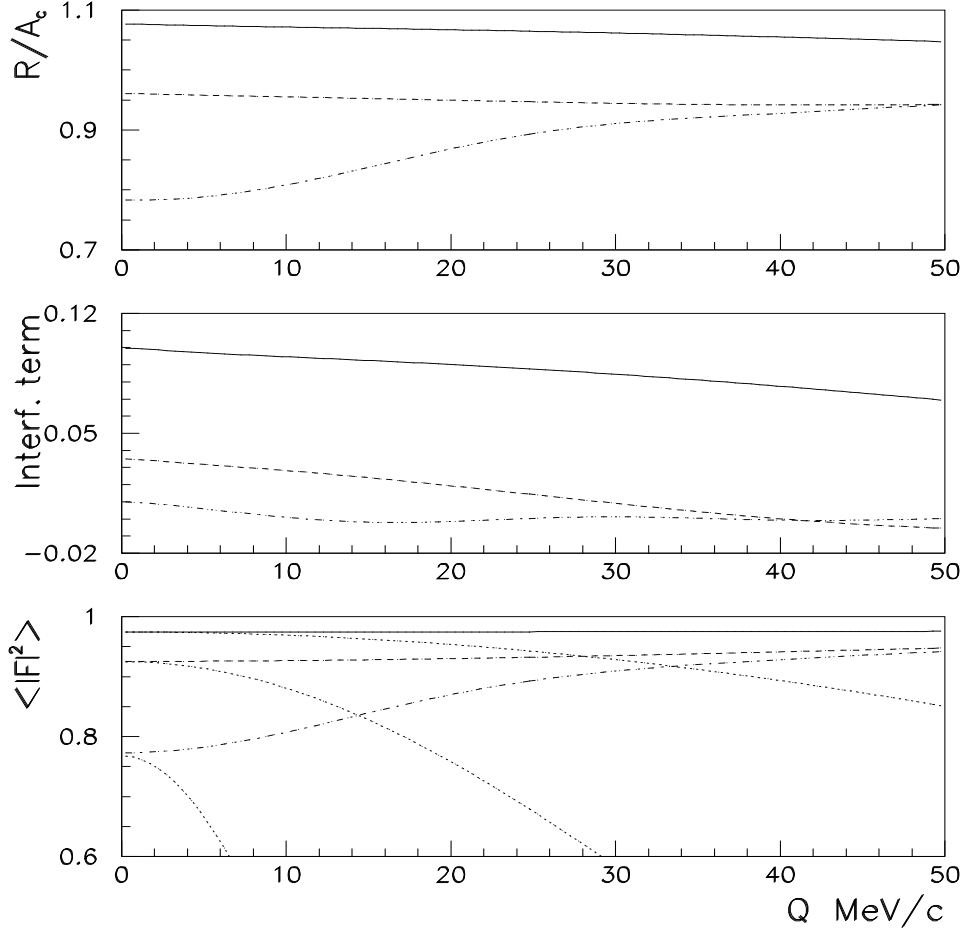


Figure 8: The $\pi^+\pi^-$ correlation function at a fixed separation r^* divided by the Coulomb penetration factor: $\mathcal{R}/A_c = \langle |e^{-i\mathbf{k}^*\mathbf{r}^*}F + f_c\tilde{G}/r^*|^2 \rangle$, and the corresponding main contributions due to the interference term and the modulus squared of the hypergeometric function (see the first of Eqs. (71)). The solid, dash and dash-dotted curves correspond to $r^* = 5, 15$ and 50 fm respectively. The calculation is done in the approximation of a constant scattering amplitude $f_c(k^*) = f_0 = 0.232$ fm, the averaging assumes the uniform distribution of the cosine of the angle between the vectors \mathbf{r}^* and $\mathbf{k}^* = \mathbf{Q}/2$. The dotted curves in the lower panel represent the s-wave Coulomb contribution $B^2(\rho, \eta)$ to the quadratic term.

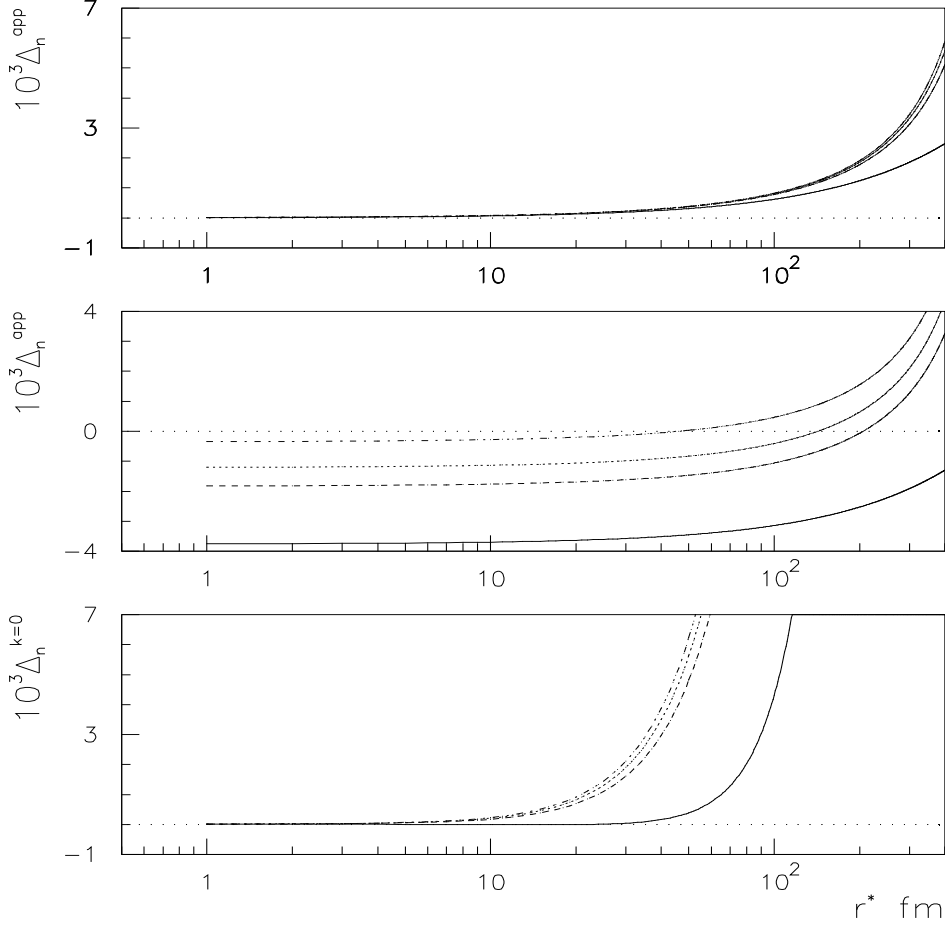


Figure 9: Comparison of the approximate $\pi^+\pi^-$ atomic wave function $\psi_{n0}^{\text{app}}(r^*)$ and the $\pi^+\pi^-$ wave function in continuous spectrum $\psi_{-\mathbf{k}^*}(\mathbf{r}^*)$ at $k^* \rightarrow 0$, respectively defined in Eqs. (91) and (62) ($f_0 = 0.232$ fm), with the exact s-wave solution outside the range of the strong interaction $\psi_{n0}(r^*)$ given in Eq. (87): $\Delta_n^{\text{app}}(r^*) = [\psi_{n0}^{\text{app}}(r^*)/\psi_{n0}(r^*)]^2 - 1$ and $\Delta_n^{k^*=0}(r^*) = \langle |[\psi_{-\mathbf{k}^*}(\mathbf{r}^*)/\psi_{-\mathbf{k}^*}^{\text{coul}}(0)]/[\psi_{n0}(r^*)/\mathcal{N}'(n)]|^2 \rangle - 1$, $k^* \rightarrow 0$; the averaging in the latter expression is done over the uniform distribution of the cosine of the angle between the vectors \mathbf{r}^* and $\mathbf{k}^* = \mathbf{Q}/2$. The central panel shows $\Delta_n^{\text{app}}(r^*)$ assuming $\mathcal{N}'(n) = \psi_{n0}^{\text{coul}}(0)$ in Eq. (91) in correspondence with the ansatz (96). The curves in the increasing order correspond to $n = 1, 2, 3, 10$.

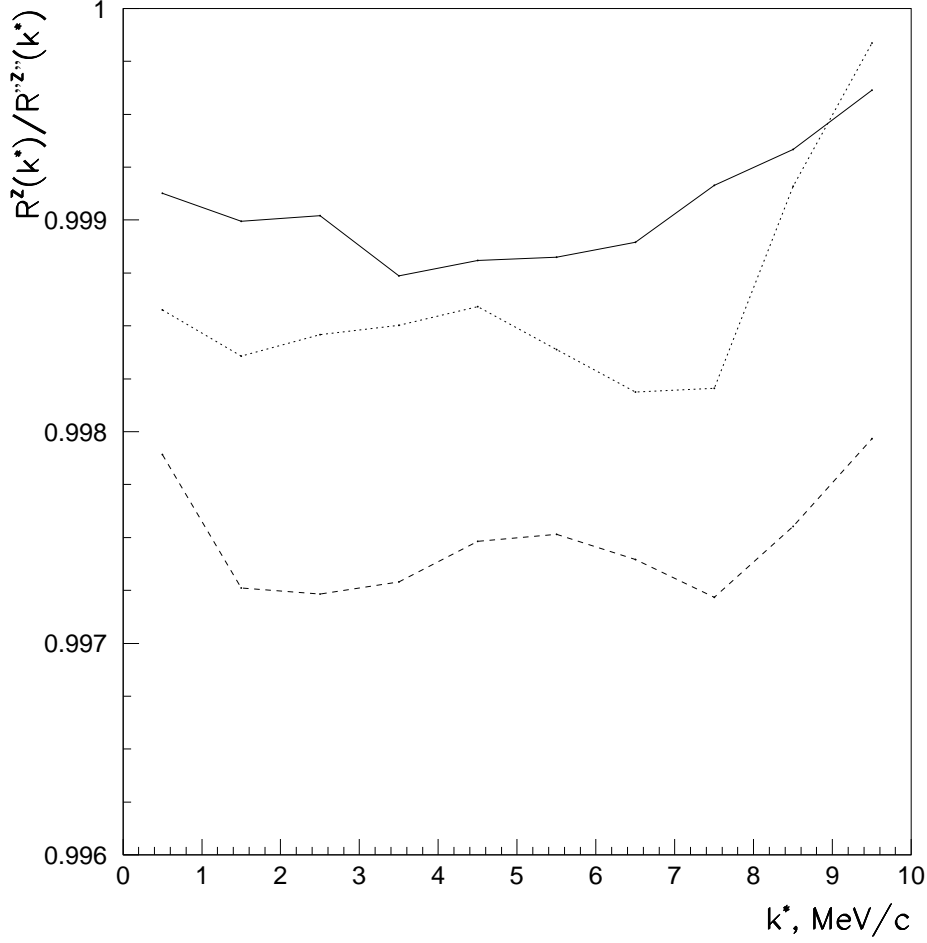


Figure 10: The ratios of the $\pi^+\pi^-$ correlation functions \mathcal{R}^Z and $\mathcal{R}^{Z''}$. For the latter, only one-particle spectra are influenced by the effective comoving charge Z . The pions are assumed to be emitted in the rest frame of a pointlike charge Z according to the thermal law with a temperature of 140 MeV. The distribution of the space-time coordinates of the particle sources is simulated as a product of Gauss functions with the dispersions $r_0^2 = c^2\tau_0^2$. The full broken line corresponds to $Z = 30, r_0 = 2$ fm, the dash and dotted ones - to $Z = 60, r_0 = 2$ and 3 fm, respectively.

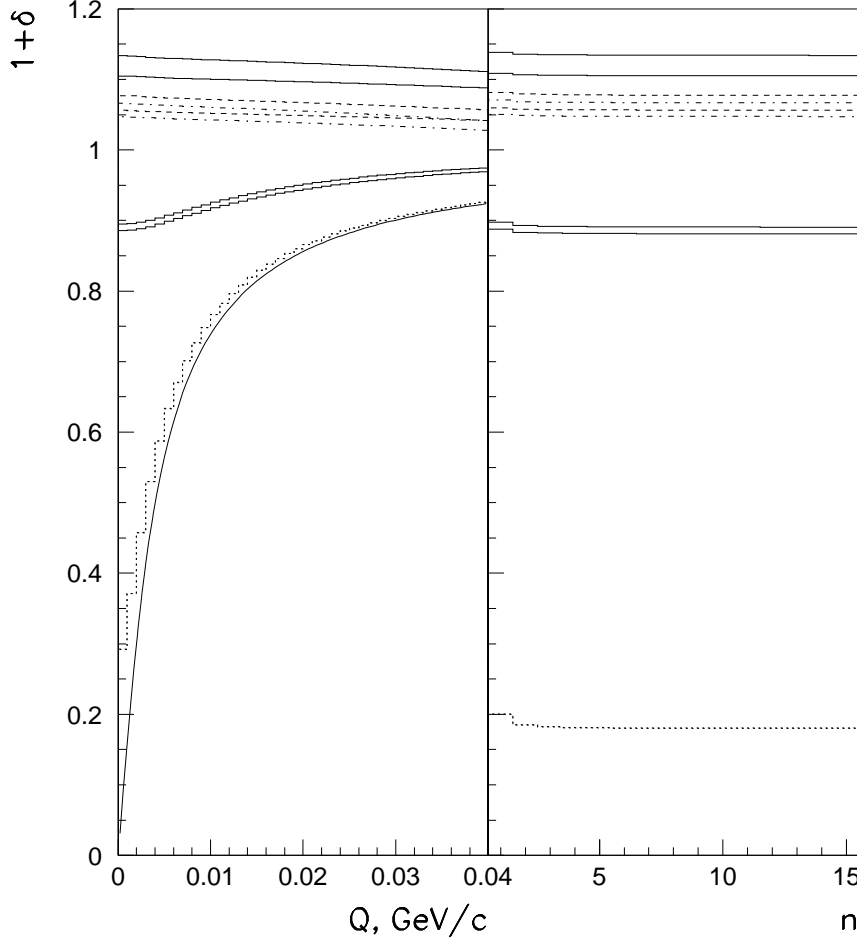


Figure 11: The correction factors $1 + \delta(k^*)$ (left) and $1 + \delta_n$ (right) as functions of the relative momentum $Q = 2k^*$ and the main atomic quantum number n respectively. They are required to calculate the $\pi^+\pi^-$ production cross sections in the continuous and discrete spectrum according to Eqs. (27) and (28). The two sets of histograms denoted by the same lines (dotted, full, dash-dotted, dashed and full) correspond to the two-pion scattering amplitudes from Ref. [6] (lower) and Ref. [4] (upper). In increasing order, they correspond to the r^* -distributions η' , ω , $\mathcal{G}(r^*; 3\text{fm})$, $\mathcal{M}(r^*; 9.20\text{fm}, 0.656, 2.86)$ and $\mathcal{G}(r^*; 2\text{fm})$ defined in Eqs. (127)-(131). The calculation was done according to the two-channel expressions given in Eqs. (133) and Eqs. (134), taking into account the correction in Eq. (125). Note that the infinite-size correction factors $1 + \delta^\infty(k^*) = 1/A_c(\eta)$ (the curve) and $1 + \delta_n^\infty = 0$.

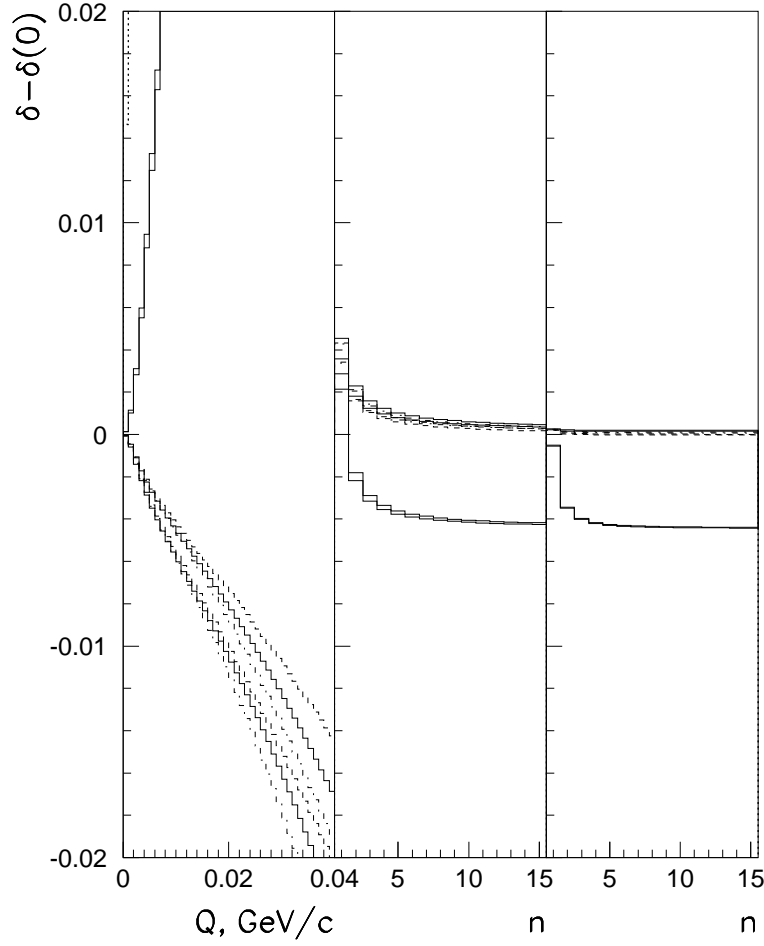


Figure 12: The differences $\delta(k^*) - \delta(0)$ (left panel), $\delta_n - \delta(0)$ (middle panel) and $\delta'_n - \delta(0)$ (right panel) calculated from the $\pi^+\pi^-$ correction factors given in Fig. 11. The latter difference is corrected for the effect of the strong interaction on the normalization of the pionium wave function according to Eq. (32). The differences corresponding to the η' contribution (dotted histograms) are seen only in the left panel first bin.

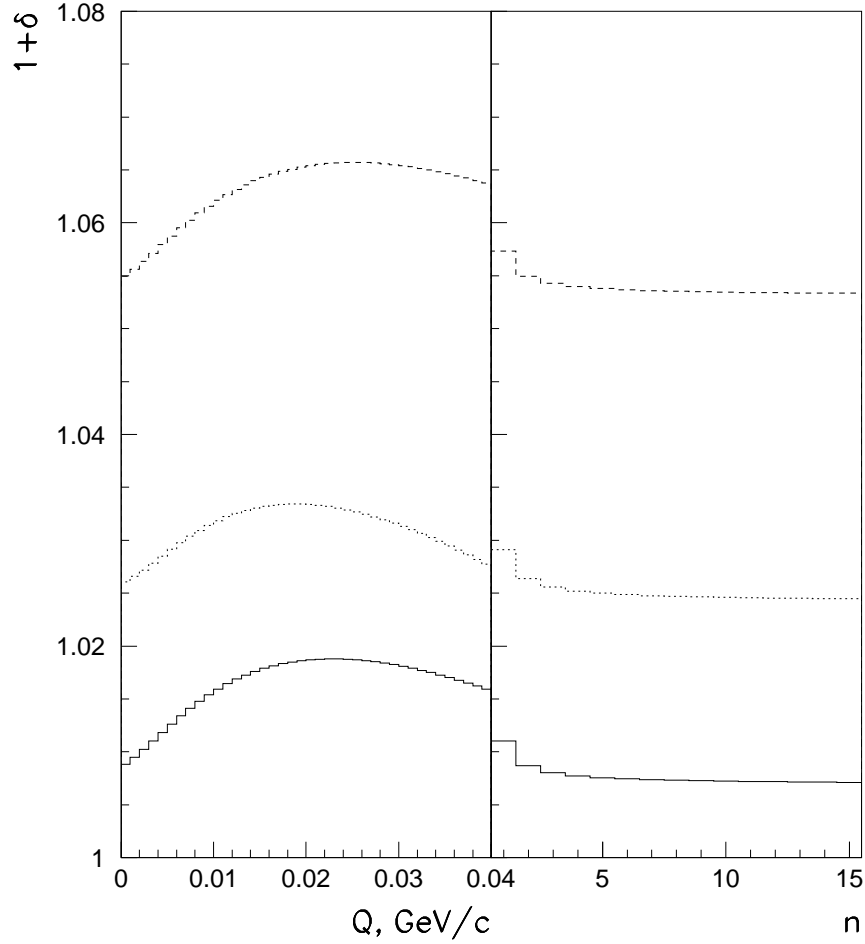


Figure 13: The $\pi^+\pi^-$ correction factors $1 + \delta(k^*)$ (left) and $1 + \delta_n$ (right) calculated in the same way as in Fig. 11 assuming the mixtures of 1% η' -, 19% ω - and 80% \mathcal{G} -contributions with $r_G = 3$ fm (lower and middle) and $r_G = 2$ fm (upper). The lower and upper histograms correspond to the two-pion scattering amplitudes from Ref. [6], the middle one - to those from Ref. [4].

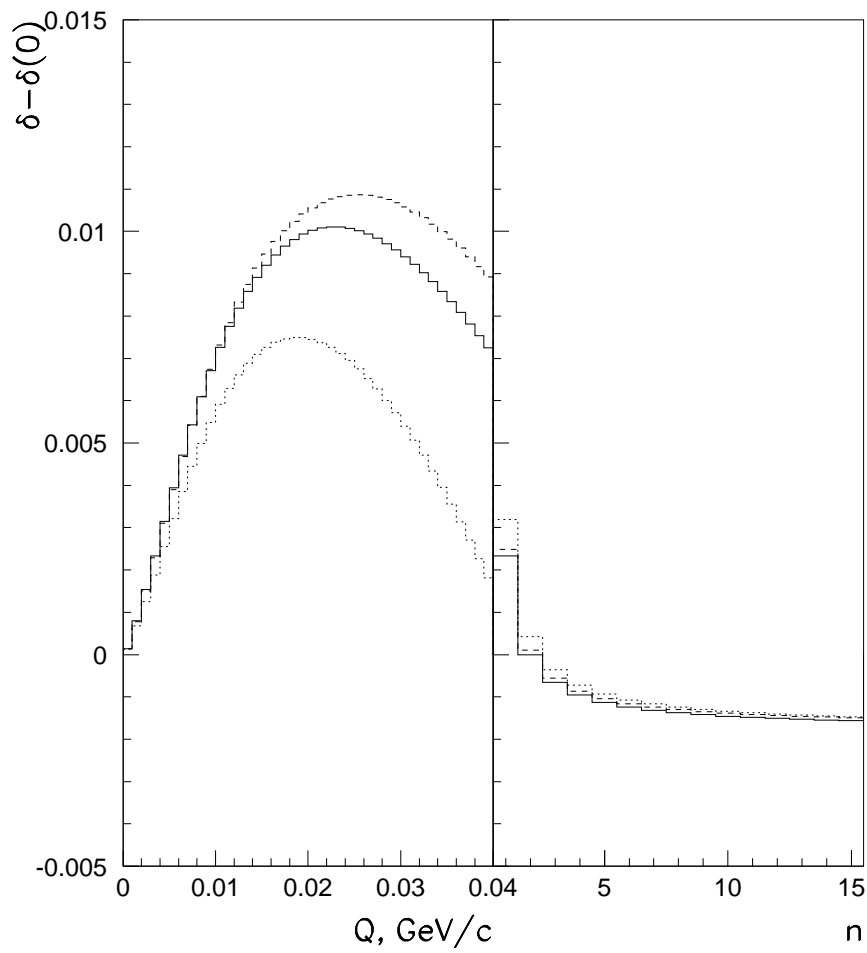


Figure 14: The differences $\delta(k^*) - \delta(0)$ (left) and $\delta_n - \delta(0)$ (right) corresponding to the correction factors in Fig. 13.

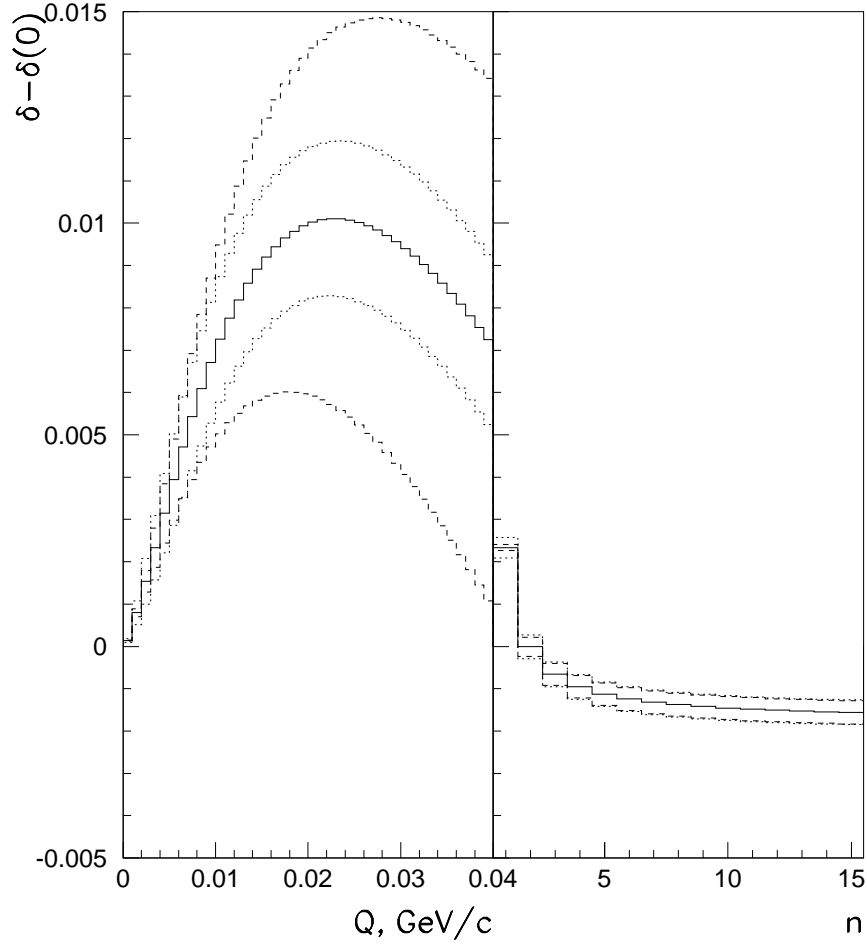


Figure 15: The differences $\delta(k^*) - \delta(0)$ (left) and $\delta_n - \delta(0)$ (right). The full histogram coincides with that in Fig. 14. The dashed ones correspond to the 0.19 ± 0.06 ω -contributions and the dotted ones - to the 0.010 ± 0.003 η' -contributions.

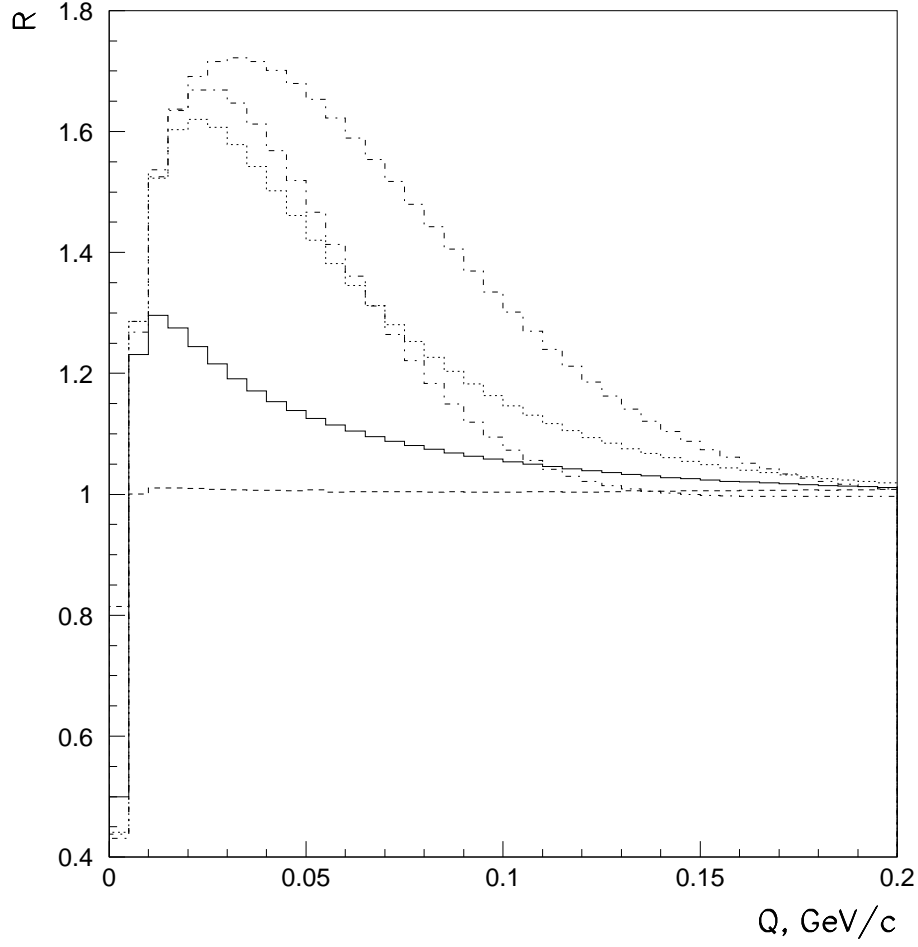


Figure 16: The $\pi^-\pi^-$ correlation functions. The histograms in the increasing order of the peak values correspond to the r^* -distributions η' , ω , $\mathcal{M}(r^*; 9.20\text{fm}, 0.656, 2.86)$, $\mathcal{G}(r^*; 3\text{fm})$ and $\mathcal{G}(r^*; 2\text{fm})$ respectively.

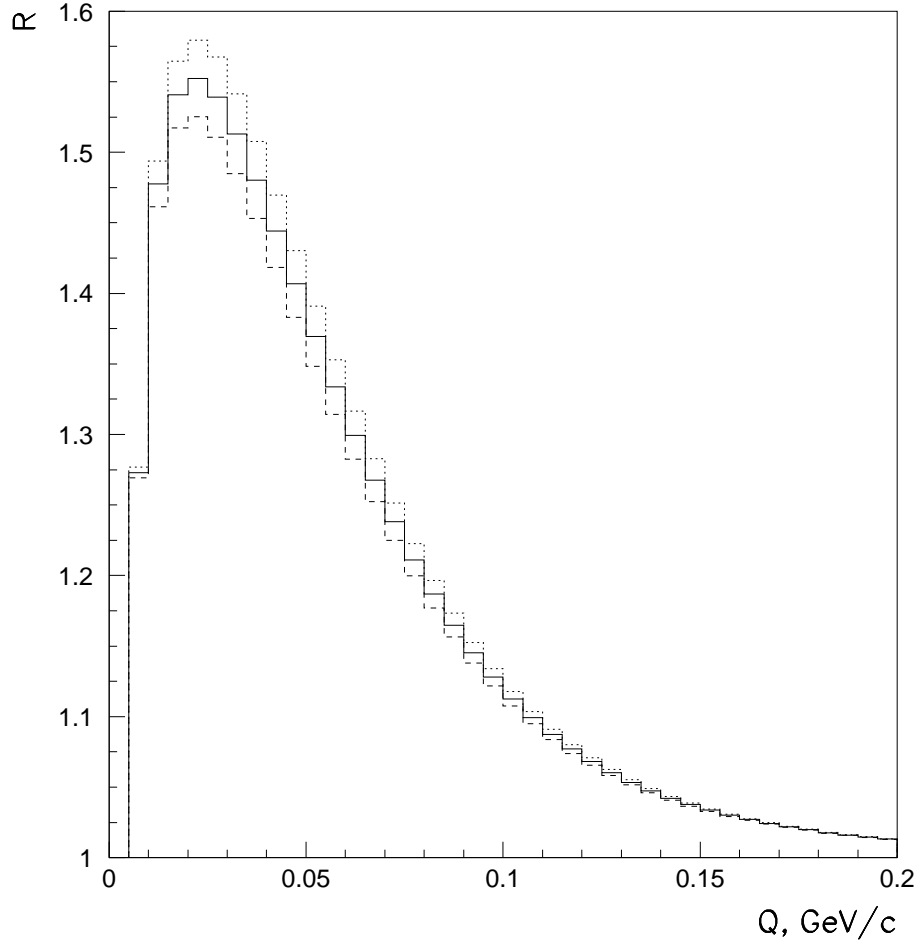


Figure 17: The $\pi^-\pi^-$ correlation functions. The middle histogram corresponds to 1% η' -, 19% ω -, 60% $\mathcal{M}(r^*; 9.20\text{fm}, 0.656, 2.86)$ - and 20% $\mathcal{G}(r^*; 3\text{fm})$ -contributions. The upper and lower histograms correspond to the 1% η' -, 19% $\pm 6\%$ ω -contributions and the unchanged ratio 3:1 of the \mathcal{M} - and \mathcal{G} -contributions (unchanged form of the short-distance contribution).